Dissection of Prosurvival and Apoptotic Signalling By Human IRE1

EMMA JOANNE FENECH

Dissection of Prosurvival and Apoptotic Signalling By Human IRE1α

Emma J Fenech

Supervised by: Dr. Martin Schröder and Dr. Adam Benham

This thesis is submitted as part of the requirements for the award of the Degree of Master of Science (Research) of the University of Durham.

October 2014

Acknowledgements:

Thank you to Dr. Martin Schröder for supporting my studies and constantly advising me throughout my Masters project. I was always well supported and have learnt so much in one year! I would also like to thank Dr. Adam Benham for his help and ideas. From the Durham microscopy team, I am very grateful to Dr. Martin Goldberg, Dr. Robert Banks, Dr. Tim Hawkins, Dr. Akis Karakesisoglou, Helen Grindley and Christine Richardson for their time, patience and expertise. An especially big thanks to Adina, Max and Jamie from Lab 2, Morris from Lab 8 and Charlotte from Lab 19. Without their knowledge and humour, this project wouldn't have been as fruitful or as fun.

A special thanks to my mum, Jane, my Dad, Albert, and sister, Clare, who have listened to me rambling about odd bits of biology and probably have a rather surprising knowledge of the subject. Thank you also to Dave and Sue and my housemates, Jenn and Sarah, for providing cake for eating and ears for listening to presentations.

And, finally, a special word of thanks to Mike who has inspired me to get to those late night and early morning time points, and whose company and I could not have managed without.

For Elsie May Allerton (‘O.G.’)

ABSTRACT

The endoplasmic reticulum (ER) is a complex organelle whose primary function is concerned with protein folding and modification. However, occasionally unfolded proteins accumulate in the ER, causing ER stress. In these cases, the unfolded response (UPR) is activated in an attempt to restore ER homeostasis. There are three mammalian UPR signal transducers. IRE1α is the most ancient of these and has two functional domains. The RNase domain is often regarded as promoting cell survival via splicing of *XBP-1* mRNA to generate the XBP-1(s) transcription factor. This domain has also been implicated in the RIDD pathway where ER-localised mRNAs are degraded. The kinase domain is thought of as proapoptotic due to its ability to activate the JNK signalling cascade.

However, recent work highlighted a potential role for IRE1α kinase activity in cell survival. This project focussed on segregating cell fate decisions according to kinase and RNase functions. This was done by comparing MEFs expressing human WT-IRE1α to MEFs expressing a kinase-deficient IRE1α mutant, or a kinase- and RNase-dead form of IRE1α. Western blotting, qPCR analysis and electron microscopy were principally used to identify biochemical, transcriptional and physical differences between these cells. Western blot analysis highlighted a correlation between the loss of IRE1α kinase activity and increased expression of the proapoptotic marker, CHOP, during ER stress. Further strengthening this observation, an increase in mRNA levels of *TRB3*, which is a downstream target of CHOP was identified by qPCR. The latter technique also suggested that ERAD, the process by which misfolded ER lumenal proteins are degraded, was also compromised. Finally, electron micrographs clearly showed loss of the ability in cells expressing either IRE1α mutants to structurally organise the proliferating ER during stress. To conclude, the results strongly argue that lack of the kinase domain negatively influences ER physiology and gene expression when the UPR is active. Therefore, this study brings to attention the importance of IRE1α kinase activity for cytoprotection which, in turn, has major implications on the role of the UPR in several different diseases.

TABLE OF CONTENTS

LIST OF FIGURES

Chapter 4

Chapter 5

Chapter 6

Appendix

LIST OF TABLES

Table of abbreviations:

Abbreviation	Full name
1NM-PP1	4-Amino-1-*tert*-butyl-3-(1′-naphthylmethyl)pyrazolo[3,4-d]pyrimidine
α1AT	Alpha 1 antitrypsin
AIP1	ASK1 interacting protein
ALS	Amyotrophic lateral sclerosis
ASK1	Apoptosis signal-regulating kinase 1
ATF4	Activating Transcription factor 4
ATF6	Activating Transcription factor 6
ATP	Adenosine triphosphate
Bcl-2	B-cell lymphoma 2
BiP/GRP78	Binding immunoglobulin protein/ Glucose-regulated protein of 78 kDa
BLOS1	Biogenesis of lysosomal organelles complex-1, subunit 1
bZIP	Basic leucine zipper
CCT	Choline cytidylytransferase
CHO	Chinese hamster ovary
CHOP	CCAAT/enhancer-binding protein homologous protein
COL6a1	Collagen, type VI, alpha1
COS-7	*Cercophitecus aethiops* kidney cells
dATP	Deoxyadenosine triphosphate
dCTP	Deoxycytidine triphosphate
DEPC	Diethylpyrocarbonate
D-Glc	D-glucose
dGTP	Deoxyguanosine triphosphate
DMEM	Dulbecco's Modified Eagle Medium
DMSO	Dimethyl sulphoxide
dTTP	Deoxythymidine triphosphate
ECL	Enhanced chemiluminescence
EDEM	ER degradation enhancer, mannosidase α-like 1
EDTA	Ethylenediaminetetraacetic acid
eIF2α	Eukaryotic initiation factor 2 (alpha subunit)
ER	Endoplasmic reticulum
ERAD	ER-associated degradation
ERdj3	Endoplasmic reticulum DnaJ homolog 3
ERdj4	Endoplasmic reticulum DnaJ homolog 4
Erk1/2	Extracellular signal-regulated protein kinases 1/2
ERO1L-α	Endoplasmic reticulum oxidoreductin-1-like α

ERO1L-β	Endoplasmic reticulum oxidoreductin-1-like beta
GADD34	Growth arrest and DNA damage-inducible protein 34
GALNT10	UDP-N-acetyl-α-D-galactosamine: polypeptide N-acteylgalactosaminotransferase 10
GAPDH	Glyceraldehyde 3-phosphate dehydrogenase
GFP	Green fluorescent protein
GRP94	Glucose-regulated protein of 94 kDa
HAC1	Homologous to ATF/CREB1
HAC1	Homologous to Atf/Creb1
HEDJ	DnaJ (HSP40) homolog, subfamily B, member 11
HEK293	Human embryonic kidney 293
HERP	Homocysteine-responsive endoplasmic reticulum stress-inducible ubiquitin-like domain member 1 protein
HGSNAT	Heparin alpha-glucosamine N-acetyltransferase
HRD1	HMG-CoA reductase degradation 1 homolog
HSP72	Heat shock protein 72
IRE1(α)	Inositol requiring 1 (alpha)
JNK	C-Jun N-terminal kinase
LC3	Microtubule associated protein 1 light chain 3
MAP7d1	Microtubule-associated protein 7 domain containing 1
MAPK	Mitogen activated protein kinase
MAPKKK	Mitogen activated protein kinase kinase kinase
MEF	Mouse embryonic fibroblast
mTOR	Mammalian target of rapamycin
mTORC1	Mammalian target of rapamycin complex 1
MTT	3-(4,5-Dimethylthiazol-2-yl)-2,5-diphenyltetrazolium bromide
NFκB	Nuclear factor kappaB
ORF	Open reading frame
p58IPK	Protein kinase inhibitor p58
PARP-1	Poly [ADP-ribose] polymerase 1
PBG	PBS and fish gelatine
PBS	Phosphate buffered saline
PCR	Polymerase chain reaction
PDGFRB	Platelet-derived growth factor receptor β
PDI	Protein disulphide isomerase
PERK	Protein kinase RNA (PKR)-like endoplasmic reticulum kinase
PFA	Paraformaldehyde
PMP22	Peripheral myelin protein 22

PP1	Protein phosphatase 1
PVDF	Polyvinylidene difluoride
RAMP4	Ribosome-attached membrane protein
RFP	Red fluorescent protein
RI332	Ribophorin encoding nonsense mutation at codon 332
RIDD	Regulated Ire1-dependent decay
RNase	Endoribonuclease
rpm	Revolutions per minute
SCARA3	Scavenger receptor class A, member 3
SERCA	Sarco-/endo-plasmic reticulum Ca^{2+}-ATPase
SRP20	Serine/arginine-rich splicing factor 3
TcRα	T-cell receptor alpha
TRAF2	Tumour necrosis factor receptor stress-induced apoptosis factor 2
TRB3	Tribbles homolog 3
TRIM16	Tripartite motif containing 16
UPR	Unfolded protein response
VCP/p97	Valosin-containing protein (97 kDa)
WT	Wild type
XBP-1	X-box binding protein 1

Chapter 1

Introduction

1.1: ER stress and the Unfolded Protein Response

A defining feature of eukaryotic cells is the presence of a cell membrane and different membrane-bound organelles. One of these organelles is the endoplasmic reticulum (ER). The ER is a large, membranous organelle which serves as a store for calcium ions (Ca^{2+}) and acts as a signalling platform. It is also responsible for synthesizing lipids and folding and modifying secretory and transmembrane proteins. If these proteins cannot be folded properly, maybe due to a mutation in their encoding gene, or a redox imbalance in the ER lumen, the ER becomes stressed and a response is elicited. This response is called the Unfolded Protein Response (UPR), which is activated to alleviate ER stress (Hussain and Ramaiah, 2007). This pathway has three principal outputs which are associated with trying to restore ER homeostasis: increased chaperone expression, translational attenuation, and upregulation of ER-associated degradation (ERAD) components and activity (reviewed in Lai *et al*, 2006).

When unfolded or misfolded proteins accumulate in the ER lumen, they bind the ER-resident chaperone, GRP78 (also known as BIP). As a result, BIP is titrated away from the three ER stress sensors: IRE1α, PERK and ATF6. IRE1α and PERK are also believed to interact directly with unfolded proteins (Gardner and Walter, 2001; Korennykh and Walter, 2012) and oligomerisation and activation of these two signal transducers follows (Bertolotti *et al*., 2000). Upon activation, the RNase activity of IRE1α induces non-conventional splicing of an mRNA encoding a bZIP transcription factor (*XBP-1*) which in turn upregulates transcription of genes that help to relieve the unfolded protein load of the ER. PERK on the other hand, phosphorylates eIF2α to attenuate protein translation. This is thought to provide the ER with more time to clear the unfolded proteins before processing new polypeptides. Finally, ATF6 is translocated to the Golgi apparatus, where it undergoes cleavage. The cleaved product, known as ATF6(f), can then travel to the nucleus, where it changes gene expression alongside spliced XBP-1 (reviewed in Ron and Walter, 2007).

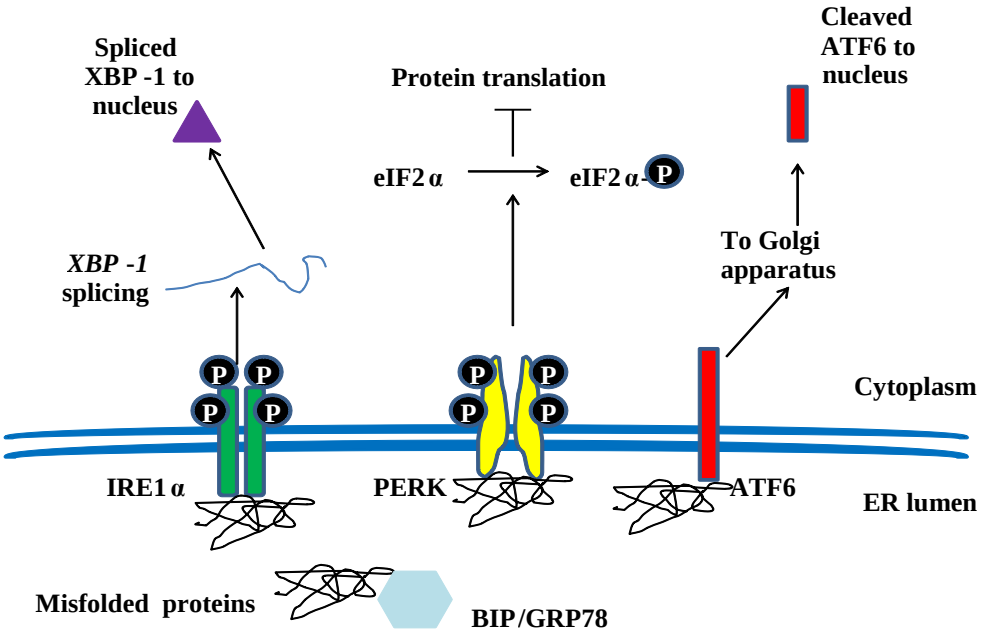

Figure 1.1: Early signalling events of the unfolded protein response.

UPR signalling can be studied relatively easily as ER-stress can be artificially induced using several different drugs. One of these drugs is tunicamycin, which activates the UPR as it blocks *N*-linked glycosylation of polypeptides in the ER (Takatsuki *et al*., 1975) which are then unable to fold correctly. Thapsigargin is also regularly used, as it is a SERCA-pump inhibitor (Lytton *et al*., 1991) and thus protein folding cannot happen normally due to loss of ER calcium homoeostasis. DTT and subtilase AB_5 are two alternative ER-stress inducing drugs which cause accumulation of unfolded proteins by inhibiting disulpide bond formation (Karlin and Bartels, 1966) and BIP inactivation (Paton *et al*., 2006), respectively. Whether or not a cell recovers from ER stress is dependent on many factors, and is the subject of research carried out worldwide. It is generally believed that persistent activation of the UPR will eventually lead to cell death, which plays a role in the pathogenesis of different human diseases (Kim *et al*., 2008). My project will focus on the signalling downstream of IRE1α, and how this influences cell fate decisions.

1.2: Activation of IRE1α

IRE1 is an ER-resident transmembrane protein which harbours both endoribonuclease (RNase) and kinase domains (Tabas and Ron, 2011). Early experiments showed that during ER stress, yeast Ire1p was necessary for transcription of *BIP* and *PDI* (Cox *et al*., 1993). Overexpression of either BIP, or PDI, which catalyses formation and isomerisation of disulphide bonds within proteins (Formenko and Gladyshev, 2003), was able to reduce UPR

signalling (Morris *et al*., 1997; Xu *et al*., 2005) suggesting ER homeostasis was being restored. Therefore, both proteins are thought to help alleviate ER stress, highlighting the protective role of IRE1.

At this point, the mechanism of IRE1 activation and how it subsequently upregulated these chaperones was unknown. Later discoveries elucidated that this transmembrane protein became activated during ER stress by a process of homo-oligomerisation and *trans*-autophosphorylation, with the latter process being fulfilled by the kinase activity of Ire1p itself (Shamu and Walter, 1996). In this study two Ire1p mutants were used: a C-terminally truncated form ('tailless') which still possessed the kinase domain, and the K702R mutant. The latter mutant had previously been shown to possess massively reduced kinase activity, whereas its close relative, K702A displayed no detectable kinase activity. The reason is presumed to be because mutation of this residue interferes with phosphotransfer ability (Mori *et al*., 1993). During ER stress, expression of 'tailless' Ire1p was able to increase the transcriptional response of the Ire1p-K702R mutant from 25% to 80% compared to WT Ire1p. If the K702R mutation was introduced into the truncated mutant, the observed 'rescue' no longer occurred. Furthermore, the K702R mutant was found to be phosphorylated on specific serine residues when expressed with the truncated form of Ire1p. It was shown that the K702R mutant was unable to undergo phosphorylation unless expressed simultaneously with a kinase-active form of Ire1p. These data along with the finding that truncated Ire1p could complex with the full length form of this protein, lead to the conclusion that kinase activity of Ire1p was required for oligomerisation of this protein. In turn, *trans*-autophosphorylation of the subunits involved in the oligomer would result in downstream signalling. It was thus concluded that only after oligomerisation Ire1p is fully active for signalling (Shamu and Walter, 1996). The different aspects of how IRE1 functions in the UPR are discussed below.

1.3: Structure and function of IRE1

IRE1 is a type I transmembrane protein. Its *N*-terminus is located within the ER lumen and in yeast this was shown to interact with the ATPase domain of BIP (Todd-Corlett *et al*., 2007). The kinase and RNase domains of IRE1 are located in the cytosolic *C*-terminus (reviewed in Schröder and Kaufman, 2005). There are several conserved amino acids in the kinase catalytic core of this protein, which if mutated are known to abolish kinase and/or RNase activities of this protein (Chawla *et al*., 2011; Lee *et al*., 2008; Mori *et al*., 1993; Tirasophon *et al*., 1998). The general consensus is that RNase activity, which is responsible for *XBP-1* splicing, is stimulated by autophosphorylation of the activation loop, which is located in the protein kinase domain (Lee *et al*., 2008 and Figure 1.2). However, the ATP-

competitive inhibitor, 1NM-PP1 has been demonstrated to activate the IRE1α RNase in mutants lacking phosphotransfer capacity (Papa *et al*., 2003). Hence, it would seem that kinase activity is actually unnecessary for activation of IRE1 by 1NM-PP1.

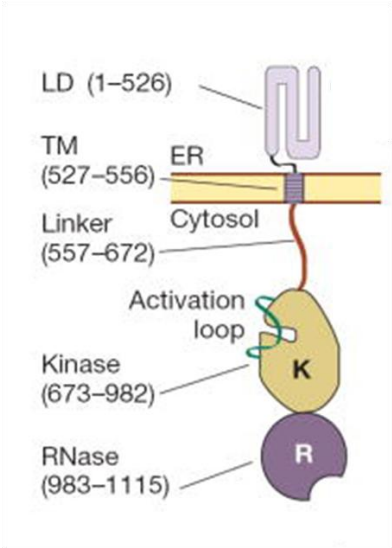

Figure 1.2: Schematic showing the different domains of IRE1α. LD is the lumenal domain and TM is the transmembrane domain (figure from Korennykh* et al.*, 2009).

The two IRE1 residues of importance to this project are K599 and D711. The catalytic lysine at position 599 is required to enable the γ-phosphoryl transfer reaction (Hodgson and Schröder, 2011). Additionally, it is thought to be required for formation of a salt bridge with the E612 residue, which in turn would play a role in the active conformation of the kinase (Korennykh *et al*., 2011). It has been established that the point mutation formed by substituting this basic lysine residue to a non-polar alanine residue (K599A-hIRE1α) results in a form of IRE1α which lacks both RNase and kinase activity. It is hence unable to splice *XBP-1* or undergo autophosphorylation (Tirasophon *et al*., 1998).

K599A-hIRE1α was used alongside the D711A-hIRE1α mutant in this project. This residue is the conserved aspartate residue in all protein kinases, which is required for coordinating the (two) Mg^{2+} ions in the kinase catalytic core (Mori *et al*., 1993). This allows the triphosphate group of ATP to be appropriately placed in the nucleotide binding pocket. Therefore, mutating this aspartate to an alanine may inhibit phosphorylation due to misplacement of the triphosphate group. As can be seen in the appendix (figure A1.1), this mutant has preserved *XBP-1* splicing capacity. Thus, the D711A-hIRE1α mutant has retained its RNase activity despite lacking kinase activity. By comparing these two mutants to the WT-hIRE1α, it can be elucidated whether or not the kinase domain is required for controlling certain aspects of cell survival downstream of the UPR being activated.

1.3.1: IRE1α endoribonuclease activity is responsible for *XBP-1* splicing

Results which were consistent with those regarding the expression of chaperone proteins during ER-stress (Cox *et al*., 1993) highlighted a correlation in yeast between activated Ire1p and UPR induction by a spliced bZIP transcription factor, Hac1p (Cox and Walter, 1996). Using Northern blotting, the Walter group showed that a 252 nucleotide intron had been removed from *HAC1* mRNA. The splicing out of this intron essentially generates a form of *HAC1* where the N-terminal DNA-binding domain is now adjacent to a C-terminal 'activation domain'. This event allows the translational block to be lifted, thus generating the active transcription factor, Hac1p (Mori *et al*., 2000). A similar system operates in mammalian cells, where IRE1α is able to splice the *HAC1* mRNA equivalent, *XBP-1*. Translated XBP-1(s) is a more active transcription factor compared to XBP-1(u) and therefore it can proceed to effectively amplify basal chaperone expression levels generated by cleaved ATF6 (Yoshida *et al*., 2001). It is important to note however, that spliced XBP-1 acts later compared to ATF6, and thus the target genes of these two transcription factors were not expected to overlap directly. This was indeed the case, and spliced XBP-1 was found to be required for upregulation of certain ERAD pathway components (Yoshida *et al*., 2003). Although ATF6 has recently been proposed to play a role in transcription of *some* ERAD related genes (Shoulders *et al*., 2013), principal transcriptional control of these genes by XBP-1(s) highlights the anti-apoptotic nature of this route, as a more effective ERAD would presumably reduce the misfolded protein load in the ER lumen.

1.3.2: The role of the IRE1α-XBP-1 branch in cell fate

One would assume that loss of XBP-1 splicing would result in events that would make cell death more favourable, due to the fact there would be less transcriptional control over genes encoding chaperones and ERAD components. Loss of *xbp-1* from embryonic liver cells correlated with the elevated levels of apoptosis observed in this model (Reimold *et al*., 2000). By default, one would expect that knockout of IRE1α should also help favour apoptosis. Cell death does indeed occur in yeast, as growth assays display inhibition of survival in *ire1*Δ strains (Back *et al*., 2005).

However, the mammalian pathway is much less simple. The Papa group used the I642G-IRE1α mutant to investigate ER stress related cell fate decisions (Han *et al*., 2009). This mutant has an enlarged kinase active site pocket which is predicted to be accessible to the ATP-competitive drug, 1NM-PP1. Use of this drug supports *XBP-1* splicing associated with active IRE1α whilst abolishing kinase-mediated phosphorylation (Papa *et* al., 2003). Using annexin V staining as a readout for cell death, it was demonstrated that *ire1α*$^{-/-}$ fibroblasts

showed much better survival after ER stress induction, compared to their WT counterparts. Although this initially seems to oppose the results obtained from the yeast system, this group was able to show that the activated I642G-IRE1α was able to *further* reduce the amount of cell death detected in the *ire1α*$^{-/-}$ cells (Han *et al*., 2009). These results support the role of XBP-1(s) in cell survival.

It was later demonstrated that the *ire1α*$^{-/-}$ fibroblasts were protected from ER-stress related cell death as caspase-2 upregulation and subsequent cleavage were unable to occur. Increased expression, but not cleavage of caspase-2 was observed in the 1NM-PP1-activated I642G-IRE1α cells. Only the WT-IRE1α cells showed caspase-2 cleavage. Thus, it was concluded that the presence of XBP-1(s) is separable from the ER stress-induced cell death pathway (Upton *et al*., 2012).

Many groups have exploited XBP-1(s) to promote cell survival. By using an expression vector encoding the spliced XBP-1 form, it was demonstrated that the presence of this transcription factor caused a decrease in CHOP expression (Guo *et al*., 2012). CHOP, also known as GADD153, is understood to contribute to ER stress-related cell death (Marciniak *et al*., 2004) and thus downregulation of this protein protects cells from death. This is consistent with data published by Sado *et al* (2009) who noted that CHOP expression increased when inducing a Parkinson's disease-like phenotype. They then successfully used adenoviral XBP-1 expression to rescue the neuronal cells from death. A separate group also demonstrated inhibition of cell death by sustained *XBP-1* splicing. Interestingly, this was achieved by overexpression of the chaperone, Hsp72 (Gupta *et al*., 2010). In general, it seems this particular IRE1-associated route offers protection against apoptosis.

1.3.3: IRE1α kinase activity leads to JNK activation

Over a decade ago, the Ron group highlighted the association between IRE1α kinase activity and IRE1α-TRAF2 interaction. Using TRAF2 dominant negative mutants, they then went on to show that the formation of active phospho-JNK required WT TRAF2 (Urano *et al*., 2000). This evidence was reinforced by coimmunoprecipitation experiments which placed JNK activation downstream of IRE1α-TRAF2 complex formation (Nishitoh *et al*., 2002). It was elucidated that the specific MAP kinase cascade which leads to JNK activation uses the MAPKKK, ASK1. It is believed that IRE1α-TRAF2-ASK1 association into a heterotrimeric complex is dependent on ER-stress activation. Formation of this complex leads to JNK activation, which in turn can contribute to cell death (Nishitoh *et al*., 2002). This idea is supported by the fact that ASK1-interacting protein 1 (AIP1), which also binds directly to IRE1α, is required for cell death signalling via the JNK pathway (Luo *et al*., 2007).

1.3.4: The TRAF2-JNK arm encourages cell death

It was demonstrated that the kinase-dead I642G-IRE1α mutant displays improved survival (Lin *et al*., 2007). As described above, this mutant has lost phosphotransfer potential but when bound to 1NM-PP1 has an active RNase (Han *et al*., 2008). This is suggestive of segregation between RNase and kinase functions and their roles in promoting life and death, respectively. This section discusses the process of cell death, followed by the relationship between this and JNK activation.

The balance between cell life and death is dictated by the balance of Bcl-2 family members (Figure 1.3). Antiapoptotic members of this family are able to sequester proapoptotic ones, thus offering protection to the cell (Bassik *et al*., 2004). Conversely, proapoptotic proteins belonging to this family are able to initiate a caspase cascade, which culminate in cell death.

The Bcl-2 proteins are thought to link the UPR to cell death. 13 years ago, it was found that the two key proapoptotic members, BAX and BAK, which are located in the mitochondrial membrane, potentiate ER stress signals (Wei *et al*, 2001). Both BAX and BAK are thought to oligomerise to create a pore in the mitochondrial membrane. This disrupts the normal calcium flux of this organelle, encouraging cell death (Eskes *et al*., 2000; Wei *et al*., 2000). However, calcium mobilisation associated with apoptosis is not only a feature of the mitochondria. BAX-deficient cell lines also show reduced calcium loss from the ER, associated with increased cell survival (Nutt *et al*., 2002). In a set of experiments where *bax* and *bak* double knockouts were reconstituted with a form of BAK targeted to the ER membrane, it was found that this Bcl-2 protein also controlled ER membrane potential (Zong *et al*., 2003).

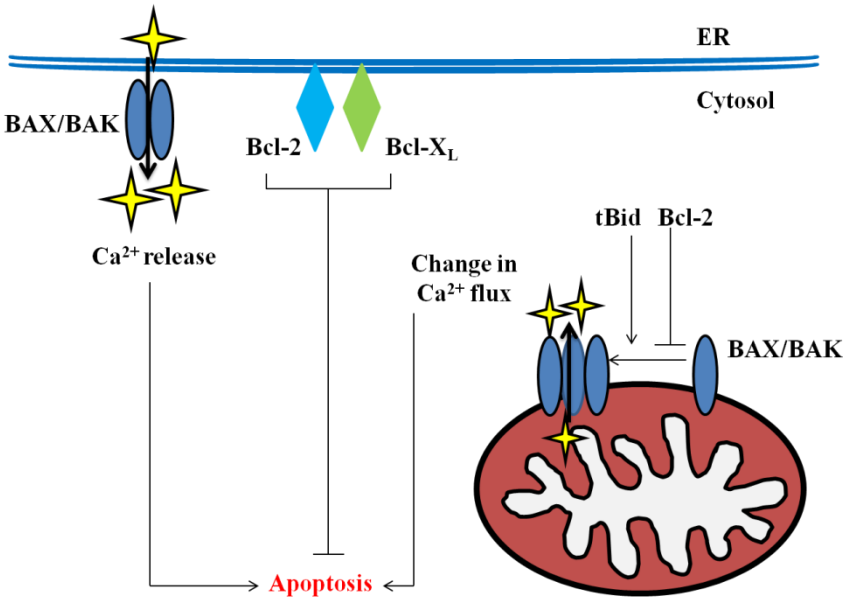

Figure 1.3: The role of Bcl-2 protein family members in influencing cell fate. As stated in the text above, BAX and BAK are able to form a pore in the ER or mitochondrial membranes where they can alter calcium ion flux. At the ER membrane, calcium ion release is thought to be inhibited by the two anti-apoptotic proteins, Bcl-2 and Bcl-X_L (Nutt* **et al.**, *2002; Wang* **et al.**,*2011). Bcl-2 impairs BAX/BAK pore formation at the mitochondrial membrane (Dlugosz* **et al.**, *2006). Conversely, tBid supports pore formation (Wei* **et al.**, *2000).

Where proapoptotic Bcl-2 proteins become active, cell death ensues via caspase activation. It was demonstrated that ER-localised procaspase-12 was only cleaved and activated as a result of ER stress, when BAX and BAK were present (Zong *et al*., 2003). Despite the mechanism of caspase-12 activation being unclear, it has been suggested that BAX and BAK enhance IRE1α signalling via direct interaction (Hetz *et al*., 2006). This, in turn, may allow more effective recruitment of TRAF-2, which itself has been implicated in cleavage and subsequent activation of procaspase-12 (Yoneda *et al*., 2001). Alternatively, caspase-12 has been proposed to be cleaved by calpains, which in turn are activated by release of calcium ions from the stressed ER (Tan *et al*., 2006). Whichever mechanism propagates cleavage of this caspase during ER stress, a caspase cascade is initiated and ends with the activation of the executioner caspase, caspase-3 (Morishama *et al*., 2004 and Figure 1.4).

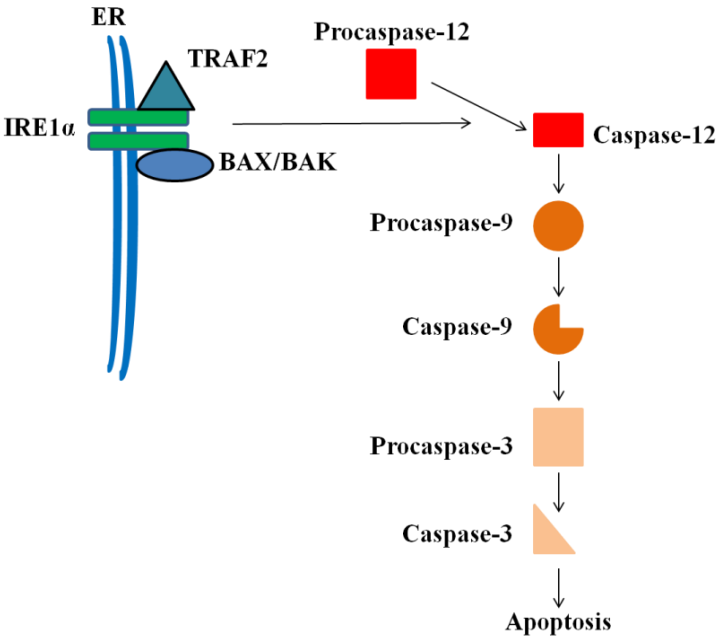

Figure 1.4: Caspase cascade triggered during ER stress-mediated cell death. The exact input of TRAF2/BAX/BAK complex with IRE1α is unknown.

So what makes JNK proapoptotic? *In vitro* kinase assays used in two different publications show that JNK is able to phosphorylate and activate proapoptotic BimL and BimEL isoforms (Lei and Davis, 2002; Putcha *et al*., 2003). The phosphorylation of BimL attenuates its sequestration by dynein light chain 1. This 'free form' of BimL is able to induce apoptosis, as shown by annexin-V staining (Lei and Davis, 2002). This cell death was found to be mediated by mitochondrial BAX, as only reconstitution of this protein into BAX knockout cells enabled cell death after Bim phosphorylation (Putcha *et al*., 2003).

JNK also phosphorylates Bcl-2, which effectively silences its antiapoptotic function (Yamamoto *et al*., 1999). Thus, amongst its interaction with other proteins, Bcl-2 can no longer inhibit the oligomerisation of BAX in the mitochondrial membrane – a process thought to potentiate cell death (Mikhailov *et al*., 2001). This data was exploited by Bassik *et al*., in 2004, who utilised a non-phosphorylatable form of Bcl-2 to enforce its cytoprotective effects.

However, it was later established that JNK also phosphorylates BAD, which subsequently releases Bcl-X_L (Yu *et* al., 2005). This in turn may oppose proapoptotic BAX activity. These findings mean there is some debate about the contribution of JNK activation to ER stress-induced cell death. To help resolve this debate, it should first be experimentally determined that it is specifically the IRE1α kinase activity that causes these changes downstream of ER stress, since many factors are known to activate JNK.

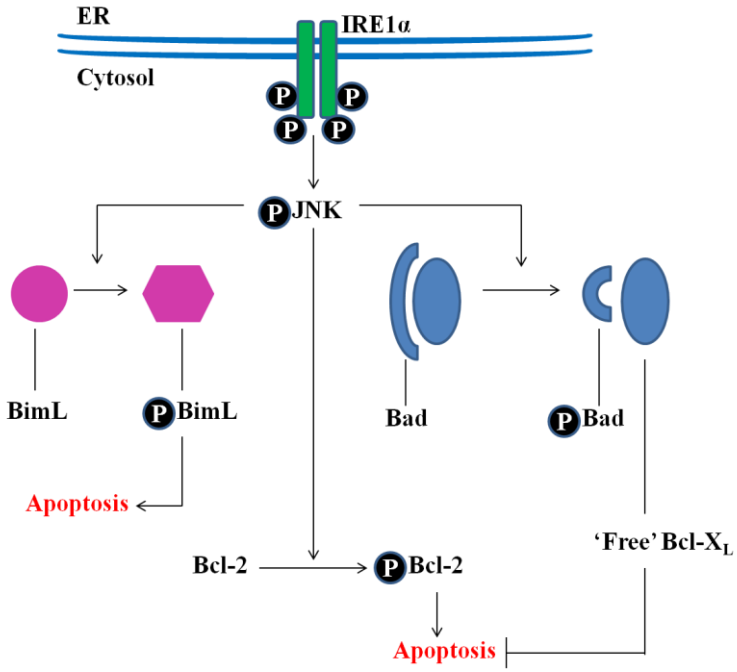

Figure 1.5: Summary of the role of phospho-JNK in apoptosis via Bcl-2 protein family members.

1.3.5: IRE1α kinase: a role in cell survival?

A different theory focussing on the IRE1 kinase activity and cell fate has recently been proposed in yeast. It was shown that an active kinase within Ire1p was required to complete the cellular recovery 'circuit' after ER-stress had been resolved, and may thus play a beneficial role (Rubio *et al*., 2011). The Walter group found that phosphotransfer incompetent Ire1p mutants were unable to recover from ER stress due to the fact that the RNase function was not 'switched off'. This complies with the theory proposed by Chawla *et al* in 2011, who suggest yeast cell death was more likely if the Ire1p RNase was not properly deactivated by a fully functional kinase domain.

1.3.6: Other functions of IRE1α endoribonuclease which influence cell survival: the RIDD pathway and beyond

Suspicions about the specificity of the RNase function of IRE1α were raised when it was discovered that *hIRE1α* was able to cleave its own mRNA transcript *in vivo* (Tirasophon *et al*., 2000). This fact was exploited by Hollien and Weissman in 2006, who, by microarray analysis, found a particular collection of genes were downregulated during ER stress. The possibility that this was due to blocking transcription was eliminated by experiments using actinomycin D – a drug which inhibits RNA synthesis (Reich *et al*., 1961). The downregulation was instead found to be a result of mRNA cleavage by the endoribonuclease of IRE1α (Hollien and Weissman, 2006).

This degradation route was later referred to as the RIDD (regulated IRE1-dependent decay) function of IRE1α (Hollien *et al*., 2009). For the Weissman group the 1NM-PP1-activated I642G-IRE1α mutant (described in section 1.3.2) served as a tool enabling them to distinguish between different endonucleolytic activities of IRE1α. They observed that RIDD only occurred under conditions of ER stress. However, in the absence of ER stress, this mutant was still able to produce spliced XBP-1, suggesting that RIDD and 'classical splicing' are different despite both requiring the endoribonuclease function of IRE1α. This group concluded that since the majority of the mRNA transcripts targeted by RIDD normally passed through the ER for modification, RIDD activity may contribute to reducing protein load in the stressed ER, thus promoting survival (Hollien *et al*., 2009).

A separate group's findings also support the fact that *XBP-1* splicing and mRNA degradation are separable. However they found that IRE1 must maintain its phosphotransfer capacity to activate RIDD, and therefore the I624G mutant would be insufficient. Furthermore, their data argues that this type of mRNA degradation correlates positively with ER stress-mediated apoptosis (Han *et al*., 2009). Further studies on the RIDD pathway need to be carried out in an attempt to reconcile the two models.

Finally, recent work involved in IRE1α RNase-mediated cleavage of microRNAs seems to be gaining importance in terms of how this transmembrane protein influences cell death. One group reported that cleavage of one particular micro-RNA (miR-17) permitted the accumulation of TXNIP, which in turn was then able to engage with inflammatory machinery thus paving the way for cell death (Lerner *et al*, 2012). At the time, it was not known whether this was IRE1α specific cleavage, although a later study from the same laboratory discovered that IRE1α mediated cleavage of miR-17, amongst others, gave rise to an increase in the proapoptotic caspase-2 protein (Upton *et al*., 2012). These data point towards a multifactorial function of the endoribonuclease activity of IRE1α that may help and/or hinder cell life depending on several variables.

1.4: The interaction between IRE1α and ERAD

ER-associated degradation (ERAD) is a proteasomal degradation route used to eliminate proteins that are unable to undergo appropriate folding in the ER lumen. Mammalian cells normally have around 30,000 proteasomes, with the 26 S proteasome representing the best characterised of all the different types (Lodish *et al*., 2008). Recognition of proteasomal substrates precedes their retrotranslocation/dislocation out of the ER, probably via the Sec61 pore (Nakatsukasa and Brodsky, 2009). Proteins can subsequently be targeted for

degradation by a process known as ubiquitination. Ubiquitin is activated courtesy of an E1 enzyme. In this ATP-dependent reaction, ubiquitin is linked to a cysteine residue of the E1. The ubiquitin can then be transferred to an E2 ubiquitin-conjugating enzyme. In the final step, the E3 ubiquitin ligase binds both the target protein to be degraded and the E2. Addition of the ubiquitin 'tag' to the misfolded protein can then be conducted by the specific E3 ligase (Hershko and Ciechanover, 1998). Normally, several molecules of ubiquitin are added to the substrate forming a polyubiquitin chain. Once this process has been carried out, the protein is translocated to the proteasome where it is degraded by resident proteases (Lodish *et al*., 2008).

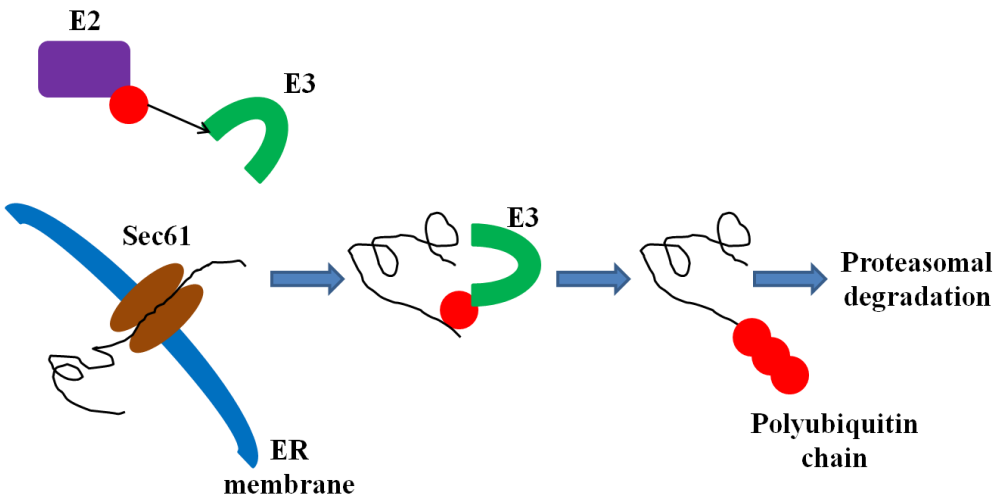

Figure 1.6: Schematic highlighting the process of ERAD: the misfolded protein is targeted to the proteasome after addition of a K48 polyubiquitin chain.

It was crucially established that there was an important interplay between the UPR and ER-associated degradation (ERAD) where the two processes could compensate for one another (Travers *et al*., 2000). This fundamental study was used to demonstrate that the Ire1p-Hac1p pathway in yeast was required for effective proteasomal degradation of misfolded proteins via ERAD. It is known that in mammalian cells components of ERAD are upregulated upon UPR activation by XBP-1(s) and ATF6(f) transcription factors (Shoulders *et al.*, 2013).

HRD1 has been recognised as a key E3 ubiquitin ligase upregulated by the UPR to facilitate ERAD (Travers *et al*., 2000 and Shoulders *et al*., 2013). The precise role of HRD1 is intriguing as it was suggested there was a correlation between the presence of this protein and the disappearance of IRE1, leading one group to believe HRD1 (also known as synoviolin) was promoting proteasomal degradation of IRE1 (Gao *et al*., 2008).

ER-localised EDEM is believed to play an important role in ERAD, as it facilitates the degradation of glycoproteins. It was demonstrated that the IRE1α-XBP-1 branch of the UPR was solely responsible for transcriptionally upregulating this gene (Yoshida *et* al, 2003). This group also observed a correlation between a less responsive ERAD pathway and the absence of the XBP-1(s) transcription factor, further highlighting the relationship between the UPR and ERAD.

Finally, HERP, whose function has not been fully characterised (reviewed in Bernasconi *et al*., 2013) has an N-terminal ubiquitin-like domain that has been proposed to function in the dislocation of polyubiquitinated proteins from the ER (Ma and Hendershot, 2004). What is known is that, unlike EDEM, it requires both ATF6 and XBP-1 pathways to converge to produce the maximal transcriptional output (Ma and Hendershot, 2004).

These three genes represent a subset of ERAD components which require IRE1α endoribonuclease to generate XBP-1(s) to drive their full expression. The capability of ERAD to degrade unfolded proteins from within the ER lumen presumably renders it 'protective' in terms of the UPR. Indeed, it is well known that inhibition of the proteasome by MG132 increases ER stress-induced cell death (Lee *et al*., 2003; Amanso *et al*., 2011; Williams *et al*., 2013). However, it has been difficult to identify exactly which ERAD components are essential for mammalian cell survival. A likely reason for this is probably due to functional redundancy within the system. For example, it is now believed that there are over 20 ER-localised E3 ligases which may target substrates for degradation from the ER (Neutzner *et al*., 2011).

1.5: The relationship between IRE1α and autophagy

Apart from ERAD, autophagy is the other cellular degradation route and it has been implicated in both cell survival and death (Kundu and Thompson, 2008). It involves the delivery of polypeptides and entire organelles to the lysosome, where they can subsequently be broken down (Lodish *et al*., 2008). The process of autophagy involves the formation of a membrane which is able to form the autophagosome. This in turn fuses to the lysosome forming the mature lysosome, or autolysosome, which contains an acidic lumen harbouring several digestive hydrolases (Aredia *et* al., 2012). There are three types of autophagy: macroautophagy, microautophagy and chaperone-mediated autophagy, each of which is considered to be part of the protein quality control system within eukaryotic cells. Several links between autophagy and the UPR have been postulated.

Autophagy begins with an event known as nucleation, where the phagophore is formed. It is thought that the ER is able to provide membrane to help generate this structure (Tooze and Yoshimori, 2010). In the presence of the ATG16 homodimer, the ATG5-ATG12 complex is believed to control extension of this structure (Mizushima *et al*., 2003). This complex is also thought to target and encourage conversion of LC3-I to LC3-II by addition of phosphatidylethanolamine in the growing phagophore membrane (Mizushima *et al*., 2001; Fujita *et al*., 2008) This, in turn, further aids the elongation and completion of the phagophore (Xie *et al.*, 2008) which encompasses cargoes such as protein aggregates. Upon completion of the phagophore, the double-membranes vesicle, known as the autophagosome is formed.

Early studies in 2006 indicated that the kinase activity of IRE1α was required to promote autophagosome formation, via an undefined TRAF2-JNK signalling cascade. This also correlated with an increase in cell survival (Ogata *et al*, 2006). To determine this, a truncated IRE1α mutant lacking the RNase domain was compared to the K599A-hIRE1α mutant, which lacks both RNase and kinase activities. Only the K599A-hIRE1α mutant displayed a decrease in autophagic activity. JNK inhibition and introduction of a dominant negative form of TRAF2 displayed similar effects. Using the knowledge that Bcl-2 is a JNK phosphorylation substrate (Bassik *et al*., 2004) and that the uncoupling of Bcl-2 from Beclin-1 could be required for activation of autophagy (Pattingre *et al.*, 2005), the mechanism for how JNK promotes autophagy has been elucidated (Wei *et al.*, 2008). Using both *jnk1*$^{-/-}$ and *jnk2*$^{-/-}$ MEFs, it was demonstrated that JNK1 was required to mediate the phosphorylation and subsequent release of Bcl-2 from Beclin-1 under conditions of stress. This free Beclin-1 was then able to bring about the autophagic response (Wei *et al.*, 2008). These data all infer that kinase function is beneficial to the cell via the autophagic route.

Despite the above evidence, a separate group demonstrated that a functional kinase domain actually impaired autophagy, and consequentially led to the accumulation of mutant huntingtin (Lee *et al*., 2011). For these experiments, autophagy was measured using a doubly fluorescent form of LC3, alongside accumulation of p62. These studies may comply with a model concerning mTORC1. This complex inhibits autophagy and was shown to stabilise the IRE1α-TRAF2-JNK arm (Kato *et al*., 2012).

Controversy over the regulation of autophagy by the IRE1α-XBP-1 arm also exists. Whilst overexpressing the spliced form of this transcription factor did not alleviate accumulation of mutant huntingtin in SH-SY5Y cells (Lee *et al*., 2011), the conversion of unspliced *XBP-1* (*XBP-1*(u)) to spliced *XBP-1* (*XBP-1*(s)) correlated with the clearance of misfolded rhodopsin in photoreceptor cells (Chiang *et al*., 2011). On the other hand, knockdown of *XBP-1* using short hairpin RNA showed an increase in autophagy and cell survival in a familial ALS motor neuron-like model (Hetz *et al*., 2009).

The role of each of the IRE1α arms in controlling degradation processes is likely to be complex and dependent on a number of variables, such as severity of stress and cell type. It is likely that both autophagy and ERAD play an important role in the UPR, and that these two processes are not mutually exclusive. For example, although a damaged proteasome would undoubtedly compromise the cells' ability to recover from the stress of unfolded proteins, it has been shown that lysosomal degradation is able to share some of the burden when ERAD is blocked chemically (Chiang *et al*., 2011).

1.6: How does IRE1α affect the physiology of the ER?

The ER is a very plastic compartment and forms a complex network of interconnected tubules and sheets. Interest regarding the morphology and biogenesis of the ER has recently been building and could help provide an alternative and complementary mechanism for the UPR to restore homeostasis to this organelle. Using fibroblasts, Sriburi *et al.*, (2004) demonstrated that retroviral expression of the spliced form of XBP-1 induced an increase in the levels of phosphatidylcholine and phosphatidylethanolamine. These two lipids are located within the membranes of intracellular structures (Lykidis and Jackowski., 2001). This correlated with the observed increase in size and volume of the ER seen in electron micrographs. They proceeded to analyse aspects of the Kennedy pathway, which is responsible for producing a large proportion of cellular phosphatidylcholine. It was discovered that the activities of both the rate-limiting enzyme and the enzymes involved in the final stage of the pathway were both higher in cells expressing spliced XBP-1 compared to cells transfected with an empty control vector (Sriburi *et al*., 2004).

The same group later elucidated that increased translation of the α isoform of the rate-limiting choline cytidylyltransferase (CCT) downstream of XBP-1(s) expression was, at least, partially responsible for the synthesis of 'excess' ER membrane lipids (Sriburi *et al*., 2007). The dependence of ER proliferation and expansion on the spliced transcription factor downstream of IRE1α RNase activity was also discovered in yeast (Schuck *et al*., 2009). By blocking the splicing of *HAC1* mRNA, the ER became disorganised and 'tangled'.

The importance of the change in ER morphology during the UPR is highlighted in mammalian cells, as it was reported that there was a degree of redundancy between XBP-1(s) and ATF6α(f). Overexpression of an ATF6α fragment was able to increase ER volume independently of XBP-1(s), however, the stage of the Kennedy pathway affected was different compared to the changes induced by the latter mentioned transcription factor (Bommiasamy *et al*., 2009).

1.7: Final remarks

This introduction has highlighted the crucial role of IRE1α in cell fate decisions. ER stress-mediated cell death has gained recent importance as it is known to play a role in several diseases, including Parkinson's disease and diabetes (Kim *et* al., 2008; Scheuner and Kaufman, 2007). Restoring ER homeostasis whilst avoiding the apoptotic pathway is the key to finding therapeutic targets to help treat disease. First though, many remaining questions regarding UPR signalling must be answered. This project attempted to elucidate whether IRE1α kinase activity contributes to cell survival independent of its endoribonuclease function. Different techniques were used to try and answer how the kinase activity was achieving this, in order to further understand the complexity of this signalling pathway.

1.8: Hypotheses and objectives:

A former PhD student in the Schröder lab, Dr. Louise Sutcliffe, generated three Flp-In T-Rex MEF cell lines encoding, WT-*hIRE1α*, D711A-*hIRE1α* or K599A-*hIRE1α*, in an *ire1α*$^{-/-}$ background. It was demonstrated that there were increased PARP-1 cleavage levels in the mutants (figure A1.2) when tetracycline was added to induce expression of the different forms of *hIRE1α* (see section 2.3 and figure 2.1). MTT tests carried out over 48 h of tunicamycin treatment showed similar decreases in viability in both mutants compared to the WT-hIRE1α, which was more able to survive ER stress (figure A1.2). For the latter experiment 100 ng/ml of the ER-stressor, tunicamycin was used despite the fact that much higher concentrations of this drug have been used (Urano *et al.*, 2000; Nishitoh *et al.*, 2002). The low concentration of tunicamycin used in this project allows the protective function of the kinase activity to be uncovered as ER stress is less severe.

From these data, it was proposed that IRE1α kinase activity protects from cell death downstream of UPR activation. This kinase domain may control this by a number of mechanisms which include: upregulation of ERAD and/or autophagy, control of the RIDD pathway, and change in gene expression. The following aims were proposed to test these ideas:

1a) Comparison of levels of apoptotic cell death markers between WT-hIRE1α, D711A-hIRE1α, and K599A-hIRE1α cells to establish and confirm previous results suggesting kinase activity protects cells from ER stress. This will be done by Western blotting against PARP-1 and caspase-3 cleavage.

b) Since JNK activation is implicated in ER stress related cell death, characterisation of this protein by analysing total JNK and phospho-JNK forms from cell lysates will follow.

c) Characterisation of the status of eIF2α phosphorylation and CHOP activation downstream of PERK signalling will be analysed using Western blotting.

2) Quantitative RT-PCR will be carried out to obtain a partial transcript profile of the WT-hIRE1α and mutant cells. The genes being analysed can be separated into genes induced by the UPR, and genes whose mRNA is cleaved by the RIDD pathway (Hollien *et al*., 2009). This may help address which mRNAs are induced in the different cell lines as a result of the UPR being activated and whether or not RIDD functions in the D711A-hIRE1α cells.

3) Preparation and characterisation of plasmids encoding ATF6, mCherry-GFP-LC3b, and ERAD substrates. The first plasmid will allow the study of changes in ATF6 activity in the different cell lines. The mCherry-GFP-LC3b plasmid will enable the question regarding

whether autophagy is defective in the mutant cells to be answered. Finally, it will be able to be determined whether there are any changes in ERAD activity between the three cell lines, by using plasmids encoding ERAD substrates. For these experiments, [^{35}S]-methionine pulse chase experiments will be carried out following transient transfection.

4) It is possible that its kinase activity may play a role in the proliferation and/or organisation of the ER during the UPR. Transmission electron microscopy will be used to analyse untreated and treated cell lines, to estimate the average width of the ER. ER-tracker will also be used to obtain an estimate for the volume of the ER.

Chapter 2

Materials and Methods

2.1: List of antibiotics, reagents and chemicals

Name	Product Number	Company
25 % glutaraldehyde	R1012	Agar Scientific, Stansted, UK
5xFirst Strand Buffer	Y02321	Invitrogen, Paisley, UK
5xgreen GoTaq®Flexi Buffer	M891A	Promega, Southampton, UK
Acetic acid (HOAc)	A/0360/PB17	ThermoFisher, Loughborough, UK
Agar 100 Resin kit	R1031	Agar Scientific, Stansted, UK
Agarose (electrophoresis grade)	MB1200	Melford, Ipswich, UK
Ampicillin	A0104	Melford, Ipswich, UK
β-Mercaptoethanol	M-6250	Sigma-Aldrich, Gillingham, UK
Blasticidin S·HCl in HEPES buffer	B1105	Melford, Ipswich, UK
Bovine serum albumin	A2153-50G	Sigma-Aldrich, Gillingham, UK
Bromophenol blue	11439	Sigma-Aldrich, Gilliangham, UK
Complete mini protease inhibitors	11836 153 001	Roche, Welwyn Garden City, UK
DAPI	D9642	Sigma-Aldrich, Gillingham, UK
dATP	R0141	ThermoFisher, Loughborough, UK
dCTP	R0151	ThermoFisher, Loughborough, UK
DEPC	A0300574	Acros Organics, Loughborough, UK
D-Glc	G/0500/61	Fisher Scientific, Loughborough, UK
dGTP	R0161	ThermoFisher, Loughborough, UK
DMSO	D5879-100ML	Sigma-Aldrich, Gillingham, UK
DTT (0.1M for reverse transcription)	Y00147	Invitrogen, Paisley, UK
dTTP	R0171	ThermoFisher,

		Loughborough, UK
EDTA	D/0700/53	ThermoFisher, Loughborough, UK
ER-Tracker™ Red	E34250	Invitrogen, Paisley, UK
Ethanol	E/0650DF/25	ThermoFisher, Loughborough, UK
Ethidium bromide	E1510-10ML	Sigma-Aldrich, Gillingham, UK
Fish gelatin	G7765	Sigma-Aldrich, Gillingham, UK
Glycerol	G/0650/17	ThermoFisher, Loughborough, UK
Glycine	BP381-1	ThermoFisher, Loughborough, UK
Glycogen RNA-grade	R0551	ThermoFisher, Loughbourough, UK
Hygromycin B	40052	Calbiochem, Nottingham, UK
LB-Agar LENNOX	LBX0202	Formedium Ltd, Hunstanton, UK
LB-Broth LENNOX	LBX0102	Formedium Ltd, Hunstanton, UK
Lead nitrate	C008	EMScope, Ashford, UK
Methanol	M/4000/PC17	ThermoFisher, Loughborough, UK
$MgCl_2$ (25mM for PCR)	A351H	Promega, Southampton, UK
$Na_2EDTA{\cdot}2H_2O$	D/0700/53	ThermoFisher, Loughborough, UK
Oligo$(dT)_{15}$ (50 µM)	C1101	Promega, Southampton, UK
Paraformaldehyde	R1018	Agar Scientific, Stansted, UK
Pepstatin A	BIMI2205	Apollo scientific, Stockport, UK
PhosSTOP	04906837001	Roche, Welwyn Garden City, UK
Potassium hydroxide pellets	P/5600/53	ThermoFisher, Loughborough, UK
Propan-2-ol	P/7490/17	ThermoFisher,

		Loughborough, UK
RNasein® ribonuclease inhibitor	N221A	Invitrogen, Paisley, UK
Sodium cacodylate	R1102	Agar Scientific, Stansted, UK
Sodium chloride	S/3120/65	ThermoFisher, Loughborough, UK
Sodium citrate	10242	BDH, Poole, UK
Sodium deoxycholate	D6750	Sigma-Aldrich, Gillingham, UK
Sodium dodecyl sulphate	BPE116-500	ThermoFisher, Loughborough, UK
Sodium hydroxide	S/4920/53	ThermoFisher, Loughborough, UK
Tetracycline	87130	Sigma-Aldrich, Gillingham, UK
Trichloroacetic acid (TCA)	T4885-500G	Sigma-Aldrich, Gillingham, UK
Tris (hydroxymethyl) methylamine	T/3710/60	ThermoFisher, Loughborough, UK
Triton X-100	282103-5G	Sigma-Aldrich, Gillingham, UK
Tunicamycin	645380	Calbiochem
Tween 20	P1379-500ml	Sigma-Aldrich, Gillingham, UK
Uranyl acetate	102088	BHD, Poole, UK

2.2: List of cell culture chemicals

Note that all chemicals used for cell culture were sterile-filtered and only opened under sterile conditions in a microbiolgical safety cabinet which was cleaned with 70% (v/v) ethanol. If necessary, filter sterilisation was carried out using a 0.2 μm sterile filter and syringe.

Name	**Product Number**	**Company**
0.25% (w/v) Trypsin-EDTA Solution	T4049-100 ml	Sigma-Aldrich, Gillingham, UK

DMEM high glucose	D5671 (500 ml)	Sigma-Aldrich, Gillingham, UK
DMEM high glucose w/o L-glutamine w/ sodium pyruvate	LM-D1112/500	Biosera, Uckfield, UK
Dulbecco's phosphate buffered saline (PBS)	D857 (500 ml)	Sigma-Aldrich, Gillingham, UK
Fetal bovine serum	S1830	Biosera, Uckfield, UK
L-glutamine	G7513-100 ml	Sigma-Aldrich, Gillingham, UK
Penicillin-streptomycin, solution stabilised, sterile-filtered, suitable for cell culture	P4333-100 ml	Sigma-Aldrich, Gillingham, UK
Tetracycline-free fetal bovine serum	FB-1001/500	Biosera, Uckfield, UK
Trypan blue solution 0.4% (w/v)	T8154 (100 ml)	Sigma-Aldrich, Gillingham, UK

2.3: List and description of cell lines used in cell culture

Cell type	Genotype	Source
MEF	*ire1α*$^{-/-}$ MEF stable Flp-In T-Rex IRE1α/Tet transfected cells h*IRE1α*	Schröder Lab, Durham University, UK
MEF	*ire1α*$^{-/-}$ MEF stable Flp-In T-Rex IRE1α/Tet transfected cells h*IRE1α*-D711A	Schröder Lab, Durham University, UK
MEF	*ire1α*$^{-/-}$ MEF stable Flp-In T-Rex IRE1α/Tet transfected cells h*IRE1α*-K599A	Schröder Lab, Durham University, UK
HEK293		Cann Lab, Durham University, UK

The *ire1α*$^{-/-}$ MEFs were received from the Kaufman lab and generation of the three stable MEF cell lines listed above was carried out by Dr. Louise Sutcliffe. Initially, the pFRT/LacZeo plasmid was transfected into the cells, introducing the FRT site and the zeocin resistance gene. Once positive cells had been selected with zeocin, the cells were transfected with pcDNA6/TR. This plasmid encodes the gene for the tetracycline repressor (TR) and the blasticidin resistance gene. After selection with blasticidin, these cells were co-transfected with pcDNA5-FRT-TO-hIRE1α and pOG44. The former plasmid encodes the tetracycline operator (TO), *hIRE1α* and the hygromycin resistance gene, and the latter expresses Flp recombinase. This enzyme allows the exchange of the zeocin resistance gene with the open reading frame of the pcDNA5 plasmid. Again, cells were selected, this time with hygromycin. This procedure was carried out with pcDNA5-FRT-TO-hIRE1α, pcDNA5-FRT-TO-D711A-hIRE1α and pcDNA5-FRT-TO-D711A-hIRE1α. Thus, the Flp-In system allowed stable integration of the three forms of the *hIRE1α* gene into the MEF genome.

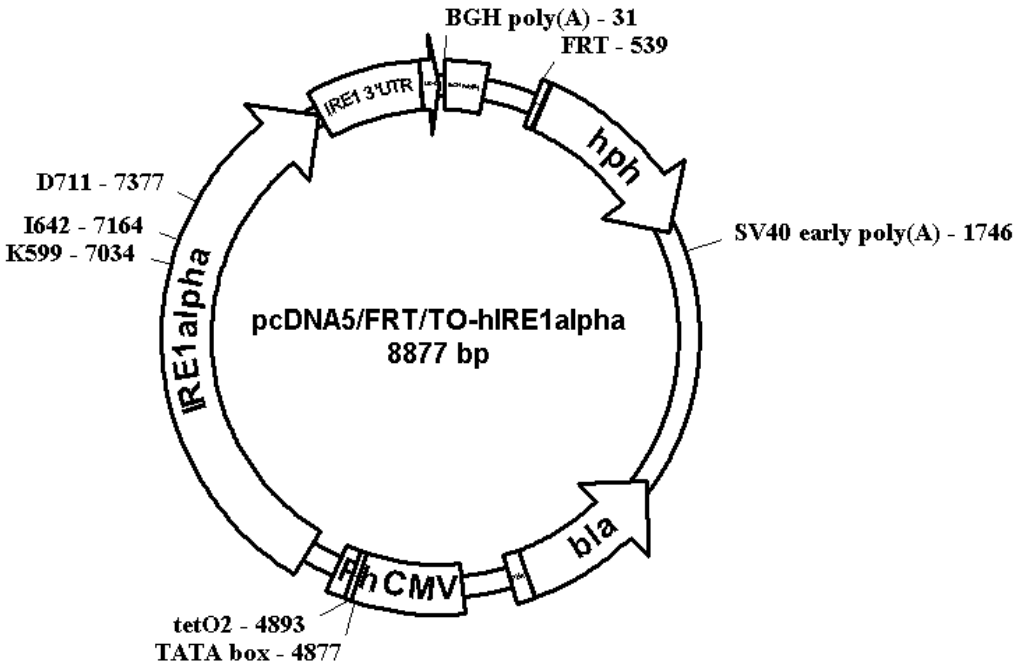

Figure 2.1: The pcDNA5/FRT/TO-hIRE1α vector from Sutcliffe, 2012.

Tetracycline binds the tetracycline repressor. This causes a conformational change in the tet repressor and it thus dislocates from the tetracycline operator, allowing expression of *hIRE1α.* This way, the role of *hIRE1α* can be closely studied, as its expression can be finely controlled using tetracycline and also because there are no 'background' effects from endogenous *IRE1α*.

2.4: List of commercially available kits

Name	Product Number	Company
Amersham™ ECL™ Western Blotting Detecting Reagents	RPN2009	ThermoFisher, Loughborough, UK
Criterion™ TGX™ Precast Gels 4-20%	567-1094/95	Bio-Rad, Hemel Hempstead, UK
DC™ Protein Assay reagent A	500-0113	Bio-Rad, Hemel Hempstead, UK
DC™ Protein Assay reagent B	500-0114	Bio-Rad, Hemel Hempstead, UK
DC™ Protein Assay reagent S	500-0115	Bio-Rad, Hemel Hempstead, UK
EndoFree® Plasmid Maxi Kit (10)	13262	Qiagen, Manchester, UK
EZ-RNA Kit (Solution A & B)	K1-0120	Geneflow, Lichfield, UK
GeneRuler™ 1 kb DNA Ladder	SM0311	ThermoFisher, Loughborough, UK
GeneRuler™ DNA Ladder Mix	SM0331	ThermoFisher, Loughborough, UK
GoTaq® qPCR MasterMix	A6002	Promega, Southampton, UK
jetPRIME	114-07	Polyplus transfection™, Illkirch, France
PageRuler™Plus Prestained Protein Ladder	26619	ThermoFisher, Loughborough, UK
Pierce® ECL Plus Western Blotting Substrate	32132	ThermoFisher, Loughborough, UK
Precision 2xreal-time PCR MasterMix with SYBR Green	Precision	PrimerDesign, Southampton, UK
Precision FAST 2xreal-time PCR MasterMix with SYBR Green	Precision-R	PrimerDesign, Southampton, UK
Restore™ Western Blot Stripping Buffer	21059	ThermoFisher, Loughborough, UK
RunBlue SDS Precast Gels 4-12% 10cmx10cm	NXG41212/27	Expedeon, Manchester, UK
Wizard®SV Gel and PCR Clean-Up System	A9282	Promega, Southampton, UK

2.5: List of *Escherichia coli* strains

Name	Genotype	Source
DH5α	F$^-$ Φ80*lacZ*ΔM15 Δ(*lacZYA-argF*)$_{U169}$ *rec*A1 *end*A1 *hsd*R17(r_k^-, m_k^+) *pho*A *sup*E44 *thi*-1 *gyr*A96 *rel*A1 λ$^-$	Agilent, Stockport, UK
XL10-GOLD	Tet^r Δ(*mcr*A)183Δ(*mcr*CB-*hsd*SMR-*mrr*)173 *end*A1 *sup*E44 *thi*-1 *rec*A1 *gyr*A96 *rel*A1 *lac* Hte [F' *pro*AB *lacI*^{q}Z ΔM15 Tn*10* (Tet^r) Am^y Cam^r]	Agilent, Stockport, UK

2.6: List of plasmid maps

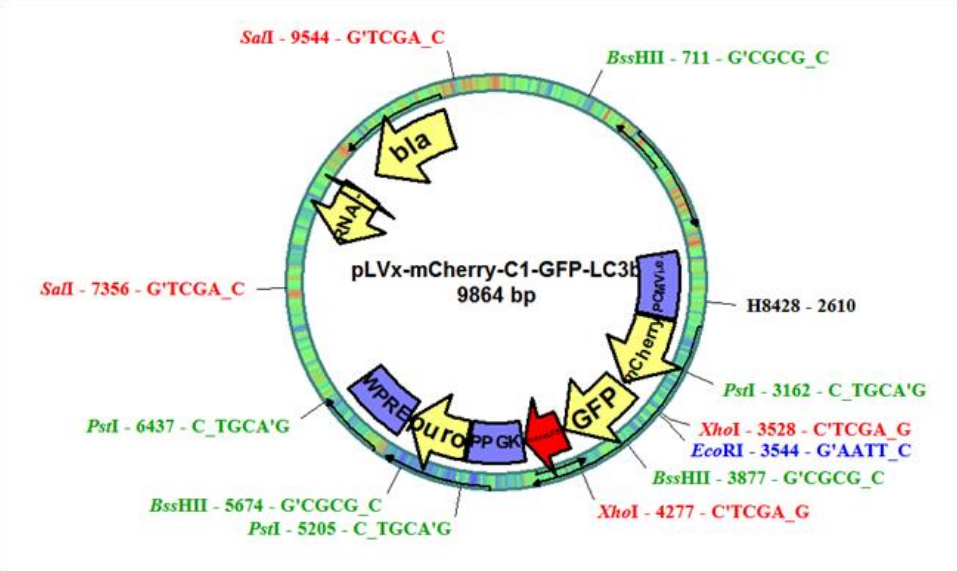

Figure 2.2: Plasmid map for the mCherry-GFP-LC3b construct. The restriction sites of the enzymes used for diagnostic digest characterisation are shown. The oligonucleotide used to sequence this plasmid is marked (H8428) and these sequences can be found in the list of oligonucleotides in section 2.8. The ORF encoding murine LC3b is highlighted in red. Other ORFs are coloured yellow, whereas promoters are blue.

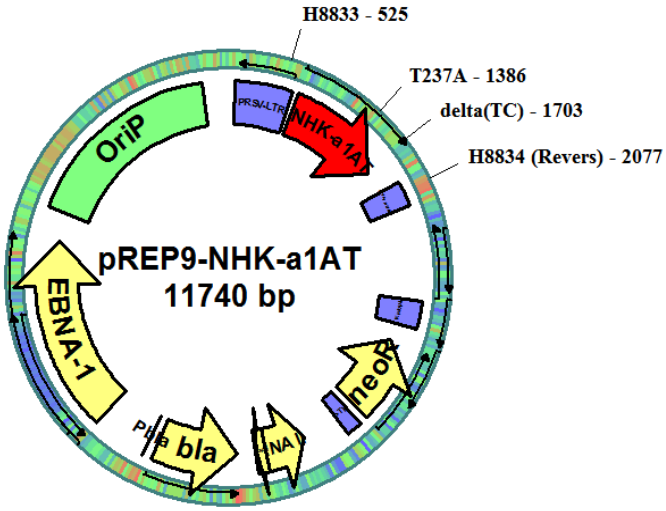

Figure 2.3: Plasmid map of pREP9-NHK-α1AT. The oligonucleotides used to sequence this plasmid are marked (H8833 and H8834) and these sequences can be found in the list of oligonucleotides insection 2.8. The point mutation (T237A) and the deletion (ΔTC) are also highlighted. The ORF for the Hong Kong null α1-antitrypsin is shown in red. Other ORFs are coloured yellow, whereas promoters are blue and origins are green.

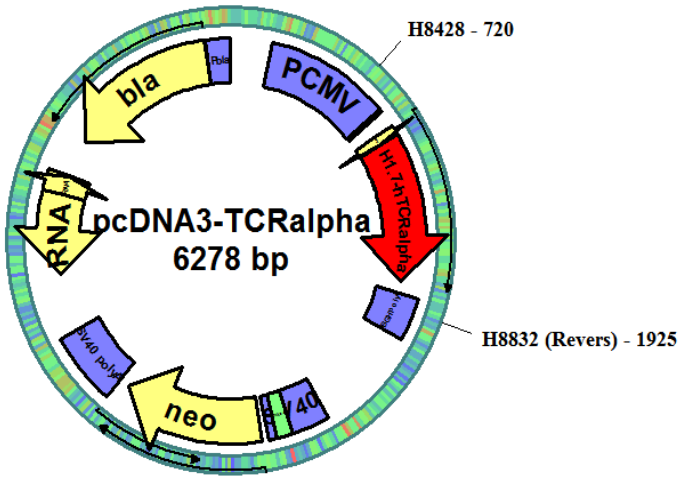

Figure 2.4: Plasmid map of pcDNA3-TCRα. The oligonucleotides used to sequence this plasmid are marked (H8428 and H8832) and details of these can be found in list 2.8. The ORF encoding TCRα is highlighted in red. Other ORFs are coloured yellow, whereas promoters are blue and origins are green.

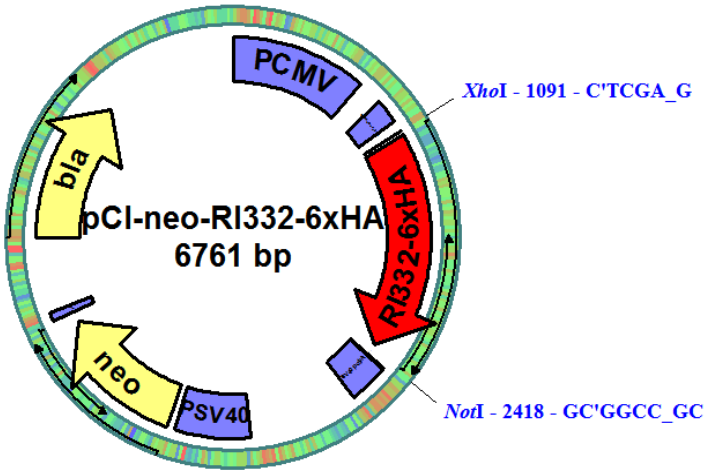

Figure 2.5: A plasmid map of pCI-neo-RI332-6xHA. The restriction sites of the enzymes used for diagnostic digest characterisation are shown. The ORF for RI332 is coloured red, whereas other ORFs are yellow. Promoters and origins are blue and green, respectively.

2.7: List of enzymes

Name	Product Number	Company
***Bss*HII**	11168851001	Roche, Welwyn Garden City, UK
***Eco*RI**	ER0271	ThermoFisher, Loughborough, UK
GoTaq® DNA Polymerase	M830B	Promega, Southampton, UK
***Not*I**	ERO591	ThermoFisher, Loughborough, UK
***Pst*I**	ER0611	ThermoFisher, Loughborough, UK
RNaseA	R-4875	Sigma-Aldrich, Gillingham, UK
***Sal*I**	ER0641	ThermoFisher, Loughborough, UK
Superscript® III Reverse transcriptase	56575	Invitrogen, Paisley, UK
***Xho*I**	ER0691	ThermoFisher, Loughborough, UK
***Xma*I**	R01805	NewEngland BioLabs, Ipswich, UK

2.8: List of oligonucleotides

Primers were all ordered lyophilised and were diluted in 1xTE (1 part 10 x TE buffer, 9 parts sterile H_2O) buffer to a concentration of 100 μM. This was used as a stock concentration from which 10 μM working dilutions were prepared using RNase and DNase-free water.

List of oligonucleotides, where F = forward and R = reverse. The annealing temperature is generally, approximately 5°C below the lowest melting temperature of each of the primer pairs. PCR and qPCR were used to optimise annealing temperatures using mouse cDNA.

Inventory Number	Purpose	Sequence	Annealing temp/°C
H8428	pcDNA3 5' primer	CAAAATCAACGGGACTTTCC	50
H8778	*CHOP* F mouse	TCTTGAGCCTAACACGTCGAT	55
H8779	*CHOP* R mouse	CGTGGACCAGGTTCTGCTTT	55
H8780	*GADD34* F mouse	TCTCTTCCAGGTGGCCTTCTA	55
H8781	*GADD34* R mouse	GAAGTGTACCTTCCGAGCTT	55
H8784	*RAMP4* F mouse	GAAGAAAAGGCGTCGGTAGG	50
H8785	*RAMP4* R mouse	CTAGGGCATCGAACATCAGG	50
H8786	*ERO1L-α* F mouse	GCGGACCAAGTTATGAGTTCC	55
H8787	*ERO1L-α* R mouse	GAAACAGGCACATTCCAACC	55
H8792	*GRP94* F mouse	TAGAAAAGGCTGTGGTGTCG	55
H8793	*GRP94* R mouse	GGGTGTCTAGGATTGATTTCG	55
H8794	*p58*^{IPK} F mouse	CGGGAAGGCTTAGAGAAAGC	55
H8795	*p58*^{IPK} R mouse	GAAATTATCTGGATGCCACTGC	55
H8796	*EDEM1* F mouse	TGGAAAGCTTCTTTCTCAGC	55
H8797	*EDEM1* R mouse	ATTCCCGAAGACGTTTGTCC	55
H8798	*HERP* F mouse	TGATGAGATAAACCGAGACTGG	55
H8799	*HERP* R mouse	CCTCTGTCTGAACGGAAACC	55

H8802	*HGSNAT* F mouse	CTGCTTTGCCTTCTTCATCC	55
H8803	*HGSNAT* R mouse	TCTTTGTGTGACTGCTCATCC	55
H8804	*BLOS1* F mouse	GTTGGTGGATCACCTCAACG	55
H8805	*BLOS1* R mouse	TCCCCAATTTCCTTAAGTGC	55
H8808	*PDGFRB* F mouse	CATCATCCCCTTACCTGACC	55
H8809	*PDGFRB* R mouse	CTTGCTGTGGCTCTTCTTGG	55
H8810	*PMP22* F mouse	GCCAGCTCTTCACTCTCACC	69
H8811	*PMP22* R mouse	GATGTAGGCGAAGCCATAGG	69
H8812	*COL6a1* F mouse	CTGGGCCAGATGAGTGTGAG	55
H8813	*COL6a1* R mouse	CATCCTTGCTCAACCGGTCA	55
H8814	*EPHRINB2* F mouse	AATCACGGTCCAACAAGACG	55
H8815	*EPHRINB2* R mouse	AATAAGGCCACTTCGGAACC	55
H8818	*SRp20* F mouse	GGCGCAGATCCCCAAGAAG	55
H8819	*SRp20* R mouse	TTTGCAAACTGGTCTTCTATTTCC	55
H8820	*TRIM16* F mouse	TCAAGTGTCTGCCATTGTCC	55
H8821	*TRIM16* R mouse	GTGGTGTTGGTGACCTTGC	55
H8824	*ERdj4* F mouse	GGGGCGCACAGGTTATTAGA	65
H8825	*ERdj4* R mouse	TTTGATTTGTCGCTCTGAGGC	65
H8826	*BiP* F mouse	GTGTGTGAGACCAGAACCGT	55
H8827	*BiP* R mouse	TCCTTCTTGTCCTCCTCCTCGG	55
H8832	pcDNA3 3' primer	GGCACCTTCCAGGGTCAAGG	60
H8833	pREP9 5' primer	GGACGAACCACTGAATTCCG	55
H8834	pREP9 3' primer	GGTTACAAATAAAGCAATAGC	50
H8944	*HEDJ* F mouse	CCTCATCGGGACTGTGATCG	55

H8945	*HEDJ* R mouse	CTTGGGGGTCATCAGGGTTC	55
H8952	*HRD1* F mouse	TCTTCCACTGCCGCATCG	55
H8953	*HRD1* R mouse	CCATGGTCATCAGAATGGCG	55
H8954	*GALNT10* F mouse	AGGCCTGATAAGGACCCGAA	55
H8955	*GALNT10* R mouse	ATTGGGCACACGATGGTCTT	55
H8956	*ERO1L-β* F mouse	AAACCTTCCGGAGAACAGCC	55
H8957	*ERO1L-β* R mouse	TGTGCTGCAACAACGCTTTA	55
H8960	*MAP7d1* F mouse	CAGCTCCCCTGGACGTAAGA	55
H8961	*MAP7d1* R mouse	CTGCGATTTCTACTGGGGGA	55
H8962	*TRB3* F mouse	TTTGGAACGAGAGCAAGGCA	55
H8963	*TRB3* R mouse	CCACATGCTGGTGGGTAGG	55

2.9: List of primary and secondary antibodies

Primary antibodies used for Western blotting. In general dilutions were made in 5% (w/v) fat-free milk solution. If the antibody was specific to a phospho-form, then the dilutions were made in 5% w/v BSA solution. In the 'host' column, R = rabbit, M = mouse and G = goat. In the 'clonality' column, M = monoclonal and P = polyclonal.

1° AB	Host	Clonality	Supplier	Product no.	Dilution	MW/kDa
anti-HA (mouse)	R	P	Sigma-Aldrich, Gillingham, UK	H6908	1:1000	Dependent on tag
BIP	R	P	Abcam, Cambridge, UK	ab-53068	1:500	78
Caspase-12	R	P	Cell Signalling, Hitchin, UK	2202	1:1000	42,55
Caspase-3	R	M	Cell	9665	1:1000	17,19,35

			Signalling, Hitchin, UK			
CHOP	Mo	M	Cell Signalling, Hitchin, UK	2895	1:1000	27
eIF2α	R	P	Santa-Cruz, Heidelberg, Germany	sc-11386	1:1000	36
GAPDH	Mo	M	Sigma-Aldrich, Gillingham, UK	G8795	1:20,000	37
Human TcRα	G	P	Santa-Cruz, Heidelberg, Germany	sc-31275	1:200	34
Human α1AT	G	P	Source Bioscience, Nottingham, UK	GTX2763	1:2000	52
IRE1α	R	M	Cell Signalling, Hitchin, UK	3294	1:1000	130
JNK	R	M	Cell Signalling, Hitchin, UK	9258	1:1000	46,54
LC3B	R	P	Cell Signalling, Hitchin, UK	2775	1:1000	14,16
PARP-1	R	P	Cell Signalling, Hitchin, UK	9542	1:1000	116,89
p-eIF2α	R	P	Cell Signalling, Hitchin, UK	9721	1:1000	38
p-IRE1α	R	M	Epitomics, Cambridge, UK	pS724	1:1000	110
p-JNK	R	M	Cell	4668	1:1000	46,54

		Signalling, Hitchin, UK		

The dilutions for all the secondary antibodies were made in a 5% (w/v) fat-free milk solution.

Secondary Antibody	Host	Supplier	Product number	Dilution
Anti-goat	Mouse	ThermoFisher, Loughborough, UK	31400	1:20,000
Anti-mouse	Goat	ThermoFisher, Loughborough, UK	31432	1:20,000
Anti-rabbit	Goat	Cell Signalling, Hitchin, UK	7074S	1:1000
Anti-rabbit	Donkey	ThermoFisher, Loughborough, UK	31458	1:20,000

2.10: Solutions and buffers

Type I laboratory H_2O was used to make the following solutions. This is defined as having: resistivity of less than 18 Ω-cm; total organic content of less than 10 parts per billion; less than 10 bacterial CFU/ml; and less than 0.03 EU/ml. Here, CFU stands for 'colony forming unit' and EU is 'endotoxin units'.

The autoclave cycle was at 121°C for 20 min at 1 atm.

Name of buffer/solution	Composition	Quantity	Recipe
0.2 N NaOH + 1% (w/v) SDS	0.2 N NaOH 1% (w/v) SDS	500 ml	4 g NaOH and 5 g SDS were dissolved in ~450 ml H_2O. H_2O was then added to a final volume 500 ml. This solution was stored in a polyethylene bottle.
1 M Tris·HCl (pH 8.0)	1 M Tris·HCl (pH 8.0)		60.57 g Tris were dissolved in ~ 400 ml DEPC-H_2O. The pH was adjusted with concentrated HCl. DEPC-H_2O was added to a volume of 500 ml. The solution was then autoclaved.
10 mg/ml tetracycline	10 mg/ml tetracycline	10 ml	100 mg tetracycline were dissolved in ~9 ml EtOH. EtOH was added so

			as the total volume was 10 ml. After filter sterilisation 1 ml aliquots were placed into brown 1.5 ml microcentrifuge tubes and stored at -20°C.
10 mg/ml tunicamycin	10 mg/ml tunicamycin in DMSO	1 ml	1 ml DMSO was added to 10 mg tunicamycin and mixed until dissolved. 50 µl or 100 µl aliquots were stored at -20°C.
10 x SDS-PAGE buffer	1.92 M glycine 0.248 M Tris 10 g/l SDS	1 l	144.13 g glycine, 30.03 g Tris and 10.00 g SDS were dissolved in 900 ml H_2O to ~ 900 ml. Once completely dissolved, H_2O was added to a total volume of 1 l.
10 x DNA gel electrophoresis sample loading buffer	20% (w/v) Ficoll 400 0.1 M EDTA 1% (w/v) SDS 2.5 g/l bromophenol blue	50 ml	35 ml of H_2O were added to 10 g Ficoll 400, 125 mg bromophenol blue, and 10 ml 0.5 M EDTA (pH 8.0). After dissolving, the volume was adjusted to 45 ml with H_2O and the solution was autoclaved. 5 ml of 10% (w/v) SDS were then added.
10 x semi-dry transfer buffer	121.1 g Tris base 144.13 g Glycine	1 l	900 ml H_2O were used to dissolve the Tris base and glycine. After the constituents had dissolved, the final volume was adjusted to 1 l.
10 x TBS	24.2 g Tris base 80 g NaCl	1 l	H_2O was used to dissolve the Tris base and NaCl and the pH was adjusted to 7.6 using conc. HCl.
10 x TE (pH 8.0)	100 mM Tris·HCl (pH 8.0) 10 mM EDTA	4 l	400 ml 1 M Tris·HCl (pH 8.0) were mixed with 80 ml 0.5 M EDTA. H_2O was added to a total volume of 4 l and the solution was then autoclaved.
100% (w/v) Trichloroacetic acid	100% (w/v) trichloroacetic acid	100 ml	100 g trichloroacetic acid was dissolved in ~80 ml H_2O. H_2O was then added to make 100 ml total volume.

2 mM dNTPs	2 mM dATP 2 mM dCTP 2 mM dGTP 2 mM dTTP 1 mM Tris·HCl (pH 8.0)	1 ml	910 µl H_2O and 10 µl 100 mM Tris·HCl (pH 8.0) were mixed together. The following were then added: 20 µl 100 mM dATP, 20 µl 100 mM dCTP, 20 µl 100 mM dGTP, and 20 µl 100 mM dTTP.
30% (v/v) glycerol	30% (v/v) glycerol	500 ml	189 g glycerol was dissolved in H_2O 400 ml, and mixed well by stirring. The remaining H_2O was added and the solution was autoclaved.
4% (w/v) PFA	4% (w/v) PFA	100 ml	90 ml of PBS was added to 4 g of PFA powder. The solution was heated to 60°C and 1 M NaOH was added dropwise until the PFA powder had dissolved. The pH was then adjusted to 7.4. PBS was added to achieve a final volume of 100 ml.
16% (w/v) PFA	16% (w/v) PFA	50 ml	50 ml H_2O was added to 8 g PFA. This was heated to 60-65 °C until the solution turned milky white. 1 N NaOH was added dropwise while stirring, until the solution cleared. This was then cooled to room temperature prior to use.
5 M KOAc, pH 4.8	5 M KOAc, pH 4.8	500 ml	147.5 ml HOAc was placed in a bottle and H_2O was added to a volume of ~ 450 ml. The pH was adjusted to 4.8 using KOH pellets while cooling in an ice/H_2O bath. H_2O was then added to a final volume of 500 ml and autoclaved.
50 mg/ml ampicillin	50 mg/ml ampicillin	50 ml	2.5 g ampicillin was dissolved in 40 ml H_2O, and then a further 10 ml H_2O was added. The solution was filter sterilized and stored in 1.0 ml aliquots at -20°C.

50 mM D-Glc, 25 mM Tris·HCl (pH 8.0), 10 mM EDTA	50 mM D-Glc 25 mM Tris·HCl (pH 8.0) 10 mM EDTA	50 ml	2.50 ml 1 M D-Glc, 1.25 ml 1 M Tris·HCl (pH 8.0), 1.00 ml 0.5 M EDTA and 45.25 ml H_2O were mixed together and stored at 4°C.
50 x TAE	2 M Tris·HOAc 0.1 M EDTA pH ~ 8.5	1 l	242 g Tris, 57.1 ml HOAc and 37.2 g $Na_2EDTA \cdot 2H_2O$ were added together and mixed. H_2O was added to a total volume of 1 l.
6 x SDS-PAGE sample buffer	350 mM Tris·HCl, pH 6.8 30% (v/v) glycerol 10% (w/v) SDS 0.5 g/l bromophenol blue 2% (v/v) β-mercaptoethanol	10 ml	3.50 ml 1 M Tris·HCl, 3.78 g glycerol, 1.00 g SDS, 500 µl 10 g/l bromophenol blue and 200 µl β-mercaptoethanol were added together. 9 ml H_2O were added to these constituents. The solution was dissolved overnight if necessary. H_2O was added to a final volume of 10 ml.
DEPC-H_2O	H_2O	1 l	1 ml DEPC was added to 1 l type I laboratory H_2O and stirred vigorously for 30 min at room temperature. The solution was autoclaved.
LB Broth	2% (w/v) LB broth		20 g LB powder was vigorously stirred into 1 l H_2O until it had dissolved. The solution was then autoclaved.
PBG	1% (w/v) BSA 0.5% (w/v) fish gelatin	100 ml	90 ml PBS was added to 1 g BSA and 0.5 g fish gelatin. The pH was then adjusted to 7.4 and the final volume was adjusted to 100 ml using PBS.
RIPA buffer	50 mM Tris·HCl, pH 8.0 150 mM NaCl 1% (v/v) Triton X-	10 ml	0.5 ml 1M Tris·HCl pH 8.0, 0.3 ml 5 M NaCl, 0.1 ml Triton X-100, 0.5 ml 10% (w/v) sodium deoxycholate, and 0.1 ml 10% (w/v) SDS were added

	100 0.5% (w/v) sodium deoxycholate 0.1% (w/v) SDS		together. 8.5 ml H_2O were then added to the mixture. The solution was stored at 4°C. One Roche CompleteMini protease inhibitor tablet and one Roche phosSTOP phosphatase tablet were dissolved in this solution immediately before use.
TBST	24.2 g Tris base 80 g NaCl 1 ml Tween 20	1 l	The salts were added together, ~900 ml H_2O were added and the solution was stirred. The pH was adjusted to 7.6 using HCl. 1 ml Tween 20 was added and H_2O was added to a final volume of 1 l.

2.11: List of specialist equipment

Name	Product Number	Company
24 well plate Adherent	83.1836	Sarstedt, Leicester, UK
6 well plate Adherent	83.1839	Sarstedt, Leicester, UK
CellView™ Cell Culture Dish, Glass-Bottomed	627965	Greiner, Stonehouse, UK
DNA Engine® Thermal Cycler	N/A	Bio-Rad, Hemel Hempstead, UK
PVDF Transfer Membrane (0.45µm pore size)	RPN303F	ThermoFisher, Loughborough, UK
Rotor-Gene Q	N/A	Qiagen, Manchester, UK
Tissue Culture dish	83.1802	Sarstedt, Leicester, UK
Tissue culture flask 175 Adherent	83.1812	Sarstedt, Leicester, UK
Tissue culture flask 75 Adherent	83.1811	Sarstedt, Leicester, UK

2.12: Protocols

2.12.1: Cell Culture (Davis, 2002)

2.12.1.1: Preparation of DMEM culture media and culture conditions

Reagents (See list 2.2 for details)

- L-glutamine solution
- Tetracycline-free FBS
- High-glucose DMEM (without glutamine, with sodium pyruvate)

A 500 ml solution of DMEM with 4.5 g/l D-glucose, 10% (v/v) FBS, 2 mM L-glutamine, 110 mg/l pyruvate was prepared. This was done by adding 50 ml FBS and 5 ml 200 mM L-glutamine to 445 ml DMEM.

Please note that any reference to DMEM/culture medium specifically means DMEM, high glucose, +10% FBS, +2 mM glutamine, unless otherwise stated. Revival of any of the three MEF cell lines was carried out using this medium and antibiotics (hygromycin and blasticidin·HCl) were added 24 h later to achieve final concentrations of 100 μg/ml and 10 μg/ml, respectively. All cells were grown in the 37°C incubator with a humidified, 5% CO_2 atmosphere. These cell culture conditions are assumed when referring to the CO_2 incubator, unless stated otherwise.

2.12.1.2: Cell revival

9 ml warmed DMEM medium were pipetted into a 75cm^2 adherent cell culture flask. The cells were taken from the liquid N_2 tank and immediately placed into a 37°C water bath. 500 μl of medium was pipetted into the cell vial when its contents had started to thaw. The mixture was pipetted up and down a few times. 500 μl of this mixture were pipetted into the culture flask. The process of adding medium to the cells being thawed was repeated at least another two times so as to dilute the DMSO in the freeze mix, thus preventing cell damage. The contents of the vial were then all transferred into the flask. The flask was placed in the CO_2 incubator for approximately 24 h, after which any necessary antibiotics were added.

2.12.1.3: Trypsinisation of cells

The DMEM medium was placed in a 37°C water bath for 30 min prior to passaging the cells. The medium from the adherent cell culture was aspirated. The cells were gently washed with 10 ml sterile PBS. Film trypsinisation was then carried out by covering the cells evenly using 2 ml of 0.25% (w/v) trypsin-EDTA, and then removing the trypsin. The cells were incubated in the CO_2 incubator for 3 min after which they were suspended in 10 ml culture medium. Depending on the desired seeding density, a specific volume was then

transferred into a fresh flask containing new media. Antibiotics were added accordingly to the flask which was then transferred to the CO_2 incubator. The final volume in the flask was 10 ml for a 75 cm^2 flask, and 25 ml for a 125 cm^2 flask.

2.12.1.4: Cell counting with a Neubauer chamber (haemocytometer)

The haemocytometer was first cleaned using 70% (v/v) ethanol. Using a 10 µl pipette, a few drops of water were placed on the mounting supports either side of the grooves. The glass cover slip was carefully positioned over the area which contained the water drops and the counting grids.

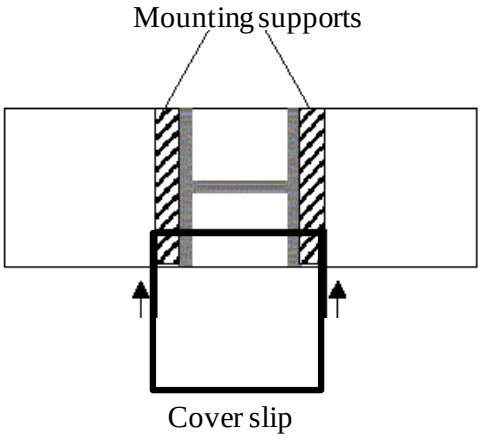

Figure 2.6: Basic schematic depicting a Neubauer chamber and the position of the cover slip.

A 1:1 ratio of trypan blue solution : cell suspension was made in a 1.5 ml microcentrifuge tube. Approximately 10 µl of sample was loaded underneath the cover slip, onto the loading groove. Each of the two counting grids were visualised using the 4 x objective lens of a microscope. The cells within a square of area 0.04 mm^2 were counted on both of the counting grids and the average number of cells was calculated.

The number of cells per ml was then calculated using the following equation:

$$\textit{Number of cells per ml} = \textit{Average number of cells} \cdot 10^4 \cdot 2$$

In this equation, *2* takes into consideration the dilution factor created as a result of mixing the given volume of cell suspension with an equal volume of trypan blue solution.

2.12.1.5: Generation of frozen cell stocks

Cells were grown until they reached 95% confluency. The above protocol for passaging cells was followed up to and including the trypsinisation stage. The cells were then resuspended in a volume of 90% (v/v) FBS, 10% (v/v) DMSO. The volume of freeze mix was determined by the number of cryotubes to be filled, with 1 ml of freeze mix per cryotube. For cells

grown in a T75 flask, 4 ml freeze mix were used. The cell suspension was transferred into the cryotubes and these were placed in the -80°C storage in an insulated container (CoolCell, BioCision) to slow the rate of freezing. The vials were removed from the container the following morning and transferred to storage in a liquid nitrogen freezer.

2.12.1.6: Treatment of MEFs

Cells were seeded at 15% confluency on a 10 cm plate. To induce expression of human IRE1α, each of the three MEF cell lines were treated with 1 μg/ml tetracycline. A 10 mg/ml tetracycline stock solution in ethanol was diluted tenfold in absolute ethanol. This 1 mg/ml tetracycline solution was diluted 1:1000 in culture media to yield the final concentration of 1 μg/ml. The culture media containing tetracycline was then added to the cells. Control cultures received the same volume of absolute ethanol added to the media. This tetracycline dilution was only stored for a week at -20°C due to its photosensitivity.

Similarly, 100 μl of the stock of 1 mg/ml tunicamycin was added to 900 μl DMSO. Thus, when 1 μl of this 100 ng/μl concentration was pipetted into 1 ml media, the final concentration of 100 ng/ml was achieved. This media was then added to the cells. As a control, cells were treated with the same volume of DMSO in culture media.

2.12.1.7: Transfection of HEK293T cells

Cells were seeded at around 30% confluency in a 6-well plate and allowed to adhere and double in number over approximately 24 h. The volume required for 2 μg plasmid DNA was calculated and added to 200 μl of jet-PRIME buffer. 4 μl of jet-PRIME was then added to the mixture and centrifuged briefly using a benchtop centrifuge. It was then incubated at room temperature for 10 min before 200 μl were added to each well. 200 μl of a mixture containing only jet-PRIME buffer and jet-PRIME transfection agent were added to control wells so as any background expression of the gene in question could be taken into account. The cells were placed in the 37°C CO_2 incubator and 4 h later the media was refreshed. Lysates were collected after 3 washes in 1 ml PBS using 100 μl RIPA buffer, 24 and 48 h after the media had been changed. Protein expression of the transiently transfected gene was analysed by Western blotting.

2.12.1.8: Protein extraction

Reagents

- Phosphate buffered saline (PBS)
- 10ml ice-cold RIPA buffer (containing 1 Complete mini protease inhibitor cocktail tablet, and 1 phosSTOP phosphatase inhibitor cocktail tablet)

The media was removed from the plates and the cells were gently washed with 3x1 ml room temperature PBS. For protein extraction the plates were placed on ice, 100 µl RIPA buffer were added to the plates and evenly spread by gently using a cell scraper. After about 2 min the surface of the plate was thoroughly scraped using the blade-edge of a cell scraper, to collect the cell lysate at one end of the plate. The lysates were transferred into a 1.5 ml microcentrifuge tube and stored at -80°C.

The protein samples were thawed and then centrifuged at 13,000 g for 15 min at 4°C. The supernatant containing the protein was transferred into a fresh 1.5 ml microcentrifuge tube prior to carrying out a protein assay.

2.12.1.9: RNA isolation (GeneFlow)

Reagents

- EZ-RNA Solution A (contains guanidine thiocyanate)
- RNA-grade pipette tips and 1.5 ml microcentrifuge tubes were used

For RNA extraction, 500 µl of EZ-RNA Solution A were added to the plates. A pipette tip was used to dislodge the cells from the plate using the lysis buffer. The samples were collected in RNase-free 1.5 ml microcentrifuge tubes and stored at -80°C.

After thawing the samples in EZ-RNA Solution A, 500 µl of EZ-RNA Solution B was added. Each sample was inverted vigorously for 15 s to mix the contents. The mixtures were incubated at room temperature for 10 min before being centrifuged at 12,000 g for 15 min at 4°C. 500 µl ice-cold isopropanol were added to fresh tubes. The supernatant which formed as a result of centrifugation was added to the isopropanol. The mixtures were shaken. At this stage, the samples were either stored overnight at -20°C, or at -80°C for 1 h or longer before the remainder of the protocol was carried out. Storage at these low temperatures was particularly useful if the amount of RNA harvested was believed to be low, as it helped to increase the final yield.

0.5 µl of 20 mg/ml RNA-grade glycogen was added to aid RNA precipitation. The samples were then centrifuged at 12,000 g for 10 min [*1] at 4°C. The supernatant was discarded using a pipette. 1 ml of 75% (v/v) EtOH in DEPC water was added and the samples were gently shaken. Again, one was able to store at -20°C at this stage, especially if cDNA synthesis was not going to follow immediately.

The final stage of the protocol consisted of a centrifugation step at 7,500 g for 5 min [*2] at 4°C. The supernatant was discarded carefully using a pipette. The samples were left to air-

dry for about 20 min at RT. 20 µl DEPC water was added to each RNA pellet and the preparations were incubated in a heat block at 55°C for 10 min before being stored at -80°C for future use.

Note, to improve RNA yields centrifugation [*1] should be carried out at 16,000 g for 30 min, and centrifugation[*2] at 16,000 g for 15 min.

2.12.2: Protein chemistry

2.12.2.1: Preparation of a standard curve for use in protein assay

100 µl of 20 mg/ml BSA stock were added to 900 µl RIPA buffer. 500 µl of this 2 mg/ml dilution were added to 500 µl RIPA buffer to create a 1 mg/ml dilution. The process of adding 500 µl of the most recently created dilution to 500 µl RIPA buffer was repeated, creating the serial dilutions of 0.5 mg/ml, 0.25 mg/ml, 0.125 mg/ml and 0.0625 mg/ml.

2.12.2.2: Protein assay (Bio-Rad)

Using RIPA buffer 1:5 dilutions of the protein samples were made in separate 1.5 ml microcentrifuge tubes. In a 96-well plate, 5 µl RIPA buffer was loaded as the blank sample. 5 µl of each of the standard curve dilutions and the protein samples were loaded into wells. Each sample including the blank was in duplicate.

A solution containing 5 ml DC™ Protein Assay reagent A and 100 µl of DC™ Protein Assay reagent S was made. This was shaken vigorously prior to use to ensure that DC™ Protein Assay reagent S had not precipitated out. 25 µl of this solution were added to each well. 200 µl DC™ Protein Assay reagent B were subsequently added to each well. The plate was incubated at room temperature for 15 min on a shaker. Using the SpectraMAX 190 plate reader and version 5.3 of the SoftMaxPro software, the absorbance values at 750 nm were determined against the standard dilutions to generate protein concentrations of the samples.

2.12.2.3: TCA (trichloroacetic acid) protein precipitation

1 volume of 20% (v/v) TCA was added to 1 volume of protein sample and mixed. This was incubated on ice for 30 min. The protein sample was centrifuged at 12,000 g, for 15 min at 4°C. The supernatant was carefully discarded, thus leaving a white pellet behind. 200 µl 10% (v/v) TCA were added ad the pellet was resuspended. This mixture was centrifuged at 12,000 g for 5 min at 4°C. The supernatant was again carefully discarded. The step involving the addition of 200 µl 10% (v/v) TCA was repeated. 200 µl 100% (w/v) EtOH were added. Here the pellet turned from white to transparent. The susepsnion was centrifuged at 12,000 g for 5 min at 4°C. The supernatant was discarded. The EtOH wash step was repeated. The samples were left to air-dry for 20 min to allow the EtOH to evaporate. The pellets were resuspended in 20 µl SDS-PAGE buffer. Note that upon addition of SDS-PAGE buffer, if the sample turned from blue to yellow, 0.5 M Tris HCl (pH 9.4) was added in 0.5µl increments to neutralise any remaining TCA.

2.12.2.4: Western Blotting

Solutions to prepare

- 1 x Semi-dry transfer buffer (18 parts sterile water, 2 parts 10 x transfer buffer, 1 part MeOH)
- 1 x TBST (1 part 1 x TBS, 9 parts sterile water, 1 ml TWEEN 20 for every litre)
- 5% w/v milk (10 g skimmed milk powder was dissolved in 200 ml 1 x TBST)

Gel electrophoresis

The appropriate amount of 6 x SDS-PAGE loading buffer was added to the protein samples so as the final concentration was 1 x SDS-PAGE. These mixtures were boiled for 5 min at 100°C. As the samples were cooling, the precast gel was placed into a tank, which was subsequently filled with the appropriate running buffer. The wells of the gel were washed with running buffer. The protein samples were loaded against 10 µl of pre-dyed protein ladder (Figure 2.2) and the gel was run at a voltage specified by the manufacturer, until the band representing 10 kDa in the protein ladder was almost at the bottom of the gel.

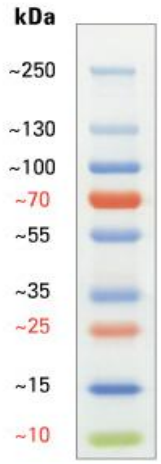

Figure 2.7: A depiction of the composition of the PageRuler™Plus Prestained Protein Ladder used for Western blotting. Product details can be found in list 2.4.

For each gel, 1 PVDF membrane (0.45 µm pore size) and 8 pieces of filter paper were cut to dimensions equal to those of the gel. The membrane was incubated at room temperature on a shaker in MeOH for 1 min. The membrane and filter papers were then incubated at room temperature in 1xsemi-dry transfer buffer for 15 min. Simultaneously, the gel was washed in 1xsemi-dry transfer buffer for 15 min.

Semi-dry transfer

Four pieces of drained filter paper were placed on the clean surface of a Semi-dry transfer machine. A 50 ml tube was used to roll across this paper to remove any air-bubbles. The membrane was placed on top of this filter paper. The gel was then carefully transferred onto the membrane, followed by the four remaining pieces of filter paper. The Falcon tube was re-used to remove any more air bubbles. The lid of the machine was carefully lowered onto the stack. The appropriate current density was set to correspond to 2 mA/cm^2.

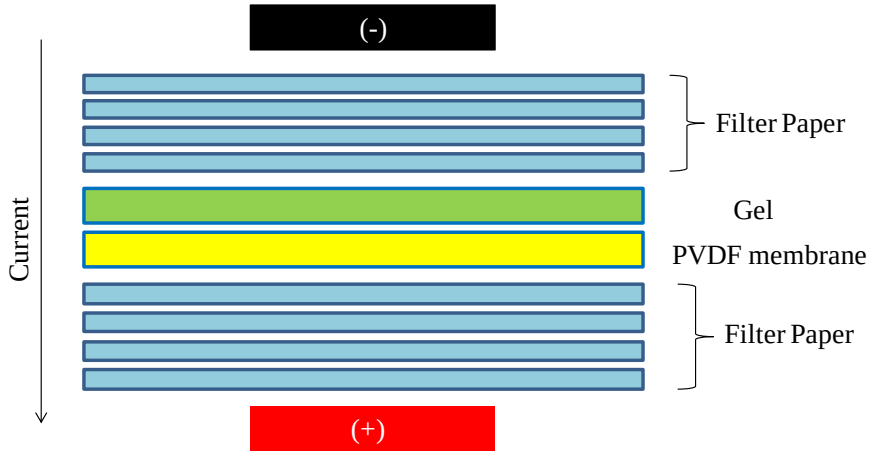

Figure 2.8: Layout of filter papers, gel and membrane in the transfer machine.

Antibody immunoblotting

Once the transfer had completed, the membrane was washed quickly in 1 x TBST and was then blocked in 5% (w/v) fat-free milk. This step was carried out either at room temperature for 1 h, or at 4°C, overnight. The membrane was then washed 3x5 min 1 x TBST. It was then cut along the 70 kDa band so as each half could be probed for a different protein. The membrane was transferred into a 50 ml falcon tube. A minimum volume of 3 ml 5% (w/v) fat-free milk was pipetted into the falcon tube and a specific amount of primary antibody was added to achieve the recommended concentration (see list 2.8). The falcon tube was placed on a roller at 4°C, overnight.

The following day, the membrane was removed from the falcon tube and washed 3x5 min 1 x TBST. It was then inserted into a fresh 50 ml falcon tube and secondary antibody was added to 5% (w/v) fat-free milk in a ratio which would produce the recommended antibody concentration (see list 2.8). The falcon tube was placed on a roller for 1 h at room temperature. The membrane was then washed in 3x5 min 1 x TBST before being placed into an exposure cassette. A solution of room temperature ECL or ECL+ was made according to product instructions to cover the surface of the membranes. A 5 min incubation stage in the dark followed.

A piece of photographic film was positioned on top of the membrane and the cassette was closed. In a dark room, the film was normally exposed for about 1 min before being developed. Following exposure times were determined by the intensity of the bands seen after this exposure.

2.12.2.5: Stripping of membranes

The membrane was removed from the cassette and washed in 3x5 min 1xTBST. Enough Restore™ Western Blot Stripping Buffer was added to cover the membrane in a tray. The membrane was incubated with the stripping buffer at room temperature for 15 min on a shaker. The membrane was then washed in 3x5 min 1 x TBST and was stored in a minimal volume of 1 x TBST at 4°C until required for further probing and imaging.

2.12.3: Molecular Biology – methods for RNA and DNA

2.12.3.1: RNA quantitation

In a 96-well plate, a 1:50 dilution of each RNA sample was made using 2 µl RNA and 98 µl DEPC water. All samples were in duplicate. Using the SpectraMAX 190 plate-reader and the Warburg-Christian analysis (Warburg and Christian, 1942) on version 5.3 of the SoftMax Pro program, the RNA concentrations were calculated against the DEPC water blank.

2.12.3.2: Reverse transcription (Invitrogen)

For this reaction, *(N+1)* master mixes were made up for *N* samples.

Reagents per sample

- 1µl 10 mM RNA dNTPs
- 1µl 50 µM oligo$(dT)_{15}$ primer
- 4µl 5xfirst strand buffer
- 1 µl 0.1 M DTT
- 1 µl 40 U/µl RNaseIN
- 1 µl 200 U/ml SuperScript III Reverse Transcriptase

The volume containing 1.5-5 µg RNA was calculated and pipetted into each PCR tube. 2 µl of the first master mix containing 10 mM dNTPs and 50 µM oligo$(dT)_{15}$ primer were added to this. A total volume of 11 µl was achieved by adding the appropriate amount of sterile, nuclease-free water. The PCR tubes were centrifuged for a few seconds to collect all the liquid at the bottom. The tubes were placed in the PCR machine and incubated at 65°C for 5 min, followed by 5 min incubation at 4°C. To each tube 7 µl of the second master mix containing 5 x first strand buffer, 0.1 M DTT, 40 U/µl RNaseIN, and 200 U/ml SuperScript III reverse transcriptase were added. The PCR tubes were centrifuged for another few seconds. The tubes were placed in the PCR machine, and a program was selected to heat the samples to 50°C for 1 h and then to 70°C for 15 min to inactivate the reverse transcriptase. The synthesized cDNA was stored at 4°C or -20°C for long-term use.

2.12.3.3: Primer Design

Primer3 and Primer-BLAST were used to design primers with the following parameters:

- PCR product of 120-150 base-pairs
- Primer length between 18 and 22 nucleotides
- Primer GC content ≥50%
- Primers flanking an exon-exon junction
- Intron length of 1000 base-pairs between the 2 exons
- Annealing temperature between 50°C and 65°C
- No mismatch bases
- Primers specific to *Mus musculus*
- Primers to amplify mRNA splice variants

Primers were diluted in 1xTE buffer to a stock concentration of 100 μM. These primer solutions were further diluted using sterile water, to a 10 μM working concentration.

2.12.3.4: Polymerase Chain Reaction (PCR) (Reed *et al*., 2013)

Reagents per sample

- 2.5 μl 10 μM forward primer
- 2.5 μl 10 μM reverse primer
- 5 μl 5xGreen GoTaq® Reaction Buffer
- 1.5 μl 25 mM $MgCl_2$
- 1.25 μl 2 mM dNTPs
- 1.25 μl 1:10 mouse cDNA dilution
- 0.25 μl Taq Polymerase (5 U/μl)
- 10.75 μl sterile water

The reagents were mixed together in a PCR tube, with the primers being added last to avoid primer-dimer formation. The total volume per tube was 25 μl. The tubes were loaded into the PCR machine and a 35 cycle program similar to the one below was run:

Table 1.1: Cycling conditions for the Thermal Cycler PCR machine.

Number of cycles	**Temperature/°C**	**Time**	**Description**
1	94	5 min	Initial denaturation
35	94	15 s	Cycle of denaturation, annealing and elongation
	55	20 s	
	72	30 s	
1	72	5 min	Final elongation

The annealing temperature was changed according to primer specifications. Once the program had finished, the samples were loaded alongside a 1kB DNA ladder on a 1% (w/v) agarose gel which contained an ethidium bromide concentration of 500 μg/l. The gel was run at 10 V per cm length of the gel.

2.12.3.5: qPCR with PrimerDesign FAST 2xMasterMix (with SYBR green)

For this reaction, *(N+1)* master mixes were made up for *N* samples.

Reagents

- 5 μl 1:10 cDNA dilution
- 10 μl FAST 2xqPCR Master Mix
- 0.6 μl 10 μM forward primer
- 0.6 μl 10 μM reverse primer
- 3.8 μl sterile nuclease-free water

A master mix containing all reagents excluding the cDNA was prepared and kept on ice. 5 μl of the cDNA were added to the qPCR tubes in triplicate followed by 15 μl of the mixture. These tubes were kept on ice at all times. The tubes were loaded into the qPCR machine and the following program was run.

Table 2.2: Cycling conditions for qPCR program on the Rotor-Gene Q using the FAST 2xqPCR MasterMix. The annealing temperature of 55°C is used here as a general annealing temperature, although this is, of course, dependent on the primers being used.

Number of cycles	**Temperature/°C**	**Time**	**Description**
1	95	1 min	Enzyme activation and denaturation
40	95	5 s	Cycle of denaturation, annealing and elongation
	55	5 s	
	72	10 s	
1	55-95	N/A	Melt curve production

Note that most of the qPCR data obtained for this thesis was done using the FAST 2xqPCR MasterMix from PrimerDesign. However, some data was obtained using the standard 2xqPCR MasterMix (Primer Design) or the Promega MasterMix kit. There were shown to be no differences in terms of data output, between these three kits (data not shown). The recipe for the former is the same as above, however the cycling conditions did vary:

Table 2.3: Cycling conditions for qPCR program on the Rotor-Gene Q using the 2xqPCR MasterMix. The annealing temperature of 55°C is used here as a general annealing temperature, although this is, of course, dependent on the primer being used.

Number of cycles	**Temperature/°C**	**Time**	**Description**
1	95	10 min	Enzyme activation and denaturation
40	95	15 s	Cycle of denaturation, annealing and elongation
	55	30 s	
	72	20 s	
1	55-95	N/A	Melt curve production

The recipe for the Promega kit was as follows:

- 5 µl 1:10 cDNA dilution
- 7.5 µl GoTaq® qPCR MasterMix
- 0.45 µl 10 µM forward primer
- 0.45 µl 10 µM reverse primer
- 1.6 µl sterile nuclease-free water

When using the Promega kit, 5 µl cDNA were added to the tubes in triplicate, followed by 10 µl master mix.

The cycling conditions which accompanied this kit were as follows:

Table 2.4: cycling conditions for qPCR program on the Rotor-Gene Q using the GoTaq® qPCR MasterMix. The annealing temperature of 55°C is used here as a general annealing temperature, although this is, of course, dependant on the primers being used.

Number of cycles	**Temperature/°C**	**Time**	**Description**
1	95	10 min	Initial denaturation
40	95	15 s	Cycle of denaturation, annealing and elongation
	55	60 s	
1	55-95	N/A	Melt curve production

2.12.3.6: Agarose gel electrophoresis of DNA

150 ml of 1 x TAE buffer were added to 1.5 g of agarose powder in a conical flask. The mixture was heated at full power in a microwave, until all the powder had dissolved. 7.5 µl ethidium bromide (10 mg/ml stock concentration) were added to the solution once the flask had cooled enough to touch. The final concentration of ethidium bromide was thus 500 µg/l. The mixture was stirred gently and poured into a gel cast. The comb was then added carefully. Once the agarose gel had set, it was placed in a gel tank filled with 1 x TAE, and the comb was removed. 10 x loading buffer was added to the samples (PCR products or digest plasmids). These were loaded into the wells of the gel alongside a 1kB DNA ladder which served (figure 2.5) as a reference marker. The voltage was set to 5 V per cm length of the gel. The gel was then photographed under a UV transilluminator (302 nm wavelength, 32 W) to analyse the DNA fragments.

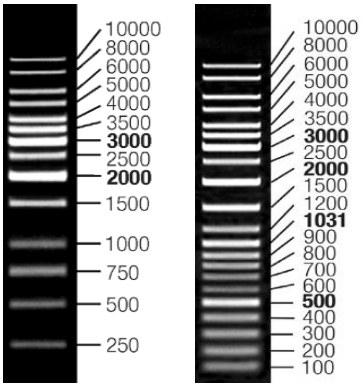

Figure 2.9: GeneRuler™ DNA Ladder Mix SM0331 (left) and SM0311 (right) used to determine fragment sizes on agarose gels.

2.12.4: Molecular biology - *Escherichia coli* methods

2.12.4.1: Preparation of LB ampicillin plates

35 g of LB-agar were suspended in 1 l of distilled water. The solution was autoclaved after being stirred. Once it had cooled to around 50°C, ampicillin was added so as a concentration of 50 µg/ml was achieved. ~25 ml of the solution was poured into each culture plate. The agar was left to solidify and then stored at 4°C.

2.12.4.2: Revival of *Escherichia coli* strains

The vial of bacterial cells was transferred from the -80°C storage to a small container of liquid nitrogen. Once removed from this container, a pipette tip was used to scrape clumps of frozen cells from the vial. A flamed inoculating loop was then used to streak the individual colonies out from one another. The plate was then incubated at 37°C overnight.

2.12.4.3: *Escherichia coli* transformation (adapted from Inoue *et al*., 1990)

After dissolving the plasmids in an appropriate amount of 1 x TE buffer, a 50 µl aliquot of competent bacterial cells (DH5α or XL10-GOLD) were added using a wide-orifice pipette tip. That was then mixed by very gently flipping the tube. These preparations were left on ice for 30 min. The vials containing DH5α cells were then heat-shocked at 42°C for 90 s whereas those containing XL10-GOLD cells were heat-shocked at 42°C for 42 s. All vials were then incubated on ice for 2 min. 1 ml LB broth was then added to each sample. The preparations were transferred to 12 ml culture tubes and then incubated at 37°C in a shaker at 240 rpm for 1 h.

200 µl of the DH5α suspension were pipetted onto LB ampicillin plates and spread using a sterile spreader. This process was repeated for the XL10-GOLD suspensions but using only 50 µl. The remaining suspensions were centrifuged at 17,000 g for 1 min at room temperature. Most of the supernatant was removed, leaving about 100 µl behind. The cell pellet was resuspended in this volume and spread onto LB ampicillin plates.

2.12.4.4: Inoculation of *E. coli* colonies

A bacterial colony was lifted off the plate using a sterile toothpick, which was handled using flamed forceps. The toothpick was then placed into a culture tube containing 4 ml LB broth and 100 µg/ml ampicillin. The tube was incubated at 37°C in a shaker at 240 rpm overnight. It was ensured that the tube caps were not fully closed to allow respiration to occur.

2.12.4.5: Generation of *E. coli* stock cultures

1 ml culture inoculation was added to 1 ml 30% (w/v) glycerol in a cryotube. Mixing was carried out by pipetting up and down. The culture was then placed in liquid nitrogen before being transferred to -80°C.

2.12.4.6: Miniprep of plasmid DNA from transformed *Escherichia coli* (Birnboim and Doly, 1979)

1.5 ml of saturated overnight culture were placed in a 1.5 ml microcentrifuge tube. The remaining culture was stored in the refrigerator at 4°C.The microcentrifuge tubes were centrifuged at 14,000 g for 1 min at room temperature. The supernatant was removed carefully using a pipette, and discarded. The process of centrifugation and removal of the supernatant was repeated.

100 µl of 50 mM D-Glc, 25 mM Tris·HCl (pH8.0), 10 mM EDTA were added to the cell pellet. These samples were resuspended by vortexing and then incubated at room temperature for 5 min. 200 µl 0.2 N NaOH, 1% (w/v) SDS were added to the tubes. The samples were mixed by inverting the tubes between 4 and 6 times. It was ensured that the samples were not vortexed from this point onwards, to avoid the chromosomal DNA being sheared. The samples were incubated on ice for 5 min. 150 µl of ice-cold 5M KOAc (pH 4.8) was added and the tubes were inverted 4-6 times to mix the contents. The samples were placed on ice for another 5 min.

The tubes were centrifuged at 14,000 g for 3 min at 4°C. The resulting supernatant containing the plasmid was transferred into a fresh microcentrifuge tube. 0.8 ml of 100% (v/v) EtOH was added to the tubes, which were then inverted 2-3 times. This was followed by a 2 min incubation at room temperature. The samples were centrifuged at 14,000 g for 1 min at room temperature. The supernatant was discarded.

1 ml of 70% (v/v) EtOH was added to each sample. This was followed by another centrifugation at 14,000 g for 1 min at room temperature. The supernatant was discarded. The tubes were centrifuged at 14,000 g for a final 10-15 s at room temperature, and any remaining liquid was carefully removed using a pipette. The pellets in the tubes were air-dried for 15 min to allow the EtOH to evaporate. 30 µl 1 x TE (pH 8.0), 0.3 mg/ml RNase A were added to the pellets. These preparations were stored at 4°C.

2.12.4.7: Diagnostic digest of plasmid DNA

Firstly, the program pDRAW32 was used to choose which enzyme/s would be most suitable for confirming the plasmid's identity by diagnostic digest.

For each clone of each plasmid a1.5 ml microcentrifuge tube containing 2 µl miniprep solution, 0.5 µl restriction enzyme, 2 µl restriction enzyme buffer and 15.5 µl sterile water was prepared. Each 1.5 ml microcentrifuge tube containing a 20 µl final reaction volume was transferred into a 37°C water bath for 1 h and then placed on ice. An undigested control was also prepared using 2 µl miniprep solution and 8 µl sterile water. The appropriate volume of 10 x loading dye was added to the control samples and digests so as the final concentration was 1 x agarose loading dye. The products were run on a 1 % agarose gel as described in 2.12.3.6.

2.12.4.8: Promega Wizard® SV Gel and PCR Clean-up System (DNA purification)

The column was placed into the collection tube. All of the miniprep was transferred into the assembly and incubated for 1 min at room temperature. Each sample was centrifuged at 13,000 g for 1 min at room temperature. The liquid in the collection tube was discarded.

375 ml 95% (v/v) ethanol were added to 75 ml membrane wash solution and then the minicolumn was washed with 700 µl membrane wash solution. The above centrifugation step was repeated and the liquid was discarded. The minicolumn was then washed in 500µl membrane wash solution and then centrifuged at 13,000 g for 5 min at room temperature. When the collection tube was emptied this time, care was taken so as the bottom of the minicolumn was not wetted with the flow through. The samples were then centrifuged at 13,000 g for 1 min at room temperature.

The minicolumn was carefully transferred to a clean 1.5 ml microcentrifuge tube. 50 µl of nuclease-free water were applied directly to centre of the minicolumn whilst ensuring not to touch the membrane with the pipette tip. Each sample was incubated at room temperature for 1 min and then centrifuged at 13,000 g for 1 min at room temperature. The minicolumn was then discarded and the microcentrifuge tube containing the purified DNA was stored at 4°C.

2.12.4.9: MAXIprep DNA preparation (Qiagen)

4 ml of inoculation culture (see 2.12.4.4) were added to ~500 ml of LB broth in a flask and placed in a 37°C shaker (240 rpm) overnight. This culture was centrifuged at 6,000 g for 15 min at 4°C. The supernatant was carefully poured off. At this stage the pellet can be stored at

-20°C. 20 ml of buffer P1, containing 100 μg/ml RNase A, were used to resuspend the pellet, and after this mixture had been split equally into 2 tubes, each one was placed on ice.

Protocol followed for each mixture:

Buffer P2 was checked for precipitation. 10 ml of this buffer were added to each mixture, which was then incubated at room temperature for 5 min. A viscous, non-homogenous liquid formed. Whilst the incubation step was taking place, one QIAfilter Maxi Cartridge was prepared per sample. To do this, a cap was screwed onto the outlet nozzle of a cartridge. This was then placed in a rack. 10 ml of pre-chilled buffer P3 were added to the mixture and was inverted 4-6 times.

The lysate was poured into the barrel of the QIAfilter Maxi Cartridge and incubated at room temperature for 10 min. The cap was then removed from the nozzle and the plunger was gently inserted into the cartridge. Pressure was applied to the plunger and the cell lysate was filtered into a 50 ml tube. 2.5 ml of Buffer ER were added to the filtered lysate. The tube was inverted around 10 times and then incubated for 30 min on ice.

1 QIAGEN-tip 500 per lysate sample was equilibriated by applying 10 ml Buffer QBT. This passed through the column by gravity flow. The filtered lysate was then poured into the QIAGEN-tip and was allowed to enter the resin by gravity flow. The QIAGEN-tip was then washed with 2x30 ml of Buffer QC. The DNA was eluted using 15 ml of Buffer QN and collected in a fresh tube which had been placed underneath the QIAGEN-tip. To the eluted DNA, 10.5 ml of room temperature isopropanol were added and mixed by inversion. This mixture was centrifuged at 15,000 g for 30 min at 4°C. Care was taken not to dislodge the DNA pellet as the supernatant was being poured away. The pellet was washed with 5 ml of endotoxin-free, room temperature 70% (v/v) EtOH. This was centrifuged at 15,000 g for 10 min at 4°C. The supernatant was again carefully discarded. Any remaining EtOH was removed with a pipette. The pellet was air-dried for approximately 10 min (longer if required) and was dissolved in a suitable volume (about 50 μl) of endotoxin-free Buffer TE.

2.12.5: Microscopy

2.12.5.1: TEM processing for cells grown in culture flasks

Solutions prepared prior to protocol

- Double strength fixative
  - -12.5 ml 16% (w/v) paraformaldehyde
  - -10 ml 25% (w/v) glutaraldehyde
  - -25 ml 0.2 M sodium cacodylate buffer

- Single strength fixative
  - -25 ml double strength fixative (see above for recipe)
  - -25 ml 0.1 M sodium cacodylate buffer

- Epon recipe (to mix with propylene oxide for final infiltration)
  - -20 ml Agar100 epoxy resin
  - -DDSA (dodecenyl succinic anhydride) hardener
  - -MNA (methyl nadic anhydride) hardener
  - -BDMA (benzyldimethylamine) accelerator

An equal volume of double strength fixative to cell culture medium was added to the flasks and incubated at room temperature for 5-10 min. After this the fixative was poured off, 10 ml single strength fixative were added to cover the cells. The flasks were incubated at room temperature for 1 h with shaking. The cells were then washed three times in 0.1 M sodium cacodylate for 5 min.

The cells were washed in 1 ml cacodylate buffer and removed from the flask surface using a cell scraper. They were then transferred into a 1.5 ml microcentrifuge tube. The cells were centrifuged at 1,000 g for 5 min. The supernatant was removed and the pellets were 'post-fixed' for 1 h in 1% (w/v) osmium cacodylate in 0.1 M cacodylate buffer. In some of the samples (for example: the tunicamycin treated K599A cells) the pellet was very small and therefore a 1000 g spin for 3 min was carried out. The supernatant was pipetted off and the pellet was washed in 0.1 M sodium cacodylate buffer.

The pellet was gently touched with a cocktail stick to test whether or not it easily fragmented. Providing the pellet remained intact, it was transferred to a glass vial and dehydrated through a series of alcohol additions. This step was carried out in the 1.5 ml microcentrifuge tube if the pellet was not intact.

Alcohol dehydration steps

- 3x5 min 50% (v/v) ethanol washes
- 3x5 min 70% (v/v) ethanol washes
- 3x5 min 95% (v/v)ethanol washes
- 3x10 min 100% (w/v) ethanol washes

The mixture was then infiltrated three times with a mixture of 100% (w/v) alcohol:propylene oxide (50:50), with each infiltration lasting 10 min. Another three 10 min infiltration steps were carried out using propylene oxide. Each sample underwent a final infiltration using a mixture of propylene oxide:resin (50:50) for 1 h to overnight with the lids open.

2.12.4.2: Sectioning and analysis of cells in resin

Ultrathin sections of the cells embedded in the resin were cut using a Leica Reichert Ultracut S ultramicrotome. These were then picked up onto a 200 mesh copper grids and stained using 1% (w/v) alcoholic uranyl acetate and Reynold's lead citrate (Reynold, 1963) for 10 min each. They were examined using a Hitachi H-7600 transmission electron microscope. Electronmicrographs were taken on an AMT Orca-ER digital camera (Deben).

2.12.5.3: Immunofluorescence

The cells for this experiment were cultured on glass cover slips placed in the wells of a 24-well plate.

Preparation:

A section of parafilm was cut and stretched over a glass square to provide a platform upon which the glass cover slips could rest. This was then placed on top of some wet tissue paper in the bottom of a plastic box to ensure that the cover slips did not become dry during the incubation steps described below. The entire box was lined with tin foil making it impenetrable to light. The primary and secondary antibodies were added to thawed PBG in 1.5 ml microcentrifuge tubes (see table 2.5 and 2.6 for dilutions) , then placed on ice.

Fixing process:

The medium was removed from the wells containing the glass cover slips. The cells were washed twice using 1ml of ice-cold PBS. After the second wash, the PBS was not aspirated off the wells. 12 µl drops of ice-cold 4% (w/v) paraformaldehyde (PFA) were pipetted onto the parafilm in the incubation box. The cover slips were removed carefully using fine tweezers and dabbed gently onto dry tissue paper to remove any excess PBS. They were then placed 'face-down' (cells facing down) onto the drops of PFA in the incubation box. The lid

of the box was replaced and the cover slips were incubated with PFA at room temperature for 15 min.

Permeabilisation process:

After the fixing stage was complete, the cover slips were placed into a 24-well plate containing PBS, ensuring they were now 'face-up' (cells facing up). They were washed twice in 1 ml ice-cold PBS. At this stage, the cover slips can be stored in PBS at 4ºC.

10 µl drops of 0.5% (w/v) Triton X-100 (dissolved in PBS) were added to the parafilm in the incubation box, and the cover slips were positioned on top, as before. The lid was replaced and the cover slips were incubated at room temperature for 10 min.

Blocking process:

The cover slips were replaced into the wells (again ensuring they were 'face-up') and washed once in 1 ml of ice-cold PBS. This time, 10 µl drops of 0.5% (w/v) fish gelatin in PBS were added to the parafilm layer. As before, the cover slips were transferred into the box and incubated at room temperature for 15 min.

Antibody staining and mounting slides:

Table 2.5: Primary antibodies for immunofluorescence. Dilutions were made in PBG.

Name	Host	Clonality	Supplier and Product Number	Dilution
Emerin (4G5)	Mo	M	Abcam (ab-49499)	1:200
Sun-1 (282)	R	P	Karakesisoglou lab collection	1:200
Nesprin-2 (pAbK1)	R	P	Karakesisoglou lab collection	1:200

Table 2.6: Secondary antibodies used for immunofluorescence. Dilutions were made in PBG.

Name	Host	Supplier and Product Number	Conjugated dye	Dilution
Anti-mouse IgG	Donkey	Invitrogen A-21202	Alexa Fluor® 488	1:2000
Anti-rabbit IgG	Goat	Invitrogen A-11011	Alexa Fluor® 568	1:2000

10 µl drops of primary antibody were added to the parafilm in the incubation box. The cover slips were transferred directly from the blocking step onto the primary antibody and incubated at room temperature for 1 h. Afterwards, the cover slips were replaced in the wells and washed three times with 1 ml ice-cold PBS. 10 µl drops of the secondary antibody were added to the parafilm layer and the cover slips were incubated for another h at room temperature. During this time, the mounting media was thawed.

The cover slips were again replaced in the wells and were given five washes in 1 ml ice-cold PBS. Approximately 7 µl of mounting media was added to a slide for each cover slip. The cover slips were dabbed gently on tissue paper as above and lowered 'face down' onto the solution on the slides. These were placed flat in a slide box and stored in the fridge to dry overnight before being imaged.

2.12.5.4: Confocal microscopy (visualisation of the ER)

MEFs were seeded onto 9.6 cm^2 glass-bottomed plates to allow visualisation under the confocal microscope. There were given 24 h to adhere to the plate, followed by 24 h of tetracycline treatment. Tunicamycin was then added and the cells were taken down to image as soon as it was noticed they were beginning to detach from the surface of the plate. This was done to avoid not being able to visualise the cells due to them completely detaching from the plate as a result of apoptosis.

1 µl of ER-Tracker™ Red (pre-dissolved in DMSO) was added per ml of culture media and left to incubate in the dark at 37°C for approximately 10 min. The media was then replaced. The cells were then visualised using the Zeiss 510 Meta CLSM inverted microscope. The lipophilic dye stains the ER red by binding sulphonylurea receptors of the potassium channel in the ER membrane (Invitrogen). Making sure the settings of the microscope were constant between taking images, approximately 10 pictures of each cell and treatment were taken.

Chapter 3

The protein expression profile of WT, D711A and K599A human IRE1α in mammalian cells during ER stress

3.1: Rationale for studying protein expression in the three cell lines

Several proteins induced by the UPR have been implicated in both cell life and death. As discussed in chapter 1, *XBP-1* splicing, courtesy of the IRE1α RNase domain, has been shown to play an integral role in the cytoprotective component of the UPR (Gupta *et al.*, 2010; Han *et al.*, 2008; Sado *et al.*, 2009; Lin *et al*,., 2009, Reimold *et al*., 2000). Regarding kinase activity of IRE1α, some groups demonstrated it is responsible for aiding cell death mechanisms via JNK activation (Nishitoh *et al.*, 2002; Urano *et al.*, 2000). However, a separate group more recently suggested the kinase's principal function in terms of yeast cell fate, was to control the state of the endoribonuclease and thus has at least some protective function (Rubio *et al*., 2011). The MTT and PARP-1 cleavage in the appendix show that the D711A-hIRE1α and K599A-hIRE1α mutants undergo cell death before the WT-hIRE1α cells, raising the possibility that the kinase activity of hIRE1α is important for cell survival. This project was hence designed to bring certain mechanisms via which the kinase may dictate cell fate decisions to attention, principally by comparing transcription and protein levels, and ER physiology during ER stress in the three cell lines.

The differences in protein levels were investigated in this chapter. Many of the proteins analysed have been demonstrated to play a role in ER stress-induced cell death. Since the K599A-hIRE1α cells have a compromised cytoprotective response (Figure A1.3), the cell death markers should be elevated in this mutant. By comparing the D711A-hIRE1α response to the one seen in the WT-hIRE1α and K599A-hIRE1α cells, some light should be shed onto the role the kinase plays in cell life decisions downstream of UPR activation.

To validate activation and expression of human IRE1α, phospho-IRE1α and IRE1α were probed for. BIP was also imaged so as to confirm that ER stress induction was taking place as expected. Proteins involved in UPR-mediated cell death include caspase-12, caspase-3 (an executioner caspase activated downstream of caspase-12 cleavage), PARP-1, phospho-JNK and CHOP (Kim *et al*., 2006). All of these were analysed by Western blotting. To evaluate whether or not there are differences in protein translation potential, phospho-eIF2α and total eIF2α were probed for. LC3 was also analysed, so as to help indicate differences in the autophagic programme between the three difference cell lines.

3.2: Differences in protein expression in the three MEF cell lines

Using the culture conditions described in chapter 2, phospho-IRE1α and IRE1α proteins were probed for to confirm the tetracycline-inducible expression system was working as expected. Western blotting confirmed that human IRE1α was induced after 4 h of tetracycline treatment in all three cell lines, and expression reached a maximum after 10 h of this treatment, independent of the presence of tunicamycin. A low level of IRE1α phosphorylation was observed in the WT-hIRE1α samples after 4 h of induction, suggesting that overexpression had caused dimerisation and subsequent autophosphorylation of this UPR signal transducer in the ER membrane. There was a large increase in phospho-IRE1α expression between 4 and 10 h of tetracycline addition, which was maintained throughout the remainder of the time course and again was independent of tunicamycin treatment. The antibody used against phospho-IRE1α specifically detects phosphorylation of the S724 site on hIRE1α. Phosphorylation of this particular site was not observed in either of the mutant cell lines, confirming impaired kinase activity.

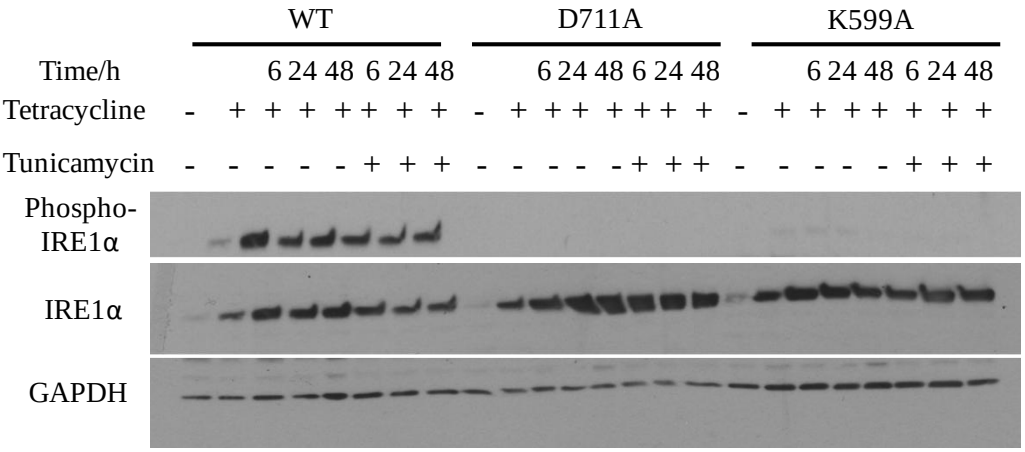

Figure 3.1: Western blot showing levels of IRE1α and its phospho-form from WT-hIRE1α, D711A-hIRE1α and K599A-hIRE1α MEF lysates. – and + indicate absence or presence of the appropriate drug, respectiely. Cells treated with tetracycline were harvested after 4 h, then after 6, 24 and 48 h of combined tetracycline and DMSO treatment. ER-stressed cells were harvested after 6, 24, and 48 h of combined tetracycline and tunicamycin treatment. GAPDH was used as the loading control. Figure A3.2 represents the repeat obtained.

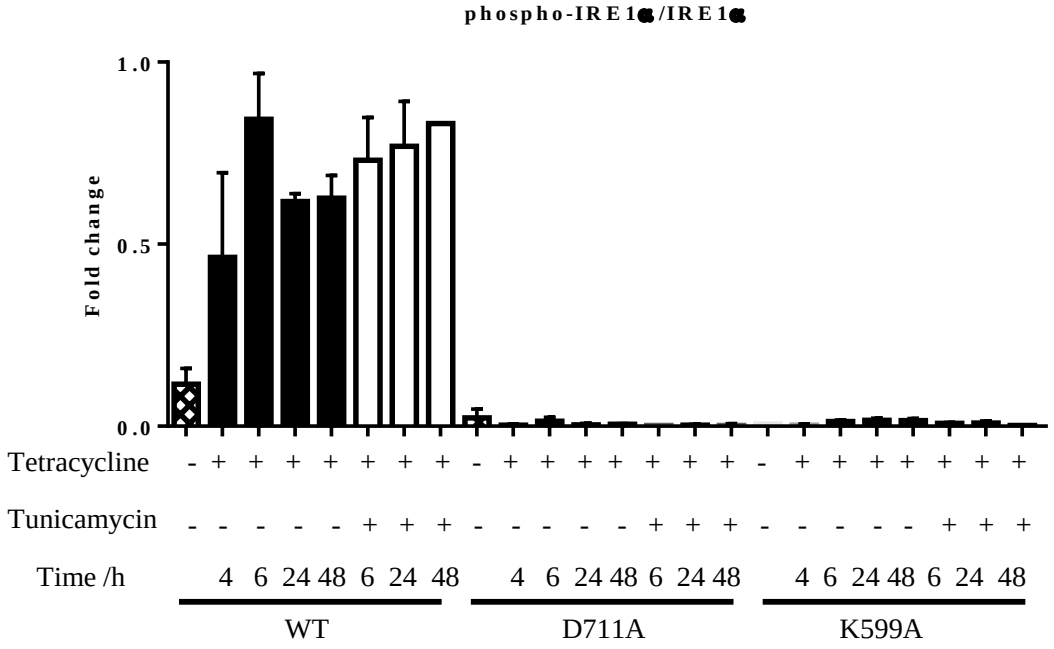

Figure 3.2: Graphical representation of the Western blot in Figure 3.1. The bands were quantified using ImageJ and phospho-IRE1α/IRE1α was calculated. The error bars show the standard error. An unpaired t-test was carried out and the confidence limits were set to 95%. There was no significant difference between the tetracycline-only and the tetracycline and tunicamycin treated cells in the WT-hIRE1α.

BIP was also used as a positive control to highlight induction of ER-stress. Since a protocol for the BIP/GRP78 antibody had not been established, ECL+ was initially used to visualise the bands on the PVDF membrane. This gave a very smeary blot at the molecular weight predicted for this protein. However, the second time the treatment course was run, only ECL was used, and this showed much clearer, more distinct bands in all three cell lines. In the WT-hIRE1α and D711A-hIRE1α cells there was a large upregulation of BIP 24 h after ER-stress induction. This increase was slightly less impressive in the K599A-hIRE1α mutant, which is consistent with Western blotting carried out in XBP-1 knockout MEFs by Lee *et al*., 2003. However, this is not consistent with what was observed by Tirasophon *et al* (2000) who observed no differences in BIP induction between WT and *ire1α*$^{-/-}$ cells. Therefore, after obtaining a repeat for these data, it may be useful to compare BIP mRNA and protein levels in *ire1α*$^{-/-}$ cells and K599A-hIRE1α cells.

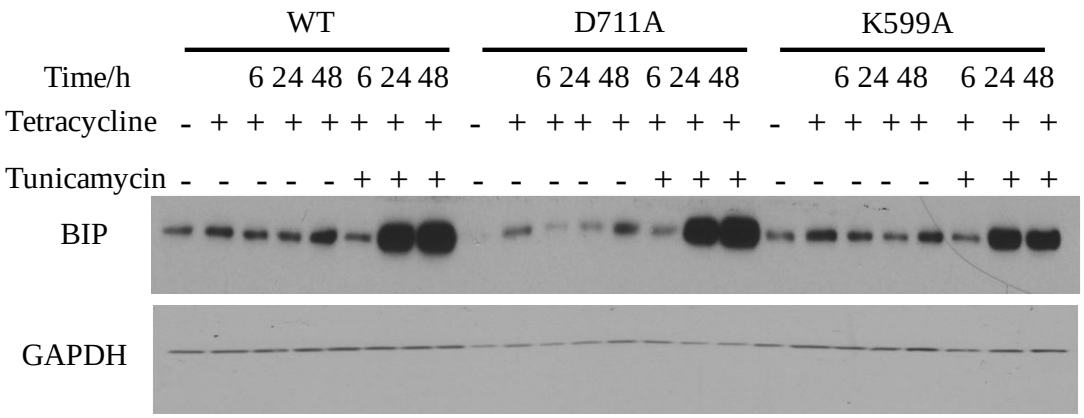

Figure 3.3: Western blot showing levels of BIP from hIRE1α WT-hIRE1α, D711A-hIRE1α and K599A-hIRE1α MEF lysates. – and + indicate absence or presence of the appropriate drug, respectively. Cells treated with tetracycline were harvested after 4 h, then after 6, 24 and 48 h of combined tetracycline and DMSO treatment. ER-stressed cells were harvested after 6, 24, and 48 h of combined tetracycline and tunicamycin treatment. GAPDH was used as the loading control.

To address any differences in cell fate between the three different cell lines, caspase activity was investigated. Caspase activation is known to occur downstream of ER stress (Yoneda *et al.*, 2001). One way of assessing caspase activity is by analysing PARP-1 cleavage, as PARP-1 is a target of active caspases (Oliver *et al.*, 1998 and Lazebnik *et al.*, 1994). As expected, PARP-1 cleavage levels were elevated in all cell lines after 24 h of ER-stress, and increased further after 48 h (Figure 3.8 and 3.9). In both repeats, it was apparent that the PARP-1 cleaved fragment was the most abundant in the K599A-hIRE1α mutant. Since PARP-1 is a marker of apoptosis, these data suggest that cell death was most advanced in this cell line. Compared to the WT-hIRE1α, the D711A-hIRE1α mutant only displayed very slightly higher levels of PARP-1 cleavage that was not statistically significant. These results imply that the kinase- and RNase-dead mutant was most compromised.

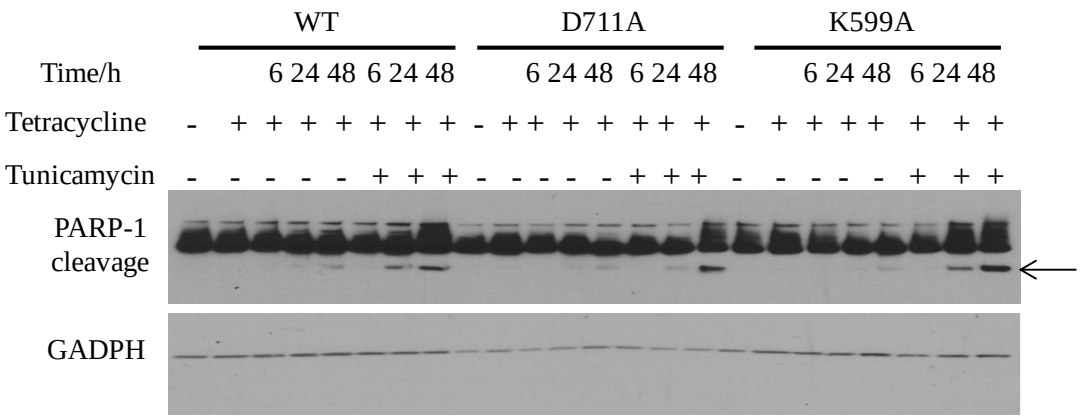

Figure 3.4: Western blot showing the ratio of cleaved PARP-1 to total PARP-1 from WT-hIRE1α, D711A-hIRE1α and K599A-hIRE1α MEF lysates. The arrow represents the cleaved fragment. – and + indicate absence or presence of the appropriate drug, respectively. Cells treated with tetracycline were harvested after 4 h, then after 6, 24 and 48 h of combined tetracycline and DMSO treatment. ER-stressed cells were harvested after 6, 24, and 48 h of combined tetracycline and tunicamycin treatment. GAPDH was used as the loading control. Figure A3.3 represents the repeat obtained.

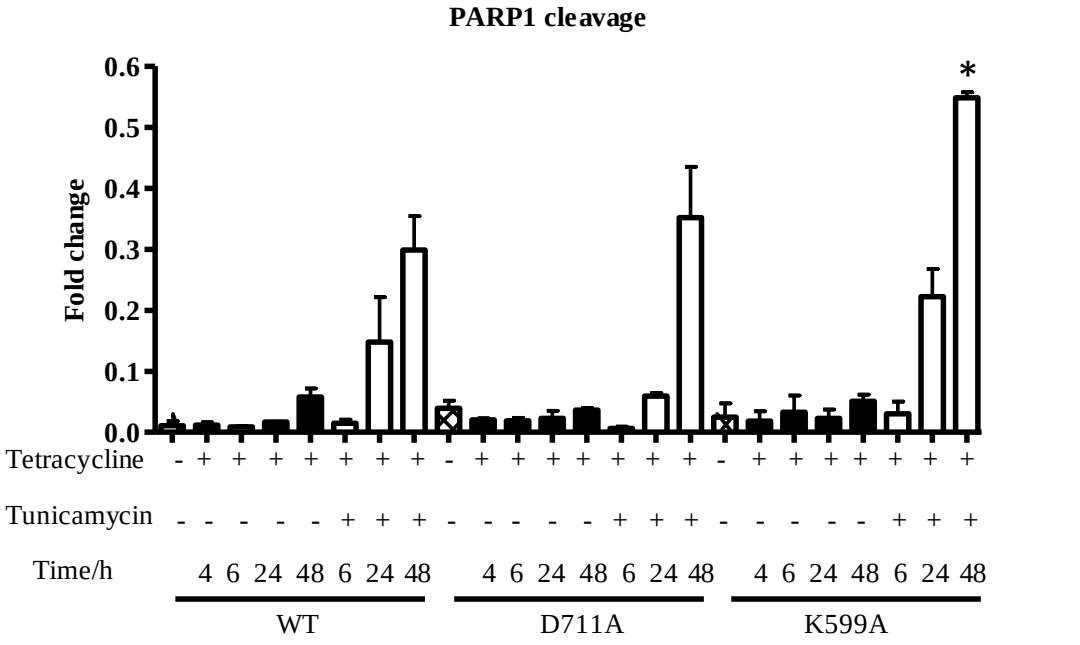

Figure 3.5: Graphical representation of the Western blot in Figure 3.4. The bands were quantified using ImageJ and cleaved PARP-1/total PARP-1 was calculated. The error bars show the standard error. An unpaired t-test was carried out and the confidence limits were set to 95%. * p = 0.0472 (WT-hIRE1α tunicamycin treated vs K599A-hIRE1α tunicamycin treated).

As with PARP-1, caspase-3 cleavage was increased in each of the cell lines when ER stress was induced. Consistent with the highest levels of PARP-1 cleavage in the K599A-hIRE1α mutant, caspase-3 cleavage was also highest in this cell line (Figure 3.10 and 3.11). These observations from the K599A-hIRE1α mutant are consistent with published data, where forced activation of the RNase domain increased cell viability (Han *et al.*, 2008; Lin *et al.*,

2009). It would appear that activation of this caspase was intermediate in the D711A-hIRE1α mutant, however, another repeat is required to validate these data. This may help explain why the D711A-hIRE1α cells die before the WT-hIRE1α cells, as was seen when observing cells in tissue culture using light microscopy (data not shown).

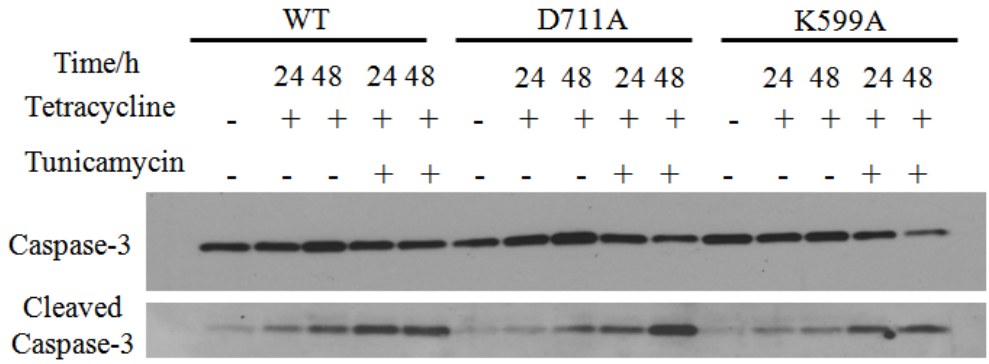

Figure 3.6: Western blot showing the ratio of caspase-3 cleavage to total caspase-3 form from WT-hIRE1α, D711A-hIRE1α and K599A-hIRE1α MEF lysates. – and + indicate absence or presence of the appropriate drug, respectively. Cells treated with tetracycline were harvested after 24 and 48 h of combined tetracycline and DMSO treatment. ER-stressed cells were harvested after 24 and 48 h of combined tetracycline and tunicamycin treatment.

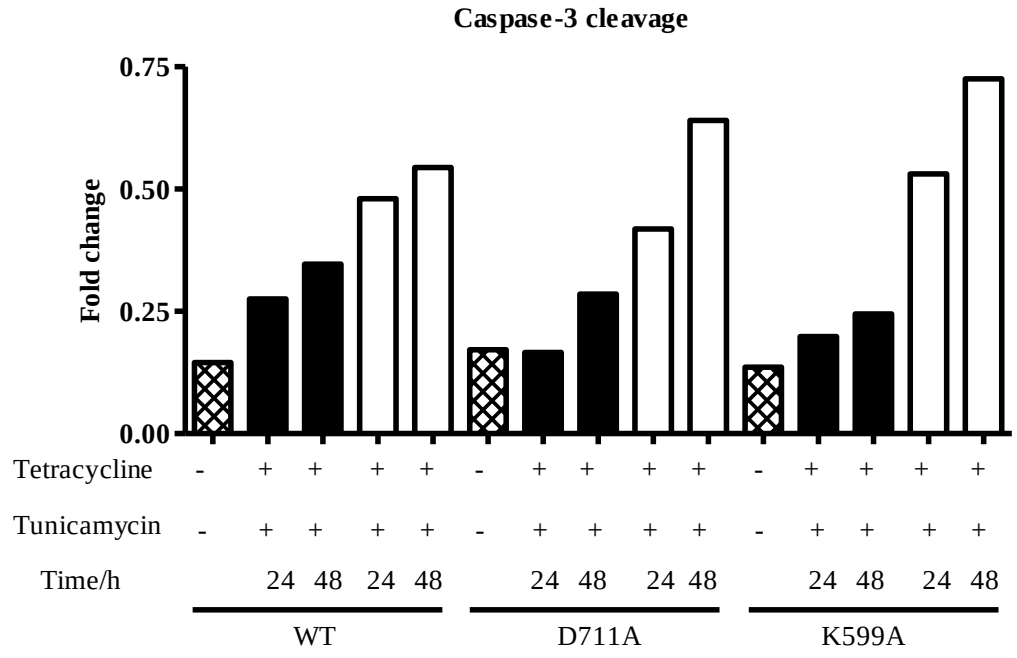

Figure 3.7: Graphical representation of the Western blot image in Figure 3.6. The bands were quantified using ImageJ and cleaved caspase-3/total caspase-3 was calculated.

Unfortunately, there was not enough time to optimise the Western blotting conditions for caspase-12, which is upstream of caspase-3 cleavage (reviewed in Lai *et al*., 2007). It was found that if the primary antibody was incubated at room temperature for 4 h after incubation at 4°C overnight, then the image seen in figure 3.12 was obtained. Here the 'upper' bands were observed to be just above the 55 kDa mark, and the lower bands were

very slightly below this mark. Since the predicted molecular weights of the uncleaved and cleaved caspase-12 are 55 and 42 kDa respectively, it is possible that the top band may be non-specific. Another reason this may also be true is because if the top bands did represent the uncleaved caspase-12 form, then it suggests that there was as much caspase-12 cleavage in the WT-hIRE1α untreated cells as there was in the K599A-hIRE1α tunicamycin treated cells (48 h). Further research needs to be conducted to prove that the lower band is uncleaved caspase-12. Loading a larger amount of protein onto the gel and increasing film exposure times will help identify the lower band.

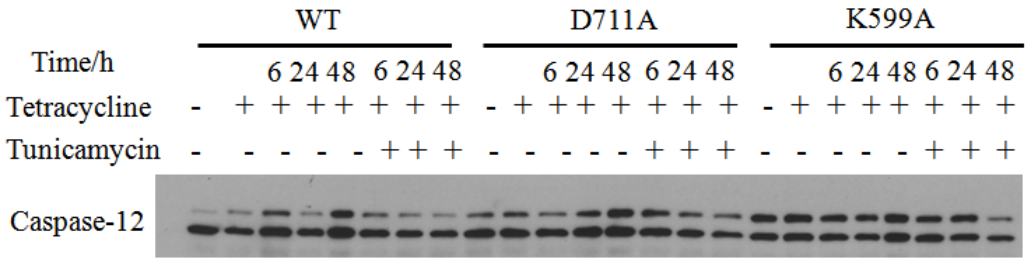

Figure 3.8: Western blot showing the ratio of caspase-12 cleavage to total caspase-12 form from WT-hIRE1α, D711A-hIRE1α and K599A-hIRE1α MEF lysates. – and + indicate absence or presence of the appropriate drug, respectively. Cells treated with tetracycline were harvested after 4 h, then after 6, 24 and 48 h of combined tetracycline and DMSO treatment. ER-stressed cells were harvested after 6, 24, and 48 h of combined tetracycline and tunicamycin treatment.

CHOP$^{-/-}$ MEFs are protected against cell death downstream of the UPR being activated (Zinszner *et al*., 1998) and this protein is often used as marker of ER stress-induced apoptosis. It was hypothesized that expression of this protein would be the lowest in the WT cells. From initial observation of the Western blot, it seemed as though CHOP was most upregulated in the K599A-hIRE1α mutant, followed by D711A-hIRE1α and finally WT-hIRE1α (Figure 3.13). This was expected since endoribonuclease activity of IRE1α confers cytoprection through XBP-1. It also correlated well with figure A3.4. However, upon normalisation to GAPDH, a different pattern emerged, where the highest levels of CHOP were in the D711A-hIRE1α mutant after 24 h of ER stress induction. Since the K599A-hIRE1α mutant should, in theory, be most compromised, and because the CHOP qPCR data supported this idea (figure 4.3), it is possible that the loading control conditions require further optimisation. It could be that a 1:20,000 dilution of the GAPDH antibody is too weak for such an abundant protein and thus probing for GAPDH should be repeated with a higher concentration of this antibody.

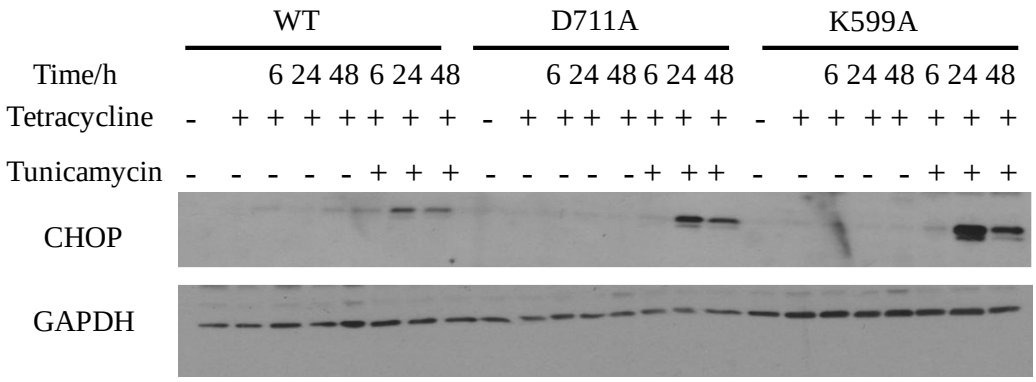

Figure 3.9: Western blot showing CHOP activation from WT-hIRE1α, D711A-hIRE1α and K599A-hIRE1α MEF lysates. – and + indicate absence or presence of the appropriate drug, respectively. Cells treated with tetracycline were harvested after 4 h, then after 6, 24 and 48 h of combined tetracycline and DMSO treatment. ER-stressed cells were harvested after 6, 24, and 48 h of combined tetracycline and tunicamycin treatment. GAPDH was used as the loading control.

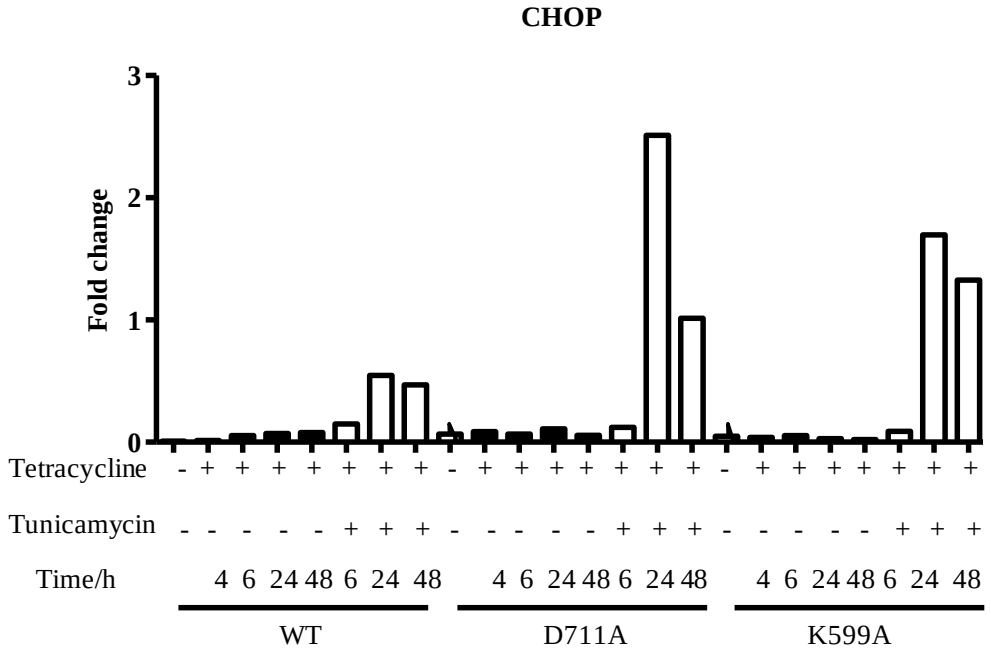

Figure 3.10: Graphical representation of the Western blot image in Figure 3.9. The bands were quantified using ImageJ and normalised against GAPDH.

Since translation of *CHOP* mRNA occurs downstream of the PERK-peIF2α-ATF4 branch (Ohoka *et al*., 2005) it was expected that the phospho-eIF2α expression profile would show a similar pattern relative to that observed for CHOP expression. However, this was not the case, and it was the WT-hIRE1α which consistently displayed the highest levels of phospho-eIF2α during ER stress (Figure 3.15 and 3.16). More data will need to be obtained to determine the significance of these findings. This phenomenon may contribute to the earlier death of the mutant cells before the WT-hIRE1α. It is known that phosphorylation of the eIF2α subunit blocks general (but not all) mRNA translation into protein (Harding *et al.*, 2000) reducing the rate of translocation of new proteins into the ER lumen. Conversely,

dephosphorylation of this subunit restarts polypeptide production and it has been shown that inhibiting this reaction using salubrinal increases cell viability (Boyce *et al*., 2005). It may be informative to use salubrinal in conjunction with cell death assays, such as MTT, to determine whether any of the three cell lines displayed better survival as a result of this treatment during ER stress.

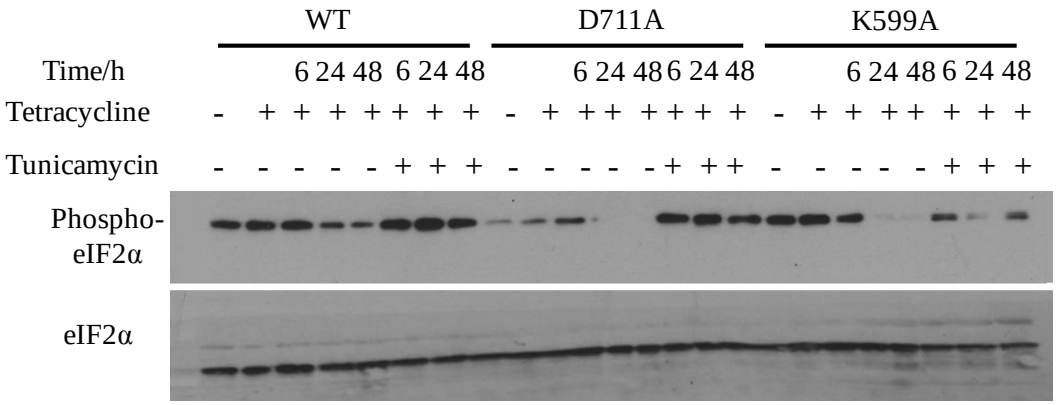

Figure 3.11: Western blot showing eIF2α and its phospho-form from WT-hIRE1α, D711A-hIRE1α and K599A-hIRE1α MEF lysates. – and + indicate absence or presence of the appropriate drug, respectively. Cells treated with tetracycline were harvested after 4 h, then after 6, 24 and 48 h of combined tetracycline and DMSO treatment. ER-stressed cells were harvested after 6, 24, and 48 h of combined tetracycline and tunicamycin treatment. Figure A3.5 represents the qualitative repeat obtained.

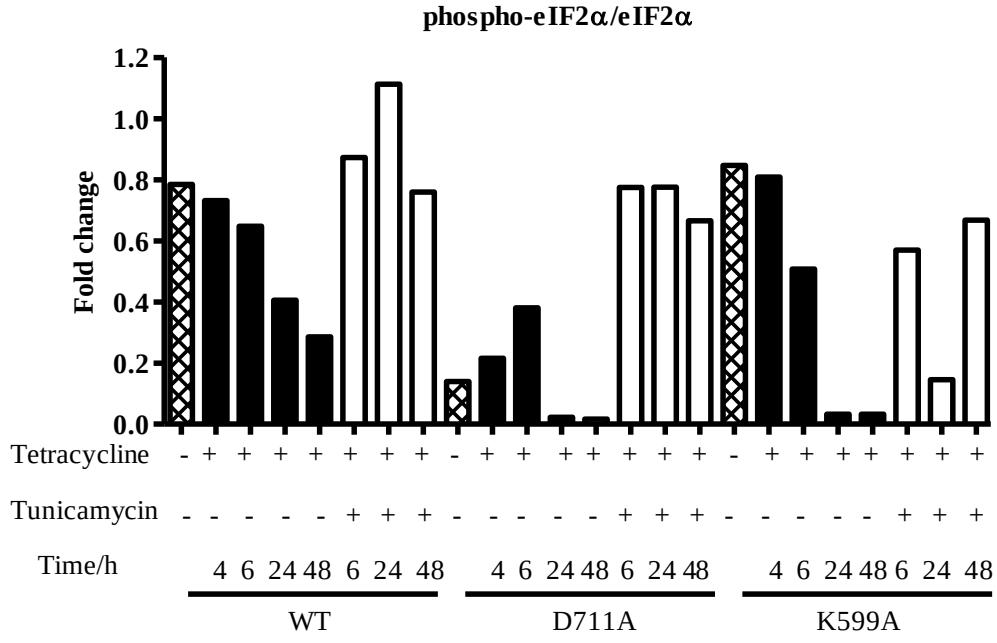

Figure 3.12: Graphical representation of the Western blot in Figure 3.11. The bands were quantified using ImageJ and phospho-eIF2α/total eIF2α was calculated.

JNK phosphorylation should also indicate differences in cell viability (see Chapter 1), however, it was found that levels did not change dramatically during ER-stress. There was only a real increase in phospho-JNK after 6 h tetracycline addition, independent of cell line and independent of whether tunicamycin was added or not. The disappearance of the phospho-JNK signal at 24 h tetracycline treatment was also consistent across the three cell lines. There is a small increase in the intensity of the 54 kDa phospho-JNK form (uppermost band of the top panel in Figure 3.17) after 48 h tunicamycin treatment. Again, this does not differ between each of the cell lines and does not indicate as strong an expression as 6 h tetracycline treatment. Overall, one can conclude that using 100 ng/ml tunicamycin to induce ER stress, does not elicit a different response in terms of JNK activation in either WT-hIRE1α, D711A-hIRE1α or K599A-hIRE1α cells.

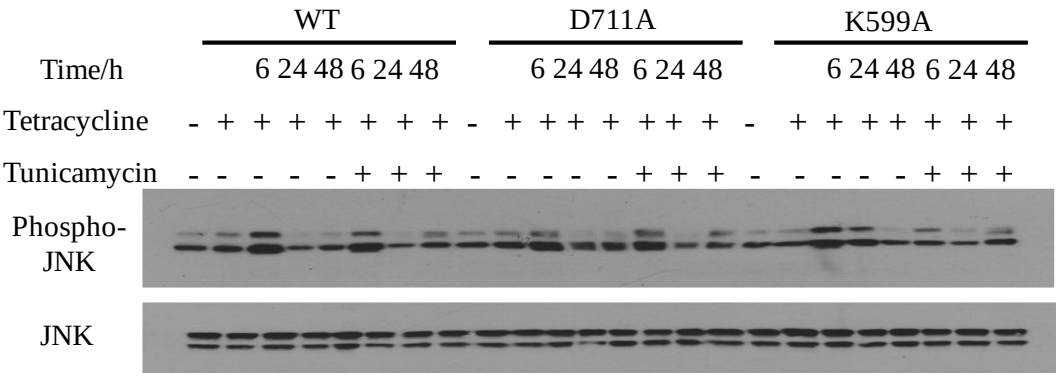

Figure 3.13: Western blot showing JNK and its phospho-form from WT-hIRE1α, D711A-hIRE1α and K599A-hIRE1α MEF lysates. – and + indicate absence or presence of the appropriate drug, respectively. Cells treated with tetracycline were harvested after 4 h, then after 6, 24 and 48 h of combined tetracycline and DMSO treatment. ER-stressed cells were harvested after 6, 24, and 48 h of combined tetracycline and tunicamycin treatment. Figure A3.7 represents the qualitative repeat obtained.

Finally, since autophagy is known to play a role in determining cell fate decisions, LC3 conversion was analysed. Lipidation of LC3-I to LC3-II is thought to signify whether or not autophagy is taking place and can simply be detected by Western blotting. It was hypothesised that autophagy may have been compromised in the mutant cell lines, therefore contributing to their earlier cell death phenotype compared to the WT cells. However, figure 3.18 and 3.19 indicate the lowest conversion in the WT-hIRE1α cells during ER stress. Further experimentation is required to validate the significance of these data and to determine the autophagic state in each of the cell lines, since it was recently found that LC3 conversion could in fact indicate a blockage in the process of autophagy (Xavier *et al.*, 2008).

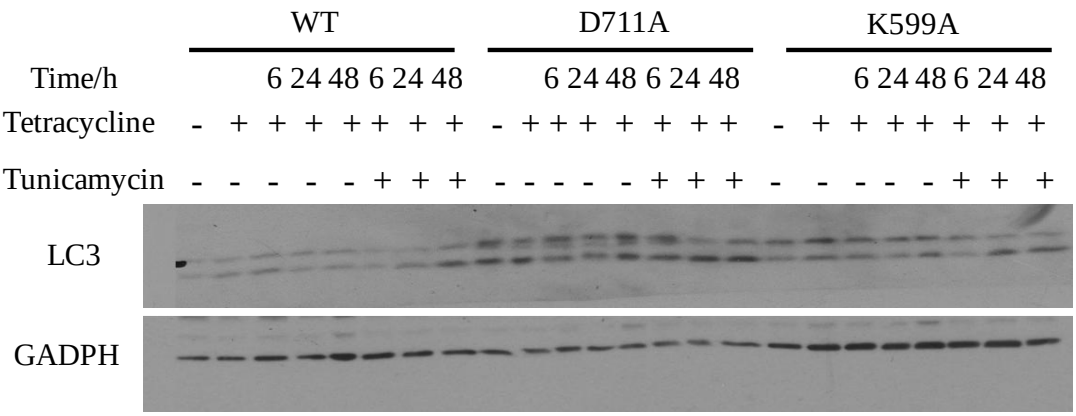

Figure 3.14: Western blot showing conversion of LC3-I (19 kDa) to LC3-II (17 kDa) from WT-hIRE1α, D711A-hIRE1α and K599A-hIRE1α MEF lysates. – and + indicate absence or presence of the appropriate drug, respectively. Cells treated with tetracycline were harvested after 4 h, then after 6, 24 and 48 h of combined tetracycline and DMSO treatment. ER-stressed cells were harvested after 6, 24, and 48 h of combined tetracycline and tunicamycin treatment. GAPDH was used as the loading control.

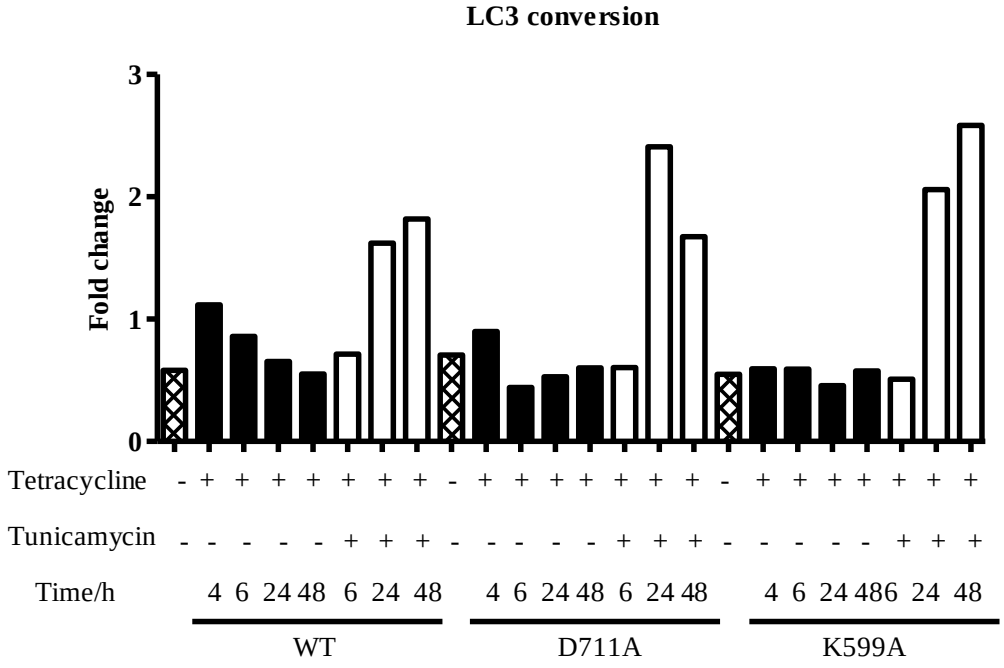

Figure 3.15: Graphical representation of the Western blot image in Figure 3.14. The bands were quantified using ImageJ and lipidated LC3/total LC3 was calculated.

3.3: Discussion

In summary, the highest PARP-1 cleavage was observed in the K599A-hIRE1α cells. However, there were repeatable differences detected in CHOP expression and phosphorylation of the eIF2α subunit in the D711A-hIRE1α cells compared to their WT counterparts. These results suggest that IRE1α kinase activity does play some role in determining cell fate of these ER-stressed MEFs.

Analysing both PARP-1 cleavage and caspase-3 activation, the K599A-hIRE1α cells appear to be most compromised in terms of cell fate downstream of ER stress. However, the lack of statistical significance in PARP-1 cleavage between the WT-hIRE1α and D711A-hIRE1α MEFs does not conclude that cell death does not happen earlier in the latter cells. PARP-1 cleavage analysed in this project is only a marker of apoptosis (Gobeil *et al*., 2001) and therefore, one cannot rule out that the D711A-hIRE1α cells may be dying via the necrotic route or another cell death mechanism. Krysko *et al.*, 2008, describe a set of methods, which together can be used to discriminate between apoptosis and necrosis. It would be interesting to determine whether these different cell lines were dying by taking different cell death pathways, as it would help characterise the role of IRE1α kinase activity.

It does, however, seem as though the kinase domain plays some role in cross-talk between IRE1α and PERK. It would be useful to show that the differences in phospho-eIF2α observed between the mutants and WT-hIRE1α are due to PERK activation by using PERK knockout MEFs, as three other proteins are able to phosphorylate eIF2α (referenced in Boyce *et al*., 2005). Additonally, one cannot rule out that the differences in eIF2α phosphorylation are due to differential induction of one of the eIF2α phosphatases.

Supporting the idea of cross-talk between IRE1α and PERK, it does appear that the D711A-hIRE1α mutant is more susceptible to cell death due to CHOP upregulation. To further support the observation that CHOP levels are elevated in the D711A-hIRE1α MEFs, it would be useful to show an increase in expression of TRB3 in D711A-hIRE1α by Western blotting. This death-inducing protein is downstream of CHOP (Ohoka *et al*., 2005), and *TRB3* mRNA expression was found to be upregulated in D711A-hIRE1α expressing cells by qPCR analysis (Chapter 4).

Similar to eIF2α, the phosphorylation status of JNK is dependent on multiple stress pathways (Lui and Lin, 2005). Since there were no differences in JNK phosphorylation when the three cell lines were treated with tunicamycin, it would be informative to check whether the response was any different using other ER stress inducing drugs, such as thapsigargin, subtilaseAB_5 or DTT. Of course, the appropriate concentration of these drugs would first have to be optimised to generate similar levels of ER stress compared to 100

ng/ml tunicamycin. However, some of these results could be difficult to interpret not least because JNK responds to different cellular stresses, but also because of off-target effects of drugs.

Finally, autophagy is a likely candidate which could help account for the differences in cell death observed. Due to the fact that there seemed to be more lysosomal structures in the WT-hIRE1α cells (See Figure 5.4) it would seem there was an increased autophagic response in the WT-hIRE1α cell compared to the mutants (Ogata *et al*., 2006). However, the upregulation of CHOP and its downstream target, TRB3 (see Chapter 4) in the mutant MEFs suggests there should be an increased autophagic response, since TRB3 inhibits the Akt/mTORC autophagic-blocking route (Salazar *et al*., 2009). This would also be consistent with the report which concluded that IRE1α kinase activity blocked autophagy (Lee *et al.*, 2011). In which cells autophagy is effective in needs to be answered using the mCherry-GFP-LC3b reporter construct, which was used by Lee *et al*., in 2011. Use of this plasmid has been shown to differentiate between autophagosomes and mature lysosomes, with the green luminescence produced by the GFP becoming less intense in the lower pH environment of the lumen of the mature lysosome (Pankiv *et al*., 2007). Further research must be conducted to elucidate whether autophagy is beneficial or detrimental in this particular model system.

Chapter 4

Investigating the transcriptional profile and the RIDD pathway as part of the UPR in WT, D711A and K599A human IRE1α mouse embryonic fibroblasts

4.1: Rationale for studying changes in gene induction between the three cell lines

It is well established that when the UPR is activated in mammalian cells, both spliced XBP-1 and cleaved ATF6 serve as two of the primary transcription factors to upregulate a large number of genes. It has been proposed that ATF6 is actually required to upregulate *XBP-1*, which can then undergo splicing by IRE1 (Yoshida *et* al., 2001). These two transcription factors are principally involved in trying to restore homeostasis within the ER (Lai *et al*., 2006). The subset of genes that were analysed by qPCR in this project, can be segregated into those which contribute to cell death, those which reside in the ER lumen (most of which have chaperone or co-chaperone activity) and those which contribute to ERAD.

Early work on the transcriptional profile of IRE1 demonstrates that the Ire1p-Hac1p pathway is required for induction of genes such as *KAR2*, which is the yeast homolog of *BIP* (Cox and Walter, 1996). In addition, BIP expression was more recently shown to be dependent on *XBP-1* splicing in fruitfly cells (Hollien and Weissman, 2006). However, in mammalian systems, the UPR seems to have deviated from this and probably relies on more than one transcription factor. Several groups have attempted to characterise which genes are strictly dependent on either XBP-1, ATF6, or a combination of these two (Lee *et al*., 2003, Yamamoto *et al*., 2007, Adachi *et al*., 2008 and Shoulders *et al*., 2013). Subsequently, a large amount of Northern blot, microarray and proteomics analyses have been carried out highlighting the importance of the IRE1α RNase domain in the transcriptional program of the UPR. However, very few studies have been dedicated to investigating whether or not the kinase activity of this transmembrane protein has any influence on which genes are expressed. For this reason qPCR analysis was carried out on the three MEF cell lines to help characterise in what ways the kinase-dead mutant might be transcriptionally deficient.

Apart from IRE1α and ATF6, the PERK branch is also associated with upregulation of certain genes *via* the phospho-eIF2α pathway. It is understood that although phosphorylation of this subunit of the eIF2 complex attenuates general translation, translation of mRNAs which harbour upstream open reading frames (uORFs) is induced (Kozak, 2002). In mammalian cells, one of these targets is the ATF4 transcription factor, which harbours two of these uORFs (Vattem and Wek, 2004). In 2011, it was shown that ATF4 along with a dimerisation partner, is capable of causing the transcription of CHOP, a protein whose function is mainly linked to cell death (Badiola *et al*., 2011). CHOP is a transcription factor which is responsible for the dephosphorylation of eIF2α via upregulation of GADD34. GADD34 can then direct the phosphatase activity of PP1 towards phospho-eIF2α (Brush *et al*., 2003). Dephosphorylation of this subunit means that protein translation is now free to restart and therefore the lumen of the ER can become full of newly synthesised polypeptides

before actually recovering from the original stress. This is one reason for linking CHOP upregulation with ER stress –related apoptosis.

Another mechanism hypothesised to encourage cell death downstream of CHOP involves TRB3. *TRB3* mRNA expression was shown to follow CHOP expression in two separate studies (Ohoka *et al*., 2005 and Shang *et al*., 2010). CHOP cooperates with ATF4 to engage with the *TRB3* promoter and cause its transcription (Ohoka *et al*., 2005). Exactly how TRB3 contributes to cell death is unknown, however one group suggested it inhibits the prosurvival function of Akt by binding it (Du *et al*., 2003). This is supported by a publication which shows that the TRB3 mediated Akt inhibition can drive the cell into apoptosis by increasing autophagic activity (Salazar *et al*., 2009).

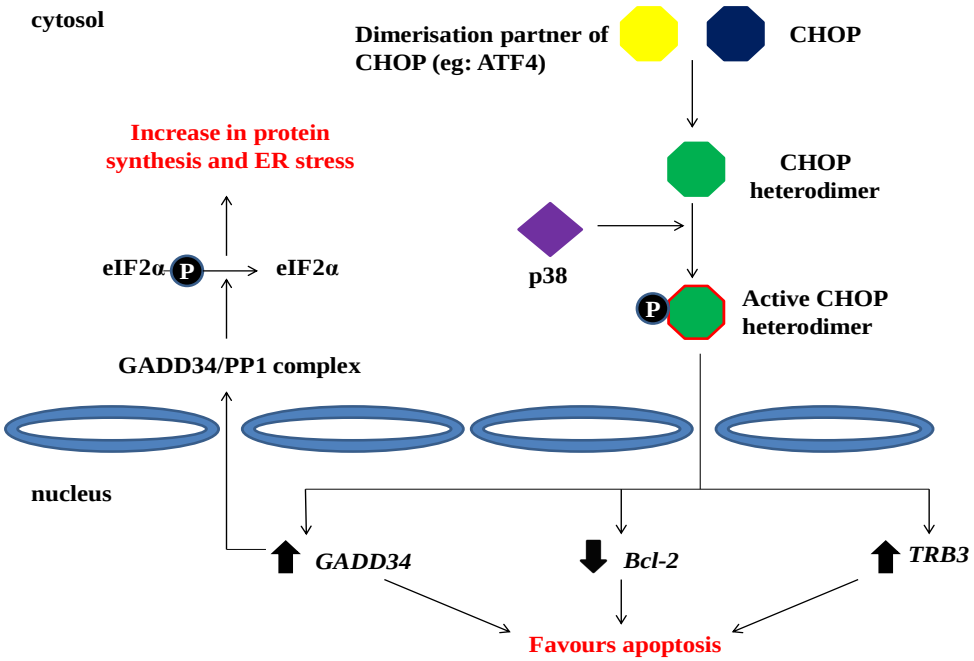

Figure 4.1: Illustration of the result of CHOP activation.

Due to the fact that CHOP plays a role in ER stress determined cell fate, this gene and downstream *GADD34* and *TRB3* were also analysed by qPCR. This was done in order to understand whether compromising the function of human IRE1α caused an over-compensatory response downstream of PERK.

The main hypothesis for the differences in transcription between WT-hIRE1α, D711A-hIRE1α and K599A-hIRE1α cells, is that the latter mutant is likely to have either decreased or elevated levels of transcript in comparison to the WT-hIRE1α. This would be due to lack of XBP-1(s), or over-compensation by ATF6(f), respectively. Alternatively, other UPR transcription factors could also play a role. The K599A-hIRE1α may display no

transcriptional differences, indicating that XBP-1(s) is not necessary for effective transcription of the gene under investigation. The principal objective of carrying out this qPCR analysis was to find evidence for differences between the WT-hIRE1α and D711A-hIRE1α cells, so as to help understand how the latter mutant is compromised. The level of involvement of the kinase domain for the transcription of each gene will be apparent depending on whether its profile is more similar to that of the WT-hIRE1α or the K599A-hIRE1α cells.

4.2: The changes in expression of induced genes between WT-hIRE1α and mutant MEFs

Each qPCR was set up on the RotorGeneQ real-time PCR machine and the data were analysed on the accompanying software. It was ensured that all primers were tested in reactions which did not contain any template cDNA, so as to ensure primer dimers or any contaminant were not responsible for the peak seen in the melt curve. All data presented here were normalised to the housekeeping gene β-actin. For normalising, the $2^{-\Delta\Delta C}{}_t$ method was used, as only the relative gene expression was of interest, rather than the absolute copy number (Livak and Schmittgen, 2001). The three MEF cell lines were treated using the time course described below.

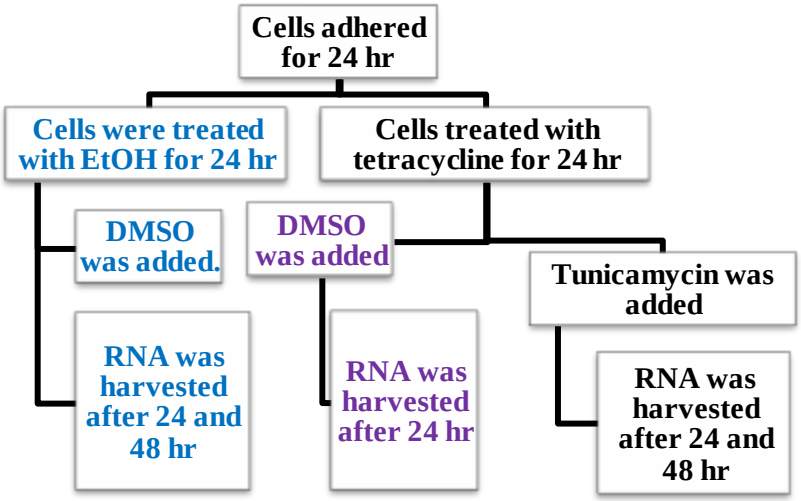

Figure 4.2: Flow chart indicating the treatments for the control and ER-stressed cells. The blue text highlights the treatments for the control cells, and the purple and black routes highlight the treatments for the tetracycline-only treated cells and the ER-stressed cells, respectively. Cells were incubated in a CO_2 incubator at 37°C. Details of chemical concentrations can be found in Chapter 2.

4.2.1: Induced genes whose function is associated with cell death

It was hypothesised that at least one of the mutants would display a higher level of *CHOP* expression relative to the WT, since partial or full loss of IRE1α function should compromise the cell during ER stress. As it can be seen from figure 4.3, *CHOP* expression was induced in all three cell lines after 24 h of ER stress induction. There was a smaller increase in transcripts between 24 and 48 h tunicamycin treatment. Any differences between the WT-hIRE1α and D711A-hIRE1α were not significant. The fold change in *CHOP* during ER stress in the K599A-hIRE1α mutant was consistently seen to be at least double the induction levels in the WT-hIRE1α and D711A-hIRE1α cells. Despite this, the *p* value obtained when comparing the WT-hIRE1α and K599A-hIRE1α using an unpaired t-test, was 0.0563. This falls just outside the 95% confidence limits, and therefore a repeat is required to validate the significance of these findings. The difference between the D711A-hIRE1α and K599A-hIRE1α cells was significant, indicating that loss of the RNase activity *in addition* to loss of kinase activity leads to increased levels of this death-inducing protein. However, what is observed in the K599A-hIRE1α mutant does not correlate with what was observed in the original publication regarding the transcriptional potential of XBP-1(s) in MEFs (Lee *et al*., 2003). This group did not observe any changes in the levels of *CHOP* between WT-hIRE1α and XBP-1 deficient MEFs. This could be due to the fact that the cells were treated with 100 ng/ml tunicamycin for 48 h, rather than 10 μg/ml for 16 h (as they were in the publication). This high concentration of tunicamycin would elicit a much stronger ER stress response, which may mask the prosurvival branch of the UPR.

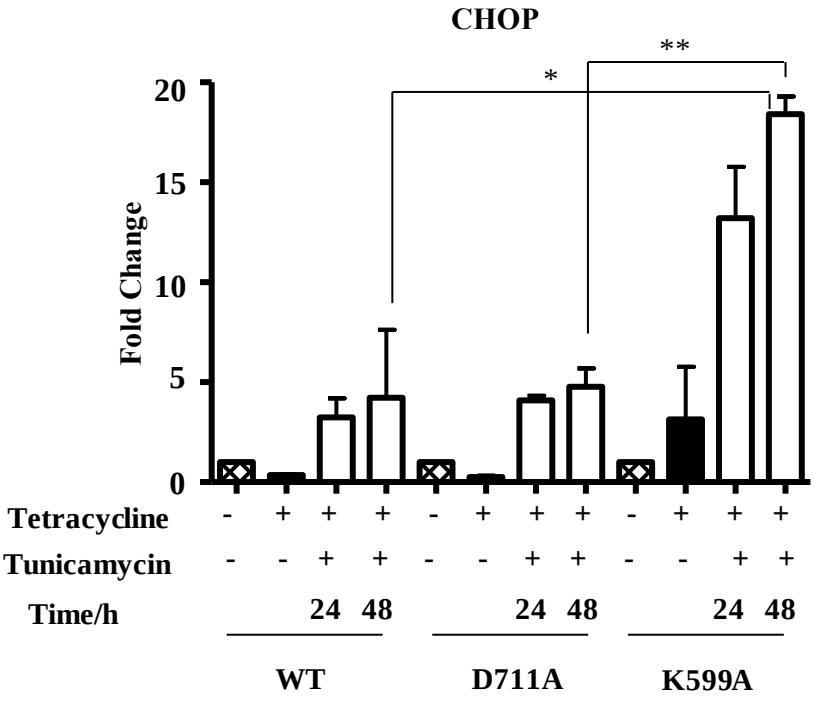

Figure 4.3:* CHOP *expression profile determined by qPCR analysis using Rotor-Gene Q software. FAST 2xreal-time PCR MasterMix with SYBR Green was used. – and + indicate absence and presence of tetracycline and/or tunicamycin, respectively. Tetracycline-only treatment was for 48 h. The time shown is the number of h that ER-stress was induced. Error bars show standard error. An unpaired t-test was performed. * p = 0.0563 (WT-hIRE1α vs K599A), ** p = 0.0087 (D711A-hIRE1α vs K599A-hIRE1α). The average C_t value error was ± 0.24.

These results suggest that the K599A-hIRE1α mutation may be responsible for causing earlier cell death via the CHOP route. Despite the fact that upregulation of CHOP is classically thought of being downstream of the PERK pathway, the upregulation seen in the qPCR data might be the cause of enhanced levels of ATF6 (Yoshida *et al*., 2000). One would expect both PERK and ATF6 to be upregulated in the K599A-hIRE1α cells to compensate for the loss of the transcriptional potential of IRE1α. Two separate groups demonstrated that *CHOP* is under regulation of ATF6(f), as well as the PERK-ATF4 branch (Ma *et al*., 2002 and Okada *et al*., 2002). Therefore, hyperactivation of ATF6 and /or PERK may be responsible for the differences seen in the K599A-hIRE1α mutant.

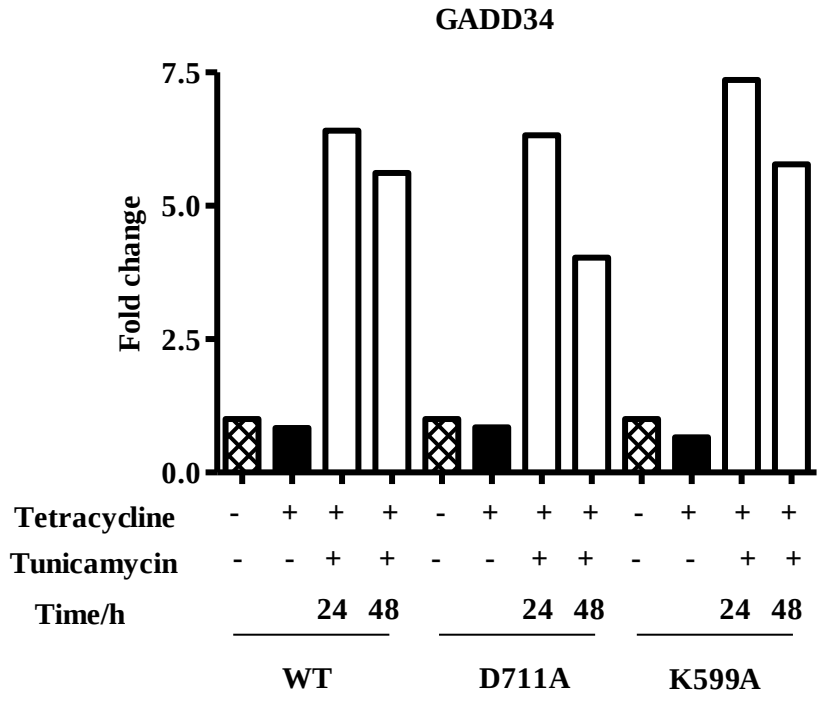

Figure 4.4:* GADD34 *expression profile determined by qPCR analysis using Rotor-Gene Q software. FAST 2xreal-time PCR MasterMix with SYBR Green was used. – and + indicate absence and presence of tetracycline and/or tunicamycin, respectively. Tetracycline-only treatment was for 48 h. The time is the number of h that ER-stress was induced for. The average C_t value error was ± 0.15.

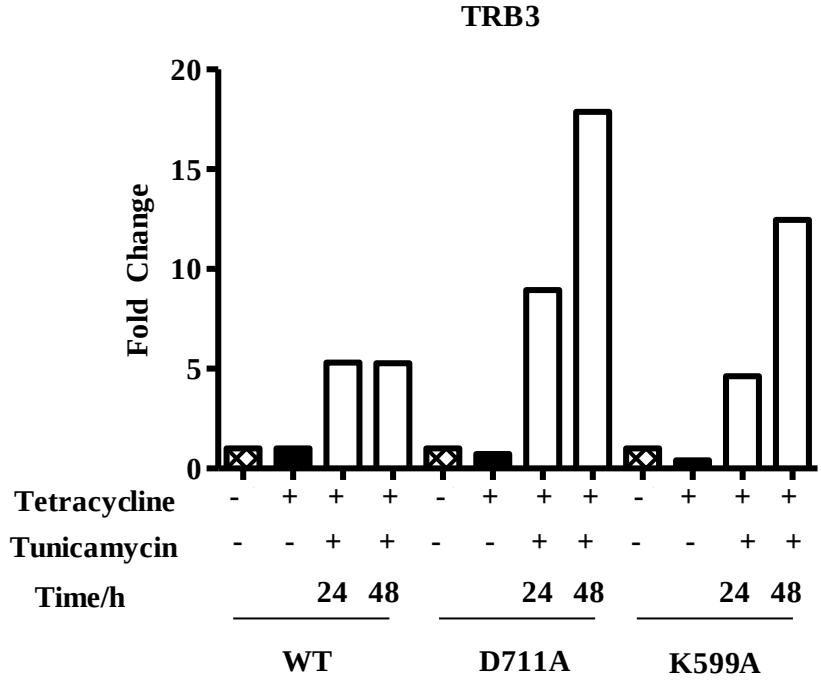

Figure 4.5:* TRB3 *expression profile determined by qPCR analysis using Rotor-Gene Q software. FAST 2xreal-time PCR MasterMix with SYBR Green was used. – and + indicate absence and presence of tetracycline and/or tunicamycin, respectively. Tetracycline-only treatment was for 48 h. The time is the number of h that ER-stress was induced for. The average C_t value error was ± 0.74.

CHOP is known to induce expression of *GADD34* and *TRB3* (Marciniak *et al*., 2004; Ohoka *et al*., 2005). Based on the *CHOP* expression profile, it was hypothesized that both *GADD34* and *TRB3* levels would be similar in the ER stress-induced WT-hIRE1α and D711A-hIRE1α cells, and highest in the K599A-hIRE1α-IRE1α MEFs. However, figure 4.4 argues that the levels of the *GADD34* gene are upregulated to a very similar fold induction (>6) in all three cell lines treated with tunicamycin for 24 h. After 48 h of ER stress, the levels of this gene had diminished somewhat, but still displayed at least a 4-fold induction compared to the untreated cells. The slightly higher fold induction in the K599A-hIRE1α mutant treated MEFs could be a result of the higher *CHOP* expression, although a repeat would be required to validate this. The reason *GADD34* levels might not rise as dramatically as expected in the K599A-hIRE1α mutant might be due to the fact that even though CHOP expression is the highest, it might not become dimerised and/or phosphorylated. These two processes are required to render CHOP a fully capable transcription factor (Zinzsner *et al*., 1998 and Wang and Ron, 1996). For this reason it might be beneficial to study the phospho-p38 pathway by Western blot analysis, as this is believed to be responsible for CHOP phosphorylation (Wang and Ron, 1996).

However, in support of the *GADD34* qPCR profile obtained, in 2008, Adachi *et al*., saw no fluctuations in levels of GADD34 parallel to changes in CHOP expression, which suggests there may be another transcription factor controlling this gene. The presence of an alternative transcription factor may also explain why the *TRB3* expression pattern did not correlate with that observed for *CHOP*. As expected, there was an increase in *TRB3* expression in each of the cell lines undergoing ER stress (figure 4.5). However, contrary to what was hypothesized based on the CHOP profile, the highest expression of *TRB3* was actually in the D711A-hIRE1α mutant, where after 48 h of tunicamycin treatment, there was almost an 18-fold induction of this mRNA compared to the untreated cells. Levels of *TRB3* mRNA seemed to be at their lowest in WT-hIRE1α, where expression compared to the untreated cells was maintained at ~5-fold induction during the time course of ER stress-inducing treatment. After 24 h, K599A-hIRE1α cells induced this gene to a similar level, however after 48 h of induction levels were intermediate between the WT-hIRE1α and the D711A-hIRE1α cells. A repeat for these data is obviously required, however the differences between the WT cells and those expressing the D711A form of hIRE1α warrants full characterisation of this mutant by microarray, or RNA sequencing experiments. It is believed the TRB3 pathway within the UPR will provide an interesting route to study the function of IRE1α kinase activity in cell fate, due to its potential role in ER physiology and autophagy (see discussion).

4.2.2: Induced genes associated with ER luminal localisation

As discussed earlier, *BIP* is induced by the UPR, and its transcript levels were therefore hypothesized to increase upon tunicamycin addition. Indeed, as it can be seen in figure 4.6, there was a ~20 fold induction of this gene in the WT, after 24 h of ER stress. In the D711A-hIRE1α mutant, there was almost the same increase in levels of this transcript, however the decrease between 24 and 48 h of treatment was less striking than in the WT-hIRE1α cells. On the other hand, 24 h after activation of ER-stress in the K599A-hIRE1α mutant saw almost a 45-fold increase compared to the untreated sample. This drastic increase could be due to differences in *BIP* mRNA stability and/or an over-compensatory effect by a transcription factor, such as ATF6α. The latter idea is supported by several laboratories who demonstrate that this chaperone is dependent on the ATF6α(f) transcription factor (Yamamoto *et al*., 2007, Adachi *et al*., 2008, and Shoulder *et al*., 2013). However, although most publications focus on the transcriptional potential of XBP-1(s) and ATF6(f), Scheuner *et al*., 2001 showed that phosphorylation of eIF2α was required for complete BIP expression. For this reason, one must not rule out the PERK pathway for gene regulation.

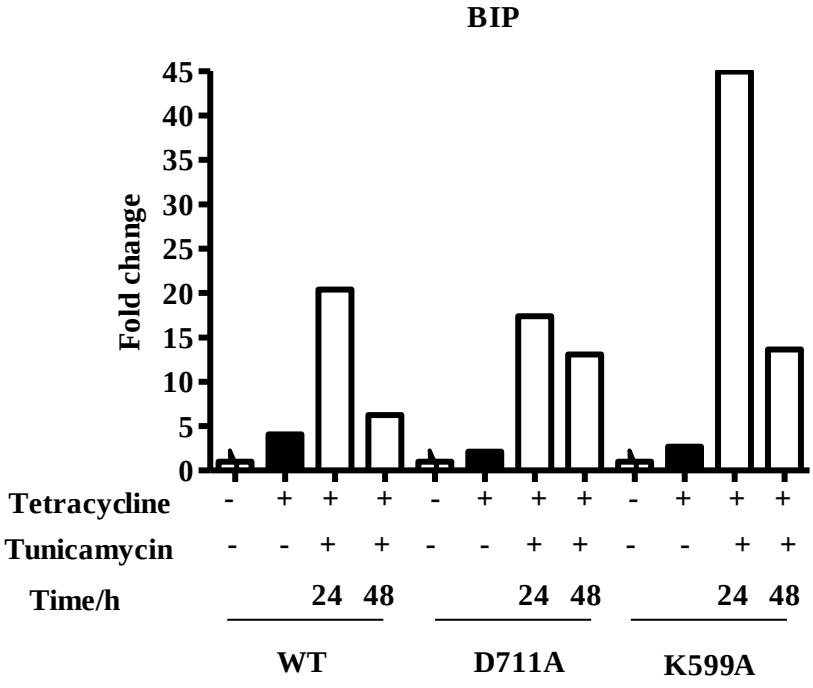

Figure 4.6:* BIP *expression profile determined by qPCR analysis using Rotor-Gene Q software. FAST 2xreal-time PCR MasterMix with SYBR Green was used. – and + indicate absence and presence of tetracycline and/or tunicamycin, respectively. Tetracycline-only treatment was for 48 h. The time is the number of h that ER-stress was induced for. The average C_t value error was ± 0.48.

The chaperone, GRP94, and co-chaperone, $p58^{IPK}$,were hypothesized to be induced by tunicamycin treatment, as they are both targets of the UPR (Lee *et al*., 2003). Figures 4.7 and 4.8 highlight that both genes display the same pattern in terms of induction. As expected, both were strongly activated in the WT-hIRE1α cells after 24 h of tunicamycin treatment, compared to the untreated samples. In both cases, the expression dropped after 48 h, more dramatically in the *GRP94* profile, compared to the one of $p58^{IPK}$. Strikingly, the levels of induction in the D711A-hIRE1α were almost identical to those present in WT-hIRE1α cells for both genes. This is suggestive of the fact that IRE1α kinase does not contribute to the control of these genes. Both genes show a comparatively low induction in K599A-hIRE1α compared to the two other cell lines, implying that IRE1α endoribonuclease function is necessary for full induction of this ER-resident chaperone.

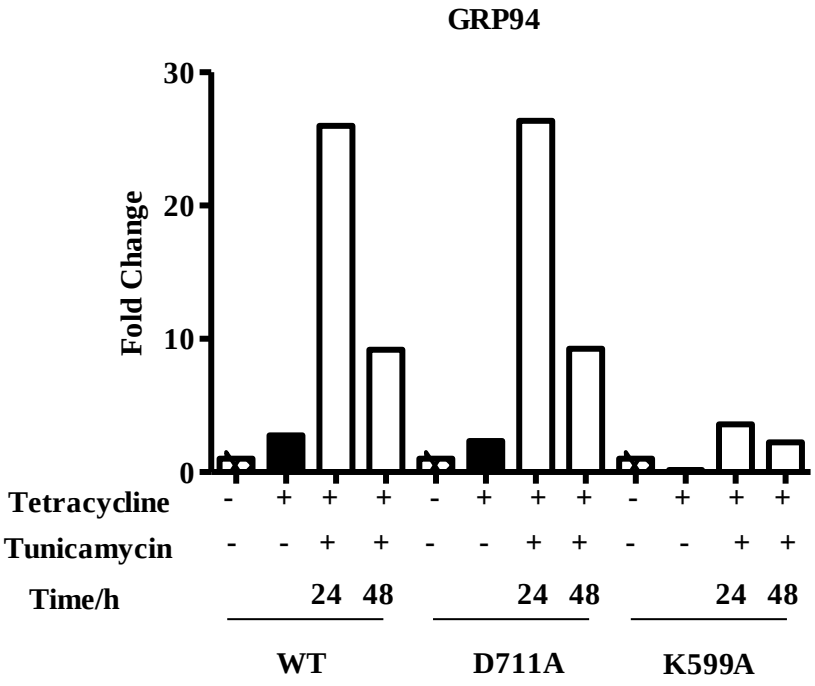

Figure 4.7:* GRP94 *expression profile determined by qPCR analysis using Rotor-Gene Q software. FAST 2xreal-time PCR MasterMix with SYBR Green was used. – and + indicate absence and presence of tetracycline and/or tunicamycin, respectively. Tetracycline-only treatment was for 48 h. The time is the number of h that ER-stress was induced for. The average C_t value error was ± 0.14.

Other laboratories imply that the ATF6(f) transcription factor would be able to induce this gene in the absence of XBP-1 (Lee *et al*., 2003; Shoulders *et al*., 2013). However, from the qPCR data displayed above, the significance of other transcription factors in the regulation of this gene during ER stress needs to be investigated. It is possible that the *GRP94* qPCR data output is a combinatorial effect of the kinase and RNase functions being absent, although a repeat is required to support this argument.

The higher relative induction of *p58^{IPK}* compared to *GRP94* in the K599A-hIRE1α mutant suggests that another transcription factor plays a significant role in the upregulation of the former gene in the absence of XBP-1(s). Both Mori (2007) and Wiseman (2013) groups suggest that this co-chaperone promoter is accessed by both ATF6 and XBP-1 and therefore ATF6 alone may be able to promote expression levels noted in the K599A-hIRE1α mutant. What is interesting is that p58^{IPK} may play a role in controlling polypeptides being translocated into the ER. These polypeptides can be degraded before fully entering the lumen during ER stress (Oyadomari *et al.*, 2006) and p58^{IPK} may therefore assist in the ERAD program. Investigating its potential role at the interface between the UPR and ERAD and exactly how it is transcriptionally regulated could provide insight into the future elucidation of IRE1α signalling.

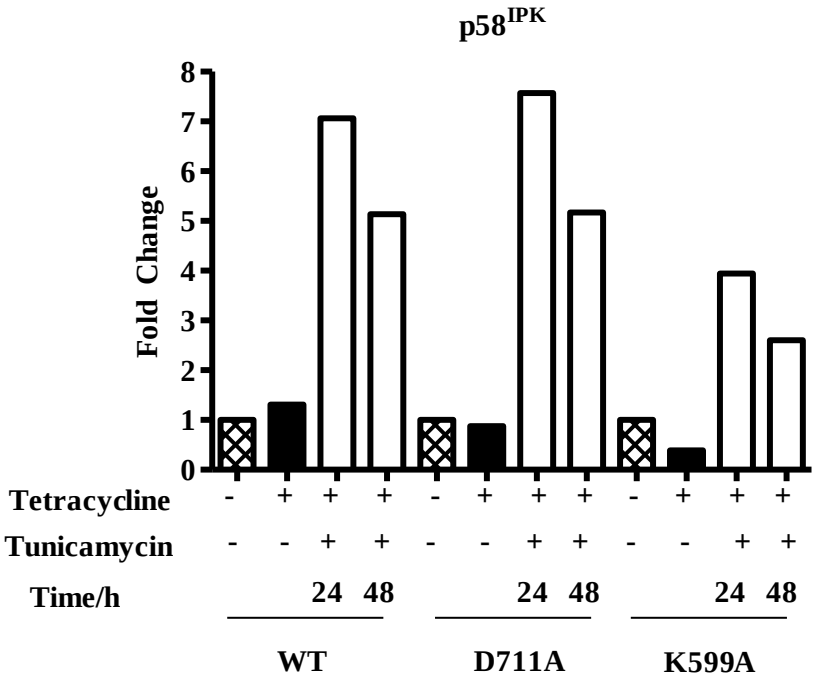

Figure 4.8:* p58^{IPK} *expression profile determined by qPCR analysis using Rotor-Gene Q software. FAST 2xreal-time PCR MasterMix with SYBR Green was used. – and + indicate absence and presence of tetracycline and/or tunicamycin, respectively. Tetracycline-only treatment was for 48 h. The time is the number of h that ER-stress was induced for. The average C_t value error was ± 0.15.

ERO1L-α and ERO1L-β are both responsible for reoxidizing mammalian protein disulphide isomerise (PDI). PDI introduces and isomerises disulphide bonds and is therefore thought to assist with protein folding (Sitia and Braakman, 2003). The yeast homolog was originally found to be upregulated downstream of the Ire1p-Hac1p pathway (Travers *et al.*, 2000) and therefore it was hypothesised that ER stress could induce its upregulation. The qPCR analysis shown in figure 4.9 suggests that IRE1α kinase activity dramatically impacts the transcriptional control for the *ERO1L-α* gene, as the transcript levels from the D711A-hIRE1α cells were decreased in comparison to WT-hIRE1α. The fold change in the WT cells

reached a maximum of ~7 after 48 h of ER stress, whereas in the D711A-hIRE1α expressing cells, maximal fold induction was only about half of this value. This was only marginally higher than the induction of this gene in the K599A-hIRE1α mutant. The differences displayed here justify that full characterisation of the D711A-hIRE1α mutant by microarray analysis or RNA sequencing should be carried out in order to begin determining the role of the kinase in transcriptional control in the UPR.

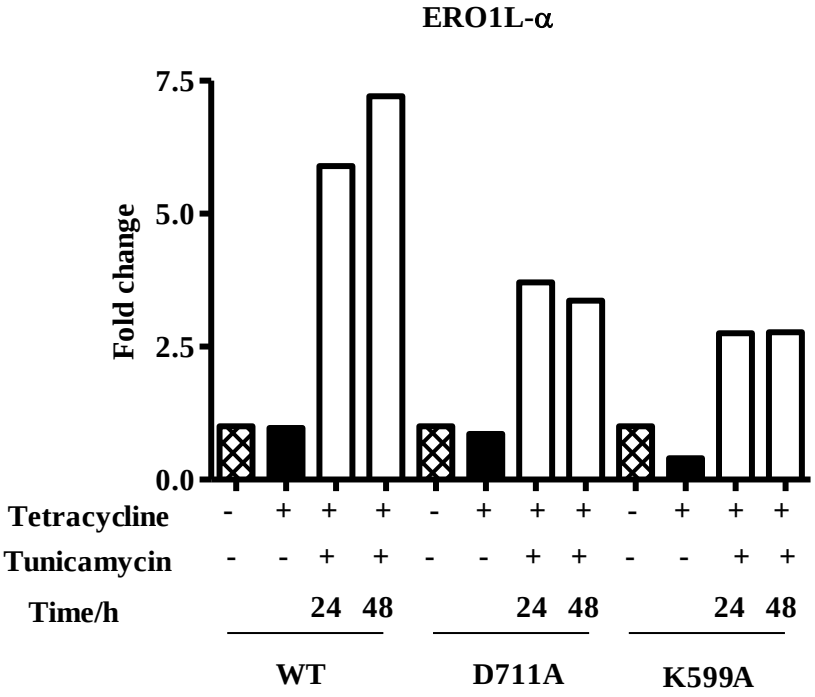

Figure 4.9: **ERO1L-α** ***expression profile determined by qPCR analysis using Rotor-Gene Q software. FAST 2xreal-time PCR MasterMix with SYBR Green was used . – and + indicate absence and presence of tetracycline and/or tunicamycin, respectively. Tetracycline-only treatment was for 48 h. The time is the number of h that ER-stress was induced for. The average*** C_t ***value error was ± 0.19.***

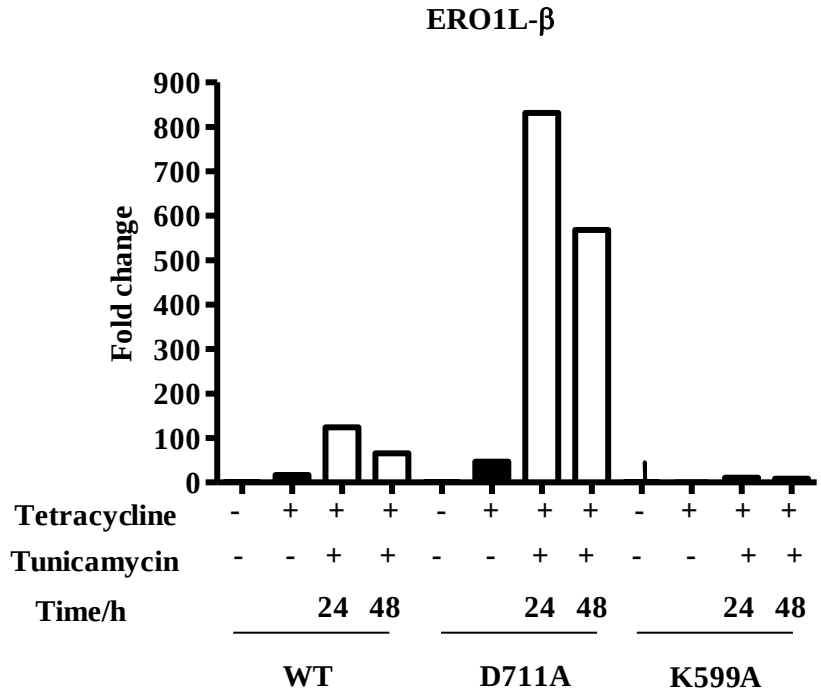

Figure 4.10: **ERO1L-β** ***expression profile determined by qPCR analysis using Rotor-Gene Q software. FAST 2xreal-time PCR MasterMix with SYBR Green was used. – and + indicate absence and presence of tetracycline and/or tunicamycin, respectively. Tetracycline-only treatment was for 48 h. The time is the number of h that ER-stress was induced for. The average*** C_t ***value error was ± 1.11.***

As it can be seen from figure 4.10, the *ERO1L-β* gene displays a different profile to *ERO1L-α.* Due to the abolishment of XBP-1(s) in the K599A-hIRE1α mutant, it was predicted that there would be little induction of this gene compared to the WT-hIRE1α and D711A-hIRE1α mutant (Sriburi *et al.*, 2007 and Shoulders *et al*., 2013). This was indeed the case, however, the D711A-hIRE1α mutant displayed massively elevated levels of this gene. Perhaps this is due to the fact that it was less able to induce *ERO1L-α*, and therefore hyper-activation of this gene was a result of compensating for this loss. Again, this probes for further investigation into the IRE1α kinase domain.

Lee *et al*., 2003 suggest that ERDJ4 transcription is completely reliant on XBP-1 splicing. The profile below, obtained for co-chaperone *ERDJ4* was largely in agreement with what has been published, as the levels of transcript in the WT-hIRE1α cells after 24 h tunicamycin treatment were approximately ~14 times the untreated control. The fold induction in both mutants were greatly reduced in comparison. However the comparatively small increases of *ERDJ4* transcript in both tunicamycin-treated mutants, suggest that another transcription factor apart from XBP-1(s) may play a role in expression of this gene (albeit a much less effective one). What is interesting is that again the kinase activity seems to be important in

ensuring this gene is expressed, as the levels of transcription reached by the D711A-hIRE1α mutant are essentially equal to those in the K599A-hIRE1α mutant. This strengthens the argument that full characterisation of the former mutant is required to help understand its role in gene induction.

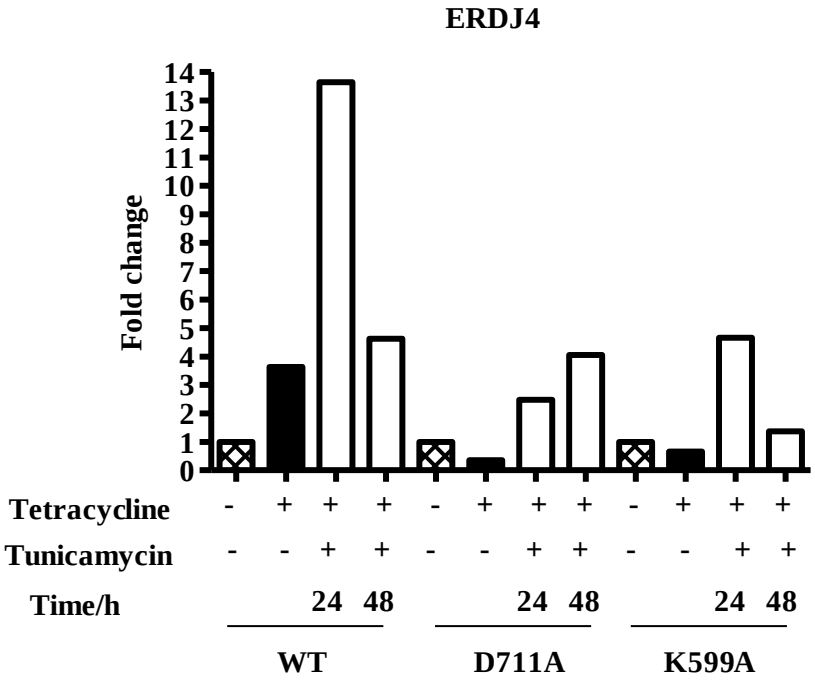

Figure 4.11: **ERDJ4 e*xpression profile determined by qPCR analysis using Rotor-Gene Q software. GoTaq® qPCR MasterMix with SYBR Green was used to obtain these data. – and + indicate absence and presence of tetracycline and/or tunicamycin, respectively. Tetracycline-only treatment was for 48 h. The time is the number of h that ER-stress was induced for. The average C_t value error was ± 0.23.***

4.2.3: Induced genes which are associated with regulating ERAD

Synoviolin or HRD1 is an indispensable E3 ubiquitin ligase for the ERAD protein quality control system. Travers *et al*., 2000 found it to be upregulated as a consequence of Ire1p-Hac1p activation and more recently it was identified as being reliant on XBP-1 for its transcription in mammalian cells (Shoulders *et al*., 2013). It was therefore hypothesized that its upregulation in the K599A-hIRE1α cells would be compromised during ER stress. In figure 4.12, *HRD1* was shown to be heavily downregulated to roughly half the fold induction in both mutants, compared to the WT-hIRE1α cells treated for 24 h with tunicamycin. A qualitative repeat was obtained for these data, and in both cases it appears there may be a very slight increase in the D711A-hIRE1α response relative to the K599A-hIRE1α. The response from the latter mutant complements the above mentioned studies, although other transcription factors must be available to achieve the smaller increases in response to ER stress induction. The results also heavily implicate IRE1α kinase in the transcriptional mechanism involved in activating this gene.

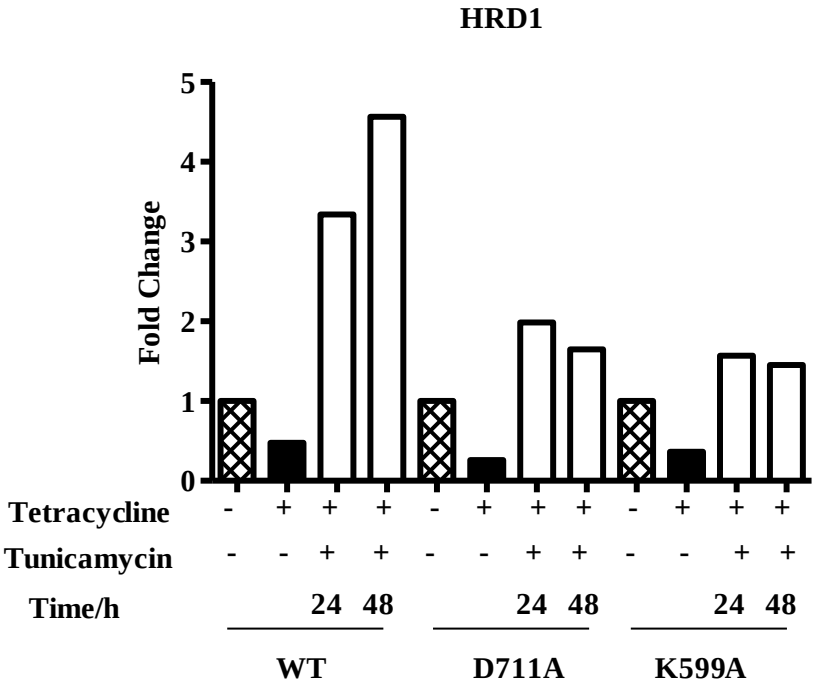

Figure 4.12:* HRD1 *expression profile determined by qPCR analysis using Rotor-Gene Q software. FAST 2xreal-time PCR MasterMix with SYBR Green was used. – and + indicate absence and presence of tetracycline and/or tunicamycin, respectively. Tetracycline-only treatment was for 48 h. The time is the number of h that ER-stress was induced for. A qualitative biological repeat was obtained for this gene (Figure A4.26). The average C_t value error was ± 0.23.

EDEM1 is proposed to recognise structures to be retrotranslocated for ERAD and Yoshida *et al*., 2003 showed that IRE1α deficient MEFs were unable to induce *EDEM1* mRNA, even though the active fragment of ATF6 was present under ER stress. This is supported by the 4-fold induction of this gene after induction of the UPR in the WT-hIRE1α, and also the lower levels sustained in the K599A-hIRE1α mutant. Again, it seems as though transcription factors other than XBP-1(s) do play a role in regulating this gene, and candidates such as ATF6 and ATF4 should be questioned. More importantly, it seems as though the kinase domain may be vital for the full transcriptional activation of the *EDEM1* gene, as expression levels in the D711A-hIRE1α mutant are intermediate between the WT-hIRE1α and K599A-hIRE1α cells.

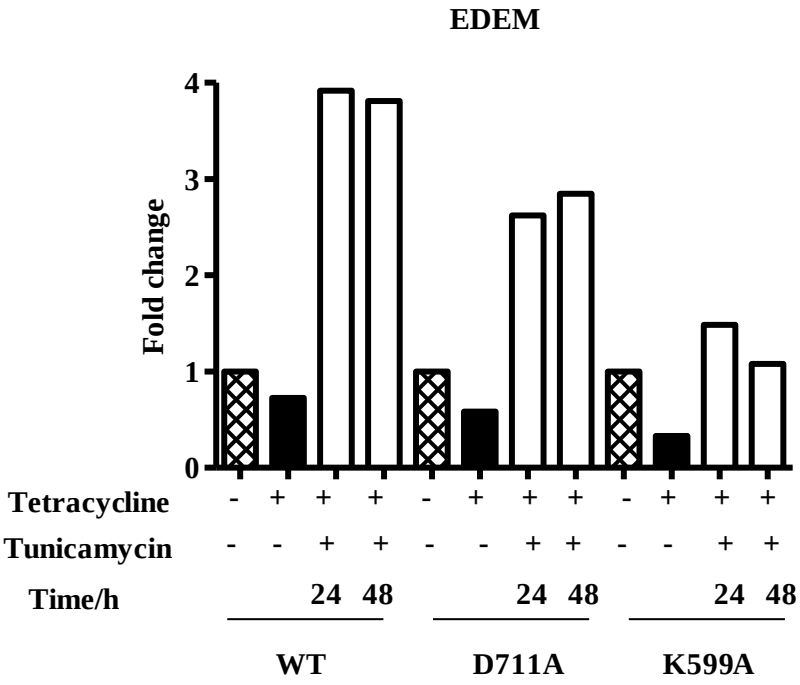

Figure 4.13: **EDEM1** ***expression profile determined by qPCR analysis using Rotor-Gene Q software. FAST 2xreal-time PCR MasterMix with SYBR Green was used. – and + indicate absence and presence of tetracycline and/or tunicamycin, respectively. Tetracycline-only treatment was for 48 h. The time is the number of h that ER-stress was induced for. The average C_t value error was ± 0.23.***

HEDJ, also known as ERDJ3, is mainly regarded as a co-chaperone for BIP as it stimulates its ATPase activity. Additionally, it has been postulated that it may play a role in ERAD by binding unfolded polypeptides chains to be targeted for degradation (Jin *et al*., 2009). The potential link to ERAD encouraged the hypothesis that this gene would show a similar profile to *HRD1* and *EDEM1*. Despite this, figure 4.14 shows that *HEDJ* is actually expressed almost identically in all three cell lines. After 24 h, levels of transcripts reach approximately a 4.5 fold induction compared to the untreated cell lines. Each displays a small decrease in transcript after 48 h of ER stress, however, the downregulation in both of the mutants is greater than in the WT-hIRE1α. In accord with this, the Wiseman laboratory (2013) showed that by inducing either XBP-1(s), ATF6, or both, resulted in almost equal increases in HEDJ upregulation. This proposed redundancy is supported by Sriburi *et al*., 2004, who essentially saw the same protein upregulation of ERDJ3 in ATF6α(373) or XBP-1(s) transduced cells. This enforces the idea that the HEDJ profile is a result of XBP-1(s) and ATF6(f) having the same capabilities regarding activation of this gene.

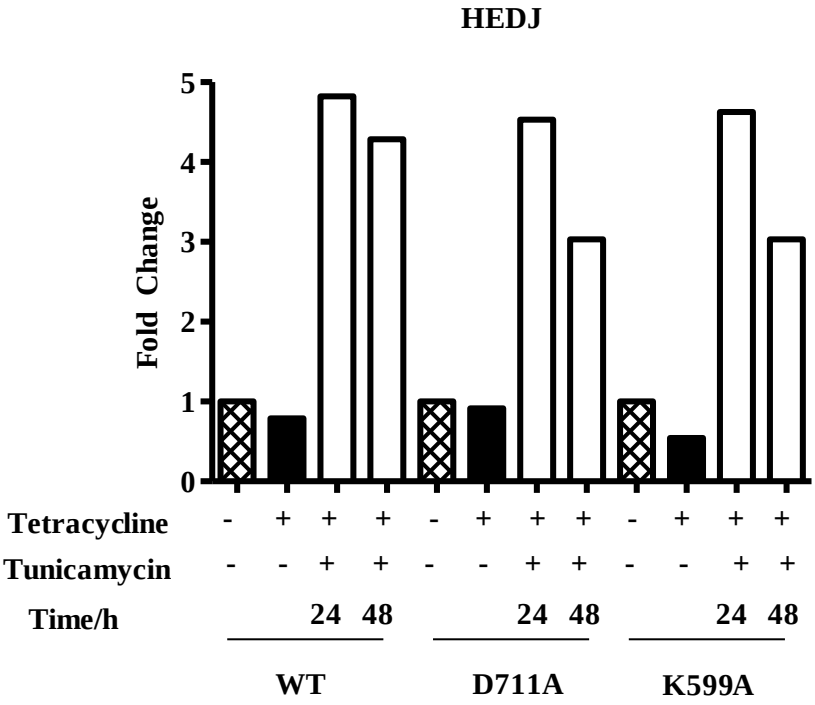

Figure 4.14: **HEDJ** ***expression profile determined by qPCR analysis using Rotor-Gene Q software. FAST 2xreal-time PCR MasterMix with SYBR Green was used. – and + indicate absence and presence of tetracycline and/or tunicamycin, respectively. Tetracycline-only treatment was for 48 h. The time is the number of h that ER-stress was induced for. The average*** C_t ***value error was ± 0.23.***

HERP is the final gene that was analysed and that is UPR-regulated for ERAD purposes. It has been postulated that all three branches of the UPR are able to cause an upregulation of this gene (Ma and Hendershot, 2004). It was shown that apart from ATF6(f) and XBP-1(s) binding the ERSE sites in the *HERP* promoter, ATF4 (downstream of the PERK-phospho-eIF2α branch) was able to complex with the composite site in this promoter. Consistently, they found the constitutively inactive eIF2α mutant (S51D) was able to generate an increase in both *HERP* mRNA and protein levels. Therefore, it was proposed that *HERP* upregulation might be similar in each of the cell lines treated with tunicamycin. Despite the fact there was no difference between the WT-hIRE1α and D711A-hIRE1α profiles, the K599A-hIRE1α mutant showed a much higher induction (~14 fold) after 24 h tunicamycin treatment. It is possible that ATF6 and ATF4 cause a higher upregulation of *HERP* in K599A-hIRE1α compared to the other two cell lines in order to try and compensate for the loss of other ERAD components. Further experimentation would be needed to validate this idea.

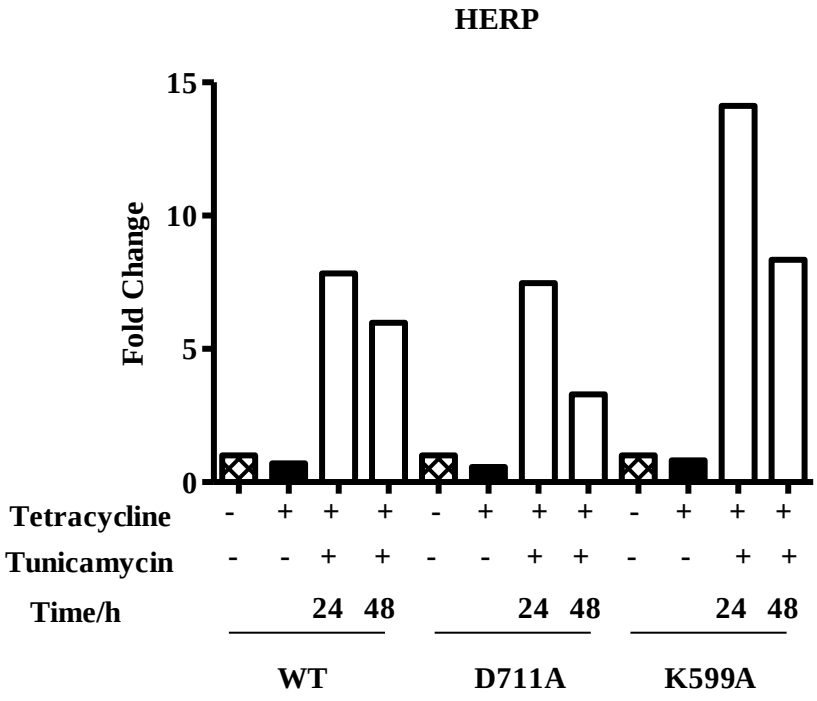

Figure 4.15: **HERP** ***expression profile determined by qPCR analysis using Rotor-Gene Q software. FAST 2xreal-time PCR MasterMix with SYBR Green was used. – and + indicate absence and presence of tetracycline and/or tunicamycin, respectively. Tetracycline-only treatment was for 48 h. The time is the number of h that ER-stress was induced for. The average*** C_t ***value error was ± 0.16.***

4.3: Rationale for studying the RIDD pathway:

A report in Science in 2006 gave evidence for a subset of mRNAs whose degradation was dependent on the presence of IRE1 (Hollien and Weissman, 2006). The presented data suggested that an internal cleavage site in these mRNAs was present to differentiate them from other mRNAs that do not get degraded, such as *BIP*. Consistent with data published recently (Gaddam *et al*., 2012) it was also demonstrated that the signal sequence targeting these mRNAs for cotranslational translocation into the ER, seemed to be required for this repression (Hollien and Weissman, 2006).

As explained in Chapter 1, the Weissman group used human IRE1α stably transfected MEFs to show that this RIDD pathway was sustained under ER stress provided the RNase was also functional. Additionally, they suggested this was maintained by using the 1NM-PP1 sensitized I642G IRE1α mutant, in which IRE1α kinase activity is abolished (Hollien *et al*, 2009). Similar data was published by the Papa group at around the same time. However, in these experiments, mRNA degradation did not occur as part of the UPR when the I642G mutant was active (Han *et al*. 2009). These two groups had opposing ideas as to how this degradation route affected cell fate, with the Weissman group proposing this would relieve

the burden on the ER, and the Papa group suggesting there was a positive correlation with apoptosis.

From these data it was hypothesized that RIDD substrates should not undergo degradation in ER-stressed K599A-hIRE1α mutants due to lack of RNase activity. Since this project was designed to find other potential functions associated with the IRE1kinase domain, determining any differences between the RIDD pathway outputs of the WT-hIRE1α and D711A-hIRE1α cells could help answer this. Since endoribonuclease activity is maintained, the D711A-hIRE1α cells may display a similar RIDD profile to what was is observed in the WT-hIRE1α cells. However, if the Papa group is correct, and full kinase function is required for an effective RIDD, then this mutant may mirror what is found for the K599A-hIRE1α mutant.

4.4: Results and discussion for analysis of the RIDD pathway by qPCR

The genes examined in the context of the RIDD pathway were those published by Hollien *et al.*, in 2009.

Table 4.1: List of RIDD target genes and their localisation as proteins, adapted from the Hollien* et al.*, paper in 2009.

Gene corresponding to RIDD target	Localisation of protein
HGSNAT	Lysosomal membrane
BLOS1	Cytosol
SCARA3	ER/Golgi apparatus membrane
PDGFRB	Plasma membrane
PMP22	Extracellular matrix
COL6	Extracellular matrix
EPHRINB2	Plasma membrane
MAP7d1	Cytoskeleton
SRP20	Spliceosome
TRIM16	Cytosol
GALNT10	Golgi apparatus membrane

Primers were designed to recognise the genes listed in Table 4.1 and tested in ordinary PCR first. Once they had also been tested for specificity using mouse cDNA (derived from pre-adipocytes and adipocytes) in the RotorgeneQ, they were finally checked for primer-dimer formation using a no template control. As with the induced genes, the raw data were normalised to *ACTB,* and the quantitation was carried out using the $2^{-\Delta\Delta C}{}_t$ method (Livak and Schmittgen, 2001). Initial experiments did show evidence for degradation in the WT-hIRE1α samples, upon induction of ER-stress. This was observed for the following genes: *BLOS1, PDGFRB, TRIM16, COL6, EPHRINB2, SRP20* and *GALNT10*. *MAP7d1* mRNA was only marginally reduced after 48 h ER-stress induction. Data were not generated for *HGSNAT, SCARA3* and *PMP22* due to time limitations.

As can be seen from figures 4.16 and 4.17 (and figures A4.28-A4.33) there is evidence for elevation of transcript levels in the K599A-hIRE1α mutant relative to the WT-hIRE1α in *COL6, EPHRINB2, GALNT10, PDGFRB, SRP20* and *TRIM16* genes. All but the latter two genes still showed a decrease in the level of transcript upon induction of ER stress compared to the untreated K599A-hIRE1α. This suggests that the RIDD pathway is not fully abolished in these cells despite the lack of IRE1α endoribonuclease activity. Only *SRP20* and *TRIM16* transcripts were increased during ER-stress compared to the untreated K599A-hIRE1α. Increased levels of *SRP20* transcript (Figure 4.17) seem to be the most significant, and a biological repeat was obtained for this gene. The profile does suggest that the kinase may play a role on effective degradation of *SRP20*. However, by observing the small increase seen at the end of the time course in WT-hIRE1α cells, one would have to question how much of was what found was simply a consequence of the length of ER stress induction.

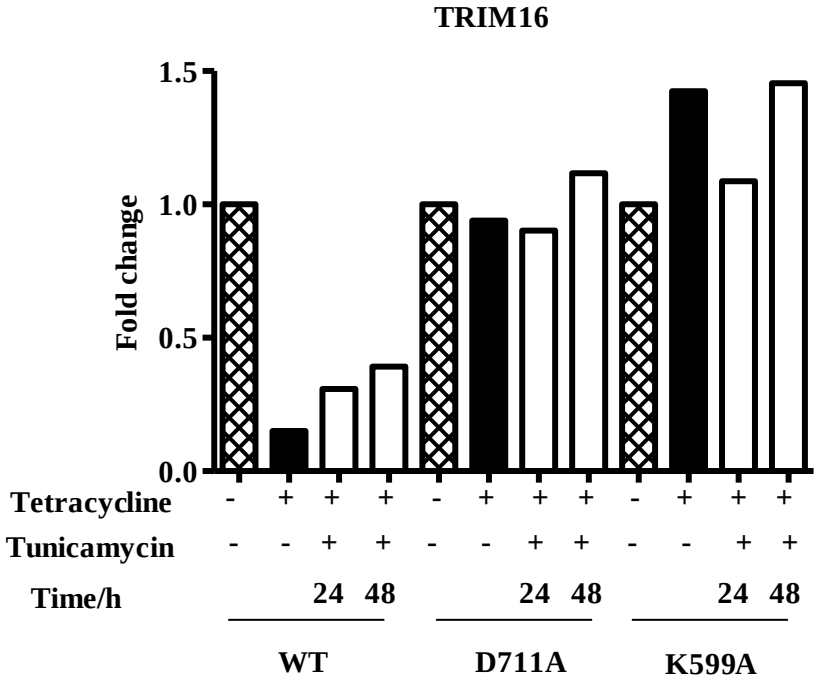

Figure 4.16: **TRIM16** ***expression profile determined by qPCR analysis using Rotor-Gene Q software. 2xreal-time PCR MasterMix with SYBR Green was used. – and + indicate absence and presence of tetracycline and/or tunicamycin, respectively. Tetracycline-only treatment was for 48 h. The time is the number of h that ER-stress was induced for. The average C_t value error was ± 0.30.***

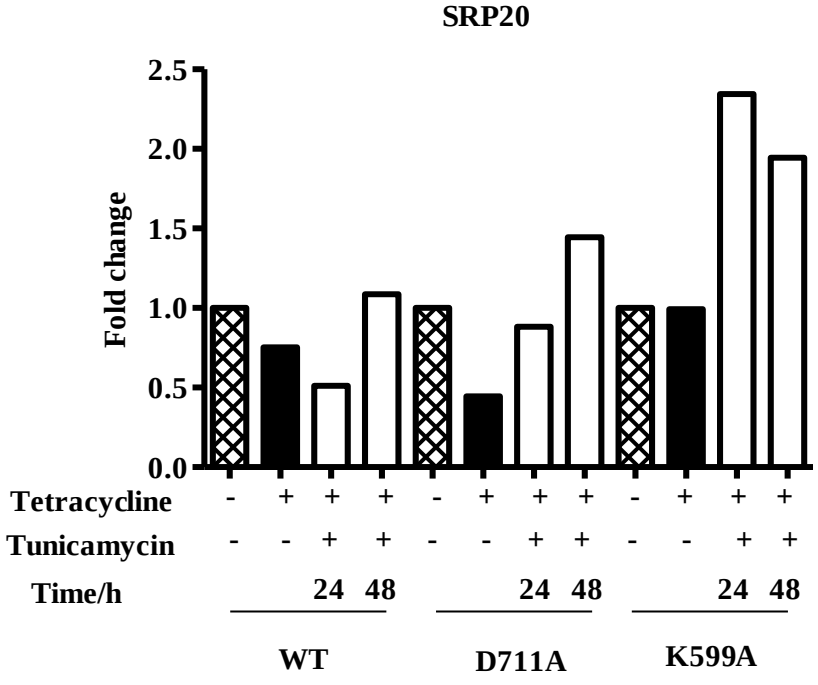

Figure 4.17: SRP20 expression profile determined by qPCR analysis using Rotor-Gene Q software. 2xreal-time PCR MasterMix with SYBR Green was used. – and + indicate absence and presence of tetracycline and/or tunicamycin, respectively. Tetracycline-only treatment was for 48 h. The time is the number of h that ER-stress was induced for. A qualitative biological repeat was obtained for this gene (Figure A4.33). The average C_t value error was ± 0.22.

Despite several attempts, no other data was generated which demonstrated a loss of RIDD in the K599A-hIRE1α expressing cells. From the data shown in this thesis it is difficult to speculate a role for the kinase activity of hIRE1α in this pathway, as the profiles for the different proposed RIDD transcripts are very variable. In general it seems as though this mutant is less effective in carrying out the RIDD function, however repeats are required to validate this observation.

It may be advisable to repeat this set of experiments using primers that have been redesigned to anneal closer to the 5' end of the genes. Most of the primers designed in this project annealed slightly closer to the 3' end than the 5' end. Therefore, if the cleavage site of the mRNA in question was upstream of the primer annealing site, it is possible that the 3' end of the mRNA may have been reverse transcribed if it had not been immediately degraded. Reverse transcription would have been able to take place as the oligo(dT)s would have still annealed to the polyA tail of mRNA, creating a starting template for the reverse transcriptase enzyme. Thus, the primers would have generated the expected PCR product despite the fact that mRNA cleavage may have taken place.

The role of the kinase domain in RIDD can unfortunately not be deduced from these studies, as from the data presented, it is still possible that some mRNAs require an active IRE1α kinase for degradation, whereas other do not. The RIDD pathway could indeed be less defined than originally portrayed by both Han and Hollien groups, and mRNAs may be subject to cleavage dependent on their proximity to IRE1α. This has in fact been proposed for *Schizosaccharomyces pombe* (Kimmig *et al*., 2012). If this is true, then qPCR analysis of single genes cannot be used to study RIDD activity, and microarray and/or RNA sequencing will be required.

4.5: Discussion

As previously discussed, the main objective was to find any differences between the WT-hIRE1α and the D711A-hIRE1α cells in terms of their transcriptional output. Changes in the cell lines expressing the kinase and RNase-dead form of IRE1α were to be expected due to loss of the XBP-1(s) transcription factor and/or overcompensatory effects by ATF6. The data obtained by qPCR analysis do indeed demonstrate that the kinase activity of IRE1α is required for a full transcriptional response. The *HRD1* and *EDEM1* profiles suggest that both mutants may have a diminished ERAD response. This, along with the fact that kinase function also seemed to be necessary for effective transcription of the ER-resident co-chaperone *ERDJ4*, and *ERO1L-α* provides a mechanism by which the kinase-activity of IRE1α may contribute to keeping the cell alive once the ER stress has been induced. These differences justify full characterisation of the transcriptional role of the kinase by using microarray and RNA sequencing in each of the three cell lines. Pulse-chase labelling and immunoprecipitation for known ERAD substrates will help confirm loss of control of ERAD in the D711A-hIRE1α cells.

Another line of interest in the D711A-hIRE1α mutant is the upregulation of *TRB3*. TRB3 is known to inhibit Akt (Salazar *et al.*, 2009) which in turn is required for function of VCP/p97 (Vandermoere *et al*., 2006). Knockdown of VCP, which is an AAA-ATPase involved in proteasomal degradation, correlated with the phenotype of dilated ER, as visualised by electron microscopy (Wócjik *et al*., 2006). As will be shown in the following chapter, the D711A-hIRE1α mutant displays very similar features to that seen in the Wócjik publication. Theoretically, elevated TRB3 levels may render VCP/p97 non-functional via Akt in the D711A-hIRE1α cells, thus leading to a drastic change in ER phenotype. Using qPCR and Western blotting to investigate the relationship between IRE1α kinase and ER phenotype could lead to discovering a novel mechanistic pathway relating the two. It may also help delineate the cell death route taken when IRE1α lacks kinase activity.

Returning to the data obtained, it was noted that differences were seen between the mRNA and protein expression levels of BIP. This is probably due to differences in protein translation in the three cell lines. Therefore the activities of phospho-eIF2α should be analysed using Western blotting at a series of close time points. Pulse-labelling could be used alongside this Western blotting to help determine levels of protein synthesis. Ribosomal profiling may also be utilised to establish the ratio of monosomes to polysomes to determine levels of translation.

Finally, the RIDD pathway should next be analysed using primers which anneal to the 5' end of the genes under investigation. It is hypothesised that RIDD activity will be lost in the K599A-hIRE1α cells compared to the WT-hIRE1α. If these experiments are successful, it may also be useful to carry out the same analyses using *xbp-1*$^{-/-}$ MEFs, in order to demonstrate that the RIDD pathway is separable from *XBP-1* splicing, as shown in Hollien *et al*., 2009.

Chapter 5

The differences in ER physiology between WT, D711A and K599A human IRE1α mouse embryonic fibroblasts

5.1: Rationale for investigating changes in ER physiology

The Walter group reported that *hac1Δ* mutants displayed normal ER characteristics when ER stress was not induced in yeast. However, by analysing the localisation of Rtn1 (an ER membrane protein) after 2 h DTT treatment, they showed that the ER became disorganised and that there was relatively more smooth ER compared to rough ER (Schuck *et al*., 2009). Earlier studies performed, using mammalian fibroblasts showed that XBP-1(s) transduction into cells resulted in an increased ER surface area and volume (Sriburi *et al*., 2004). It was also noted that this transduction correlated with increased activity of cytidylyltransferase (CCT). This enzyme is regarded as the rate-limiting factor in the Kennedy pathway (illustrated below), which produces phosphatidylcholine and phosphatidylethanolamine, both of which are required for ER membrane biogenesis. This group later demonstrated that the most efficient upregulation of these membrane components was by over-expression of XBP-1(s) and not the CCT enzyme. It is therefore thought that the product of IRE1α RNase activity is responsible for generating a greater ER surface area via increased output of the Kennedy pathway and that this is most likely achieved by upregulation of the CCT enzyme alongside other cofactors (Sriburi *et al*., 2007).

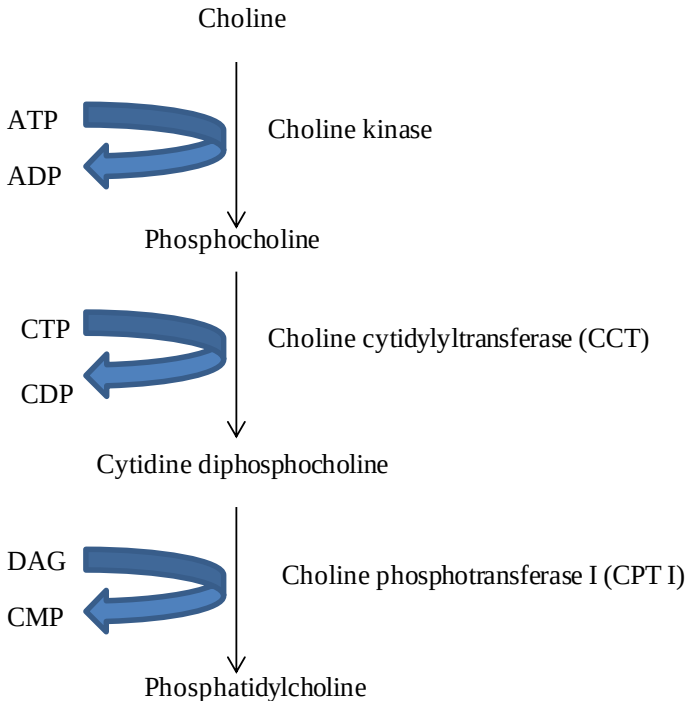

Figure 5.1: Schematic outlining the steps of the Kennedy Pathway. ATP: adenosine triphosphate, ADP: adenosine diphosphate, CTP: cytidine triphosphate, CDP: cytidine diphosphate, DAG: diacylglycerol, CMP cytidine monophosphate.

A similar phenomenon compared to that observed in yeast was observed in pancreatic acinar cells. In cells lacking XBP-1, the ER was unable to develop normally in comparison to the WT-hIRE1α cells. It was also observed that the defectively formed ER contained granules within the lumen (Lee *et al*., 2005). In agreement with this, an RNase inhibitor to IRE1α was shown to inhibit proper expansion of the ER in the AR42J pancreatic cell line (Cross *et al*., 2012).

Of relevance is the study carried out by the Brewer group, who used the transcriptionally active form of ATF6 to transfect CHO cells. They demonstrated that there was an XBP-1(s) independent ER expansion which also resulted in increased phospholipid production. In this case, it was the choline kinase (CK) enzyme (also part of the Kennedy pathway) whose activity was increased after ATF6 transduction (Bommiasamy *et al*., 2009).

As it can be seen, most work conducted in this field does not directly address ER expansion during the unfolded protein response, but rather focuses on the inductive potential of either the XBP-1 or ATF6 transcription factors. Also, the publications concentrate mainly on the size and volume of the ER, rather than the shape and structural organisation. For these reasons, it was agreed it would be informative to closely analyse the changes in ER morphology *and* size in both the D711A-hIRE1α and K599A-hIRE1α mutants compared to the WT-hIRE1α. It was hypothesized that an expansion in the ER should be seen in WT-hIRE1α and D711A-hIRE1α cells treated with tetracycline, as the PhD student Louise Sutcliffe showed that this treatment causes *XBP-1* splicing independent of ER-stress. The K599A-hIRE1α cells may be able to expand their ER via the ATF6 route, if there is indeed some functional redundancy between these two transcription factors.

5.2: Observations and results from TEM

Prior to carrying out the TEM processing protocol, all three cell lines were incubated at 37°C with EtOH or tetracycline for 24 h following a 24 h period over which they adhered to the surface of the 75 cm^2 tissue culture flasks. The control cells treated with EtOH were then treated with 10 µl DMSO for a further 48 h, whereas the cells treated with tetracycline were treated with 100 ng/ml tunicamycin for 48 h. The media and treatments were replenished every 24 h.

At least 100 electron micrographs were taken for each cell line and treatment. Most pictures were taken at a magnification of at least 15,000 to obtain a clear image of the ER, however, in some cases lower magnification images were collected to highlight the extent to which the ER filled the cytoplasm of a single cell. It was immediately apparent that there were large differences in ER physiology, in particular between the WT-hIRE1α tunicamycin treated cells and the mutant treated cells. The untreated WT-hIRE1α cells did not display any

notable abnormal characteristics. There was not a large amount of ER within these cells, and this was neither well-organised nor disorganised (Figure 5.2). Often areas of the cells completely devoid of ER were observed. In the untreated D711A-hIRE1α cells, the appearance was comparable, however at first glance, there did appear to be very slightly more ER which had a wider lumen. The untreated K599A-hIRE1α cells were very similar to the untreated D711A-hIRE1α cells, as can be seen in the figure below. None of the untreated cells displayed a continuous or extensive ER network.

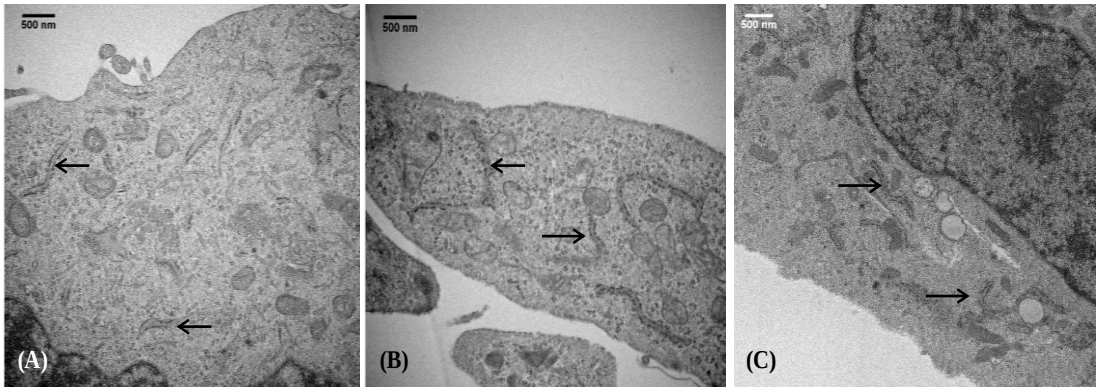

Figure 5.2: (A) denotes the untreated control WT-hIRE1α MEFs. (B) and (C) represent the untreated D711A-hIRE1α and K599A-hIRE1α MEF controls, respectively. The arrows mark typical ER. Magnification: (A): x25,000, (B): x25,000 and (C): x20,000. Scale bars represent a distance of 500 nm.

Figure 5.3 highlights the fact that there were no notable differences between the cell three lines when treated with tetracycline only. Additionally, there did not seem to be any dramatic changes in ER physiology when compared to the untreated cells.

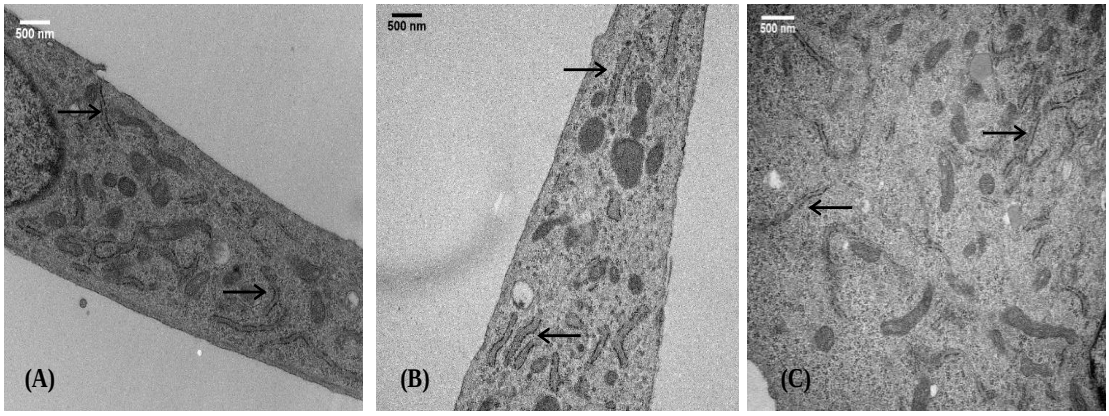

Figure 5.3: (A) is representative of the tetracycline-only treated WT-hIRE1α MEFs, whereas (B) and (C) depict average D711A-hIRE1α and K599A-hIRE1α MEFs treated with the* IRE1α*-inducing drug. The arrows mark ER. Magnification: (A): x20,000, (B): x20,000 and (C): x25,000. Scale bars represent a distance of 500 nm.

When the cells were treated with the ER stress inducing agent tunicamycin the physiology of the ER dramatically changed. In the WT-hIRE1α cells, the amount of ER increased significantly, with a large proportion of cells containing cytoplasm almost fully occupied by rough ER. This rough ER was generally not swollen and formed a very well organised network. There seemed to be an increase in the number of autophagosomes and/or

lysosomes, although through observation it was difficult to differentiate between these vacuolar structures within the cell. In some cases the ER was in close contact with these structures, as can be seen in Figure 5.4. It is possible that the ER was being directly degraded in an attempt to reduce the amount of unfolded proteins, or that the ER was 'donating' a small proportion of its membrane towards the forming vesicle.

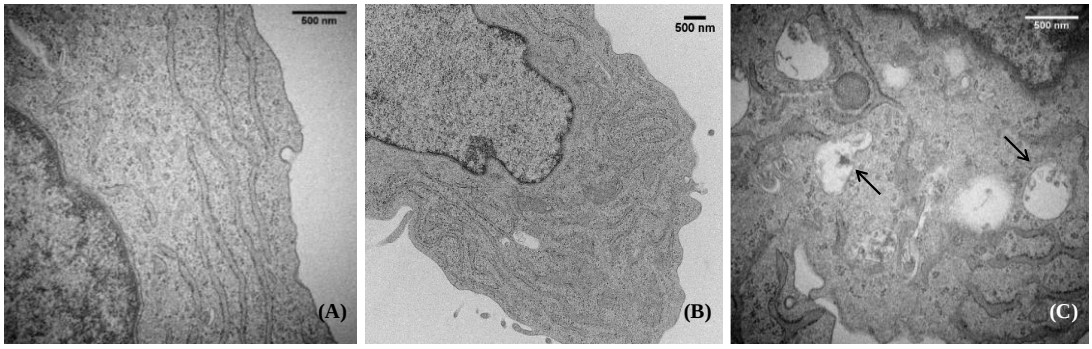

Figure 5.4: (A) and (B) show how the ER was observed to be organised in the WT-hIRE1α MEFs treated with tunicamycin. The arrows in (C) highlight the presence of lysosomal-like structures and how the ER network was seen to interact with them. Magnification: (A): x40,000, (B) x15,000 and (C) x40,000. Scale bars represent a distance of 500 nm.

On the other hand, the response of D711A-hIRE1α to the same drug was quite different (Figure 5.5). As with the WT-hIRE1α treated cells, there was a large increase in the amount of ER produced, however this was much more swollen and distorted and seemed to consist of comparatively more smooth ER. This is similar to what was observed in the yeast study carried out by the Walter group in 2009. Rather than forming an organised network, a disorganised and more 'fragmented' ER formed. The swollen ER appeared to have a less dense lumen, as opposed to the appearance of the lumen found in most of the WT-hIRE1α treated cells. This is indicative of the ER becoming expanded due to osmotic stress (personal correspondence: Dr. M. Goldberg, 19/04/2013, meeting, and Wócjik *et al*., 2006). There was a strong correlation between this phenotype and the observation of a thin white outline around the nucleus, which looked as though the outer nuclear membrane was separating from the inner nuclear membrane. This may be expected since the ER is continuous with the outer nuclear membrane. In some of the dilated and 'white-coloured' ER, small grey circles can be visualised. It is possible that these could be protein aggregates forming as a result of ER stress inducing drug treatment, or they could be analogous to the unidentified granules observed by Lee *et al*., 2005.

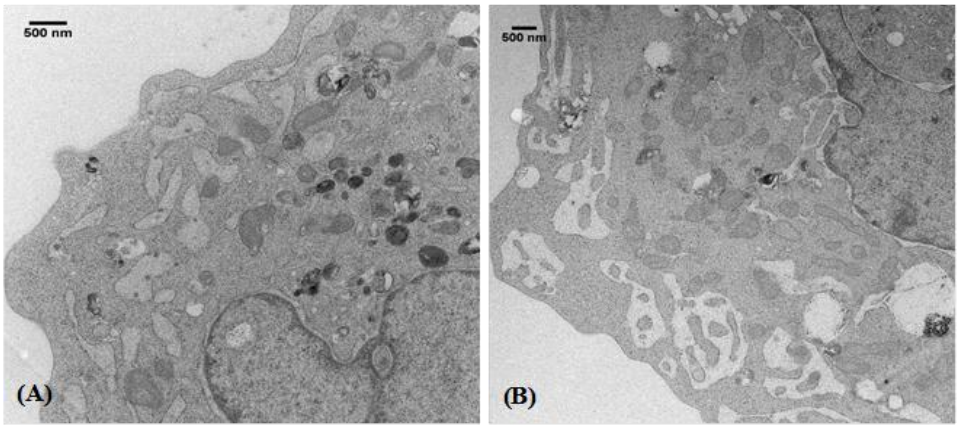

Figure 5.5: (A) and (B) show swollen, disrupted ER and also the 'white' perinuclear space in the ER-stress D711A-hIRE1α MEFs (B) also verifies that the ER is continuous with the outer nuclear membrane. Magnification: (A): x20,000 and (B): x15,000. Scale bars represent a distance of 500 nm.

In the K559A mutant, the level of ER expansion as a result of the stress response being activated was maybe very slightly less than the WT-hIRE1α and D711A-hIRE1α, but nonetheless was very badly formed. It lacked both structure and integrity, and was even less organised than the ER seen in the D711A-hIRE1α mutant. As above, there seemed to be some correlation with severely swollen ER and the white nuclear perimeter, however, this phenotype was observed less often than in the D711A-hIRE1α cells.

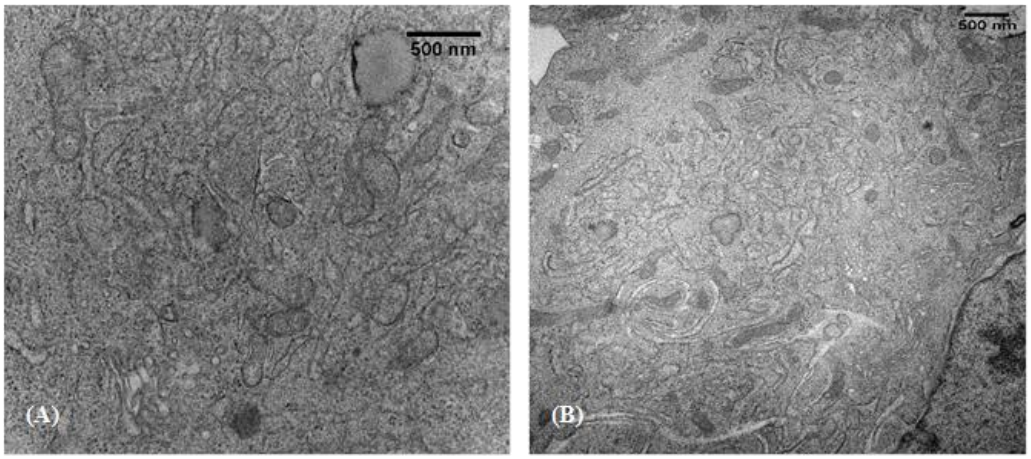

Figure 5.6: (A) and (B) show disorganised and 'tangled' ER in the K599A-hIRE1α MEFs treated with tunicamycin. Magnification: (A): x30,000 and (B): x 20,000. Scale bars represent a distance of 500 nm.

5.3: Quantification of TEM results confirms the mutants have a dilated ER

The online random number generator, random.org, was used to generate random numbers between 1 and the highest number of the photos taken for a specific cell line and treatment. For example, if 120 photos were taken for the D711A-hIRE1α mutant, random numbers were generated between 1 and 120. In total 20 random images were analysed for each cell line and treatment. Any picture taken below a magnification of 15,000 times was not quantified. This is because there would have been significant error when measuring the width of ER lumen, especially in the untreated and tetracycline-treated cells, where the ER was the most narrow. Omitting these photos would not have biased the results as only a very small proportion of pictures were taken at low magnification.

The images taken were analysed using ImageJ software. First a randomly offset grid of crosses was overlaid onto the image. From this three areas of ER were randomly selected for measurement of the ER lumen width once the appropriate scale has been set. An average was taken for each image analysed, and then from this, the overall average for the cell line and treatment was calculated.

Table 5.1: The width in nm of the ER lumen ± SE for each cell type and treatment. 'UNTR' represents the untreated, control MEFs. 'Tet' indicates where only tetracycline has been added, whereas 'Tet/Tn' highlights cells treated with both tetracycline and tunicamycin.

WT-hIRE1α			D711A-hIRE1α			K599A-hIRE1α		
UNTR	**Tet**	**Tet/Tn**	**UNTR**	**Tet**	**Tet/Tn**	**UNTR**	**Tet**	**Tet/Tn**
88.8 ± 4.5	85.6 ± 4.4	88.7 ± 8.9	89.5 ± 4.8	105.5 ± 4.8	239.9 ± 27.8	98.3 ± 6.2	86.6 ± 3.3	164.7 ± 13.4

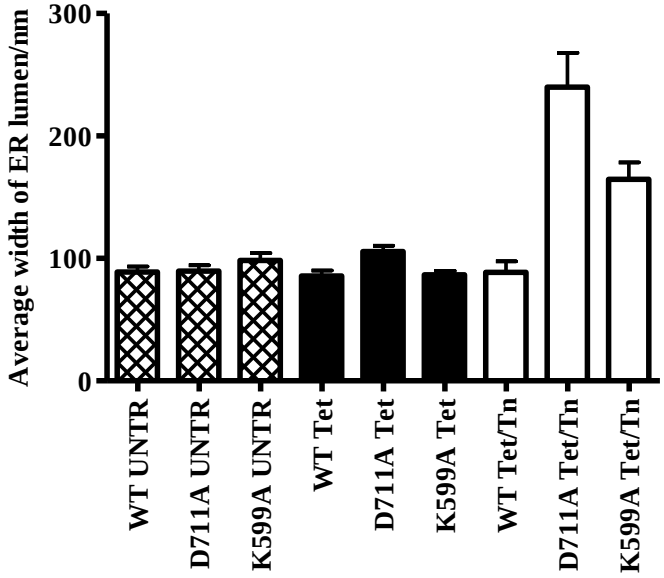

Figure 5.7: Graphical representation of the data in table 5.1 depicting the variability between the samples.

An unpaired *t*-test was carried out to determine whether the differences between the samples were statistically significant. The confidence limits were set to 95% and Welch's correction was used if the variances between the samples were significantly different in the original *t*-test. There was no significant difference between any of the untreated cells. Tunicamycin treated D711A-hIRE1α and K599A-hIRE1α were both significantly different from one another ($p = 0.02$) and also the WT-hIRE1α treated cells ($p < 0.0001$).

The values obtained for all three untreated cell lines are all quite similar to each other. Most importantly, all of these values fall within the limits of the average width of the ER lumen, between 60 and 120 nm (referenced in Klopfenstein *et al*., 2001). Interestingly, the measurement achieved for ER-stressed WT-hIRE1α cells also conforms with the average width, suggesting that the ER proliferates when under stress but provided there is normal UPR signalling, it does not become dilated and/or unstructured. The two mutants, however, show a dramatic increase in the ER width, with the most impressive increase being in the D711A-hIRE1α mutant. Combined with observations from the images taken, it would seem that the D711A-hIRE1α and K599A-hIRE1α mutants both show the capacity for ER proliferation but the organelle becomes more disorganised and presumably dysfunctional as the severity of the mutation increases from D711A-hIRE1α to K599A-hIRE1α. This would be consistent with the fact that phospholipid synthesis can be controlled by either XBP-1(s) or ATF6(f), but that specifically organising these phospholipids into sheets and/or tubules of ER requires hIRE1α kinase activity.

For the D711A-hIRE1α mutant, random pictures were chosen in the same way as described above, to measure the distance between the outer and inner nuclear membrane. This measurement was easy to take as the white colour in the perinuclear space made it possible to distinguish the inner and outer membranes from the background. The average distance was calculated to be 77.2 nm, which is much greater than the normal perinuclear distance between 20 and 40 nm (Cohen *et al.*, 2002). The interaction between SUN- and KASH-domain proteins is thought to anchor the inner and outer nuclear membranes together (Padmakumar *et al*., 2005). Therefore, the electronmicrographs suggests that D711A-hIRE1α may have abnormal or no SUN/KASH-domain interactions in the nuclear membrane. A random measurement of this distance could not be taken for the K599A-hIRE1α mutant, as too few pictures depicted this phenotype and the lack of the 'space' between the two membranes would have made it too difficult to measure accurately. It is surprising that the latter mutant is more similar to the WT in terms of this perinuclear phenotype. For this reason, it would be useful to characterise *xbp-1*$^{-/-}$ or *ire1*$^{-/-}$ cells, which have been reconstituted with a form of IRE1α which possesses kinase function, but lacks RNase activity.

5.4: ER-Tracker™ experiments validate the phenotype seen in TEM

Using ER-tracker is a very powerful tool as it enables the user to visualise live cells. Having observed that ER proliferation occurred in each of the three cell lines upon induction of stress, it was decided to attempt to quantify the relative volume of ER. Therefore, these experiments were designed to determine whether the relative ER volume in each of the tunicamycin-treated cell lines was increased by the same amount compared to their untreated and tetracycline treated counterparts. If this were the case, it would demonstrate that the mutants were lacking the capacity to structurally organise their ER but that proliferation was normal. The use of ER-Tracker™ would also help determine whether or not IRE1α kinase activity plays a role in ER biogenesis alongside XBP-1(s) and ATF6(f).

The time course of drug treatments was approximately 24 h shorter than that carried out for electron microscopy due to that fact that further into the treatment the cells start dying and detaching from the plate, making it difficult to visualise and take 'live' pictures in a short time-frame. These experiments confirmed what was seen in the electron microscopy, especially for the D711A-hIRE1α mutant. When the UPR was induced in this mutant, the dye was seen to highlight several swollen, oval-shaped fragments of ER, reinforcing that ER organisation is not maintained in this mutant. It could be seen that the ER did not form a smooth continuous network. There appeared to be some swollen 'blebs' of ER in the K599A-hIRE1α mutant, along with a disorganised network around the nucleus.

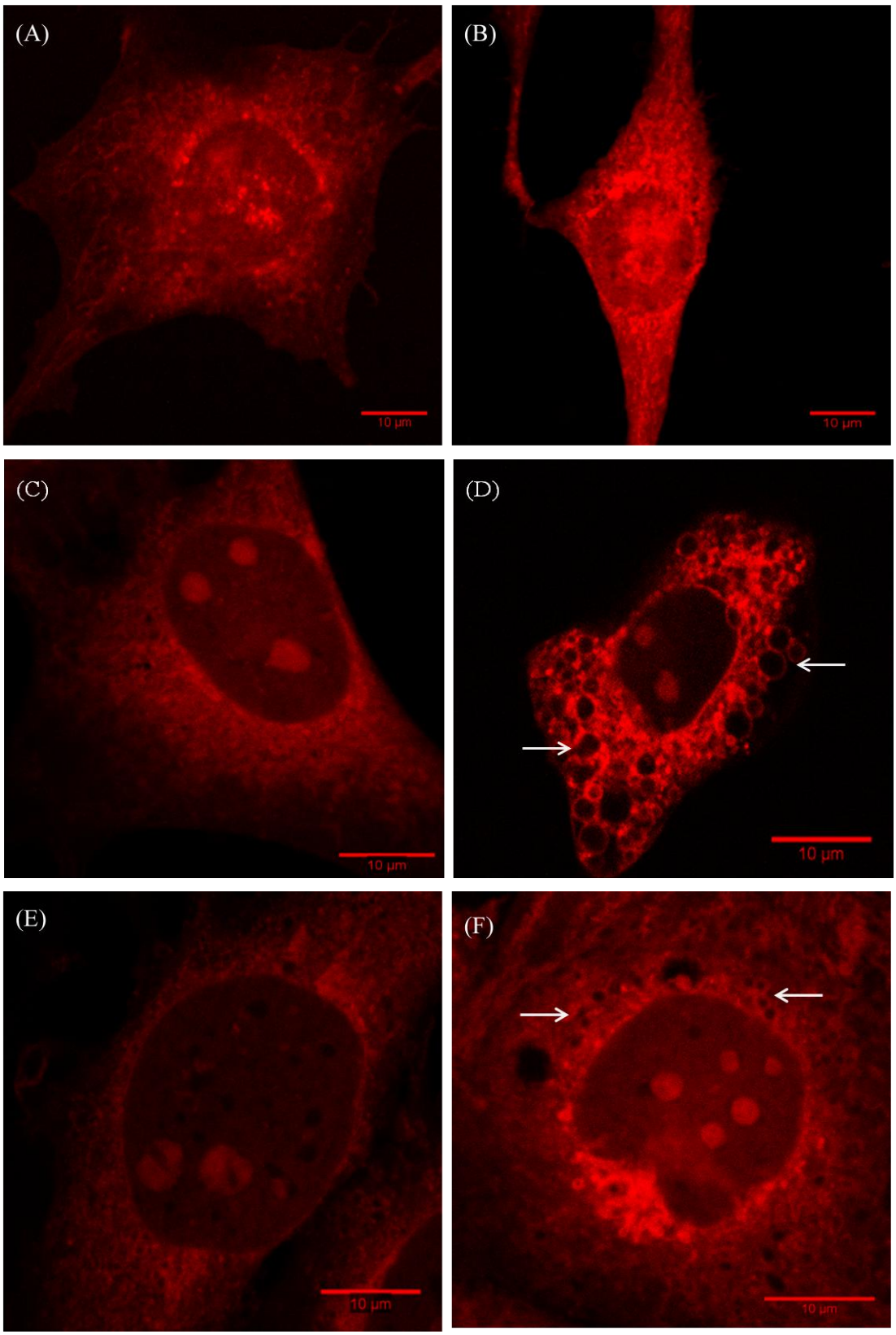

Figure 5.8: ER-tracker confocal microscopy images. (A), (C) and (E) represent tetracycline treated WT-hIRE1α, D711A-hIRE1α and K599A-hIRE1α MEFs, respectively. (B), (D) and (F) represent tunicamycin treated WT-hIRE1α, D711A-hIRE1α and K599A-hIRE1α MEFs respectively. The arrows in (D) indicate swollen areas of ER in the D711A-hIRE1α mutant, whereas the arrows in (F) show some smaller 'blebs' in the K599A-hIRE1α mutant. An image representing the untreated WT-hIRE1α can be found in the appendix. All scale bars represent a distance of 10 µm.

Despite the fact that the ER-tracker experiments validated the observations from TEM, it was not possible to obtain a value for the amount of ER. For measuring ER volume, a macro (Wojciechowicz *et al*., 2013) was modified for use on ImageJ, to quantify the 'amount' of red fluoresence. Theoretically, quantifying this fluorescence for each cell line and treatment should have given a 'relative ER volume' value. However, this could not be implemented due to that fact that there was some bias in the selection of cells imaged. How this bias arose is explained below.

Having previously looked at some stained MEFs under the confocal microscope, the parameters were set to the following:

- Scan speed: x6
- Line average of 2
- Laser intensity of 67.3
- Detector gain of 676
- HeNe lamp wavelength of 543 nm

It was important to keep these settings fixed for each picture taken, as otherwise the brightness of the image would change depending on the scan speed and laser intensity chosen. This would have effectively deemed this experiment void, as in theory there should be a positive correlation between the amount of ER present in the cell, and the intensity of the fluorescence.

Upon first observation, these settings seemed to be appropriate as none of the cells visualised were either too bright or too dim for the camera. Later however, it became apparent that some cells had taken up the dye much more effectively than others (as seen in Figure 5.8 below) and were indeed so bright that an image could not be taken. Thus, there was an immediate bias in the cohort of pictures taken and quantifying these would not have given a representative value for the volume of ER in the different cell types.

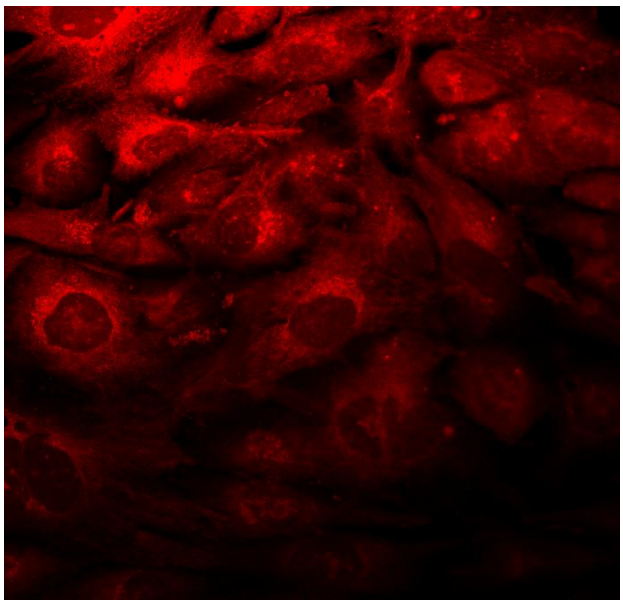

Figure 5.9: an example of K599A-hIRE1α tunicamycin treated MEFs highlighting the unequal uptake of the ER-tracker dye within a group of cells.

In general, it seemed as though the cells closest to the centre of a clump were the most brightly stained. For future work, when repeating this experiment, the cells should be sonicated prior to being seeded for the time course. It might also be advantageous to place the glass-bottomed plates onto a rocker or shaker for the whole time they are being incubated with the ER-tracker dye.

5.5: Discussion

It was established that *XBP-1* splicing is very similar in both WT-hIRE1α and D711A-hIRE1α cells, and was undetectable by RT-PCR in cDNA from K599A-hIRE1α cells (Figure A1.1). However, the fact that there is no visible increase in the amount of ER when each of the cell lines was treated with tetracycline suggests that *XBP-1* splicing alone does not suffice to induce ER expansion, and that stress is also required. The reason this may not conform with experiments conducted by Sriburi *et al*., could be because their XBP-1(s) transduction may be responsible for producing much higher levels of protein.

Since the treated K599A-hIRE1α cells show an increase in ER amount comparable to that seen in the WT-hIRE1α and D711A-hIRE1α cells, it suggests that other proteins apart from XBP-1(s), such as ATF6, might be sufficient to cause this effect in the absence of *XBP-1* splicing, as implied by Bommiasamy *et al*., 2009. Also, the difference in phenotype between the two mutant cell lines confirms that the distortions observed in both of them are not simply a result of cell death (personal correspondence: Dr. M. Goldberg, 19/04/2013, meeting).

What is most intriguing about these results is the evident loss of control over ER organisation seen in both ER-stressed mutants. The kinase inactive mutants display a severely dilated ER, which is sometimes seen in the K599A-hIRE1α mutant along with a very distorted ER phenotype. This implies that the kinase domain plays a role in structuring the ER. The reason the organisation seems worse in the K599A-hIRE1α mutant could be due to loss of activity from both domains of IRE1α, with XBP-1 playing a smaller role in organising the ER.

The results discussed argue that the kinase domain is required for proper organisation of the ER. If lack of kinase activity is partly responsible for structuring the ER, this helps answer why the D711A-hIRE1α cells die before the WT-hIRE1α cells, as suggested by the PARP-1 and caspase-3 Western blots, and the MTT assay carried out by Dr.Sutcliffe. It is also possible that this mutation directly or indirectly caused the increased perinuclear distance observed in these stressed cells. Immunofluorescence was carried out in all three cell lines using antibodies against Sun-1 and Nesprin-2 as it was hypothesized that the localisation of these proteins may have been disturbed in the D711A-hIRE1α mutant, since they link the outer and inner nuclear membranes together (Padmakumar *et al*., 2005). Unfortunately, there were not enough cells left on the cover slips to make any observations, and therefore this experiment should be repeated using poly-L-lysine coated cover slips to help the cells adhere in place while the washes are being done (personal correspondence: Dr. I. Karakesisolou, 26/06/13, meeting).

Ideally, the TEM and confocal work should be repeated making the above mentioned changes. Despite the fact that 'ER-tracker' dye has been used during activation of the UPR (Tan *et al.*, 2006) it is possible that the sulphonylurea receptors that the dye binds to (Zhang *et al*., 2010) are not as abundant and/or equally distributed during ER stress compared to during homeostasis. Synthesis of these receptors during ER stress may also be compromised. Therefore stereological techniques should also be used in conjunction with confocal microscopy to measure the volume of the ER, provided that non-biased serial sections could be taken (personal correspondence: Dr. R. Banks, 23/04/2013, meeting). As mentioned in Chapter 4, the relationship between the kinase domain and ER physiology via the TRB3 route could also provide useful information as to how the structure of the ER is maintained whilst it is proliferating to cope with ER stress. The kinase domain may indeed play a role in determining the expression of reticulons and Climp-63 – both of which are required to structure the ER into the classical tubular network (Shibata *et al*., 2010).

It would also be very interesting to determine whether there is more smooth ER in relation to rough ER in either or both of the mutants compared to the WT-hIRE1α. This can be carried out by separating these two constituents by equilibrium centrifugation and then quantifying how much there is in each fraction (Alberts *et al*., 2002).

Finally, it would be useful to show where the human IRE1α proteins are located within the ER membrane in the three different cell lines. This could be achieved by using immunofluoresecent labelling of IRE1α, or alternatively, immunogold labelling. In theory, upon tetracycline induction of each IRE1α form, the protein should become clustered in groups throughout the ER (Li *et al*., 2010). This would serve as a good control to prove there were no differences in the localisation of any of the three forms of human IRE1α.

Chapter 6

Concluding remarks and future work

The principal objective of this project was to determine pathways via which the kinase activity of human IRE1α may play a role in cell survival downstream of ER stress. Although no significant changes in PARP-1 and caspase-3 cleavage were found when comparing D711A-hIRE1α cells to WT-hIRE1α cells, there was a large increase in CHOP expression. Since CHOP is implicated in cell death (Oyadomari and Mori, 2004) this indicates that the kinase domain is required as well as endoribonuclease activity for cell survival downstream of the unfolded protein response being activated.

QPCR data showed that *TRB3* expression was also elevated the most in the D711A-hIRE1α cells. In order to determine a mechanism as to how lack of kinase activity compromises the cell, it would be useful to investigate Akt activation and expression of proteins it interacts with using both qPCR and Western blotting. One of these proteins is VCP/p97, which Akt is known to inhibit (Vandermoere *et al*., 2006). As described in chapter 4, it was found that there was a relation between the knockdown of VCP and the phenotype of swollen ER (Wócjik *et al*., 2006). This is in agreement with the D711A-hIRE1α phenotype observed by TEM and confocal techniques in Chapter 5. These data all argue that there is a relationship between the IRE1α kinase and the TRB3-Akt axis, however further research is required to elucidate whether or not this relationship is direct. Analysing this pathway could give some insights into the role autophagy plays during ER stress in the three different cell lines, as TRB3 should lift the inhibition on this degradation pathway imposed by mTOR (Salazar *et al.*, 2009). The LC3 plasmid, which was characterised and prepared for transfection, could be used to confirm these findings.

qPCR analysis also revealed that certain genes upregulated in the stressed WT-hIRE1α cells were induced to much lower levels in *both* of the mutants (not just in the K599A-hIRE1α cells). *ERO1L-α*, *ERDJ4*, and *HRD1* were essentially reduced to the same levels in tunicamycin-treated D711A-hIRE1α and K599A-hIRE1α cells, implying kinase function is required to ensure full expression of these genes encoding chaperones and ERAD proteins. These interesting differences support the idea that the D711A-hIRE1α mutant needs to be properly characterised using microarray and/or RNA sequencing. *EDEM1* was also reduced in the D711A-hIRE1α mutant, however, not as much as in the K599A-hIRE1α. Loss of expression of *HRD1* and *EDEM* suggest that the ERAD component of the UPR would also be less effective in the kinase-dead cells, providing another possible route of explanation as to why these cells are compromised. To confirm this theory, pulse-chase labelling to determine the rate of turnover of established ERAD substrates will have to be conducted. As with the LC3 construct, plasmids containing established ERAD substrates were validated and prepared for transfection, however time constraints did not allow functional experiments to be carried out.

The ATF6 reporter will need to be used to validate whether or not there is an upregulation of this UPR signal transducer. If there is, then this will explain the increased expression of certain genes detected by qPCR analysis in the K599A-hIRE1α mutant. It may also be useful to carry out ChIP assays to show ATF6 binds to the promoters of the genes upregulated in the latter mentioned mutant. However, one must not rule out the possibility that PERK may also play a role in changing the transcriptional outcome during ER stress, and therefore complimentary studies should be carried out using $PERK^{-/-}$ MEFs.

Images from microscopy implicate both kinase and RNase in controlling the width of the ER and structurally organising this organelle under ER stress. It did seem that stress was required for the ER to proliferate, and not just *XBP-1* splicing as previously reported (Sriburi *et al.*, 2004; Sriburi *et al.*, 2007). Proliferation in the K599A-hIRE1α mutant did seem slightly less in comparison to the other two cell lines. This is in agreement with the BIP profile shown in Chapter 3, however Western blotting for a different ER-resident protein (not inducible by ER stress) would be required for evidence of ER volume, preferably alongside ER-tracker experiments.

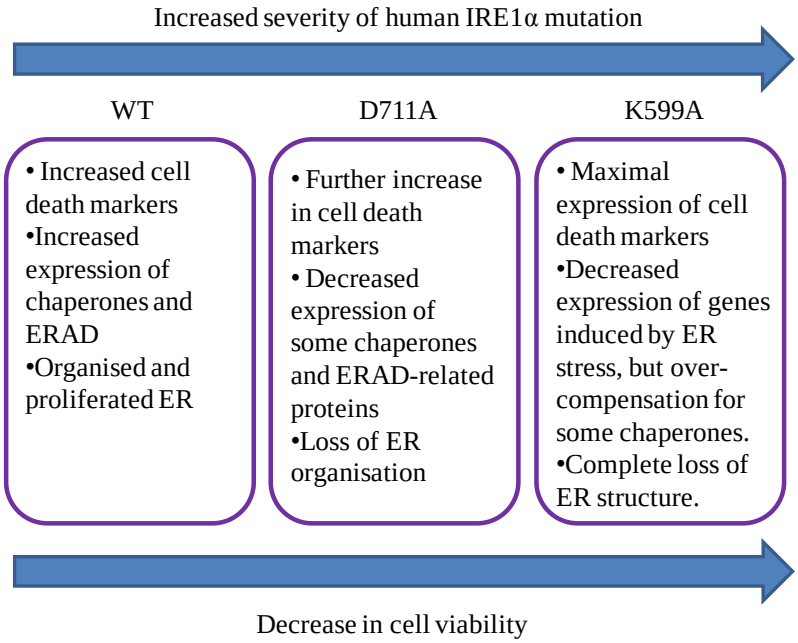

Figure 6.1: Summary of experimental findings.

The results and future experiments discussed in this thesis should help to map cell decision pathways downstream of human IRE1α as part of the UPR. Since UPR-mediated cell death plays such an important role in health and disease (reviewed in Schröder and Kaufman, 2005) this work will eventually help ascertain which areas can be targeted to either promote the survival signals, or dampen cell death massages. It is likely that the kinase can have both antiapoptotic and proapoptotic roles, depending on the precise cellular conditions. Since UPR-mediated death is attributed to cell loss in the brain and pancreas in Parkinsonism and diabetes, respectively, identifying exactly what determines the nature of this kinase activity has very important medical implications.

As an extension of this work, it would also be informative to use kinase inhibitors, such as sunitinib (Ali *et al*., 2011, Korennykh *et al*., 2011), to question the mechanism of how these chemicals affect cell fate. Development of inhibitors specific only to IRE1α kinase could prove particularly useful for inducing death in cancer cells. These cells are believed to survive the high levels of ER stress caused by their hypoxic and nutrient-poor environment (Feldman *et al*., 2005). Elucidating the role of IRE1α kinase holds the key to discovering therapeutics strategies to combat an array of varying human diseases.

APPENDIX

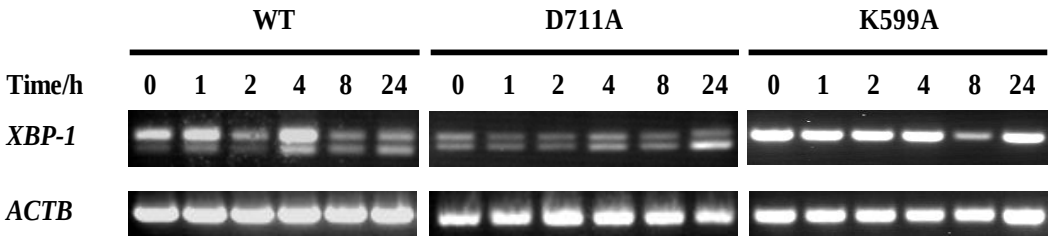

Figure A1.1: RT-PCR carried out by Louise Sutcliffe showing* XBP-1 *splicing in WT-hIRE1α, D711A-hIRE1α and K599A-hIRE1α MEFs. Times indicate treatment with 1 μg/ml tetracycline. Samples are one of three replicates (Sutcliffe, 2012).

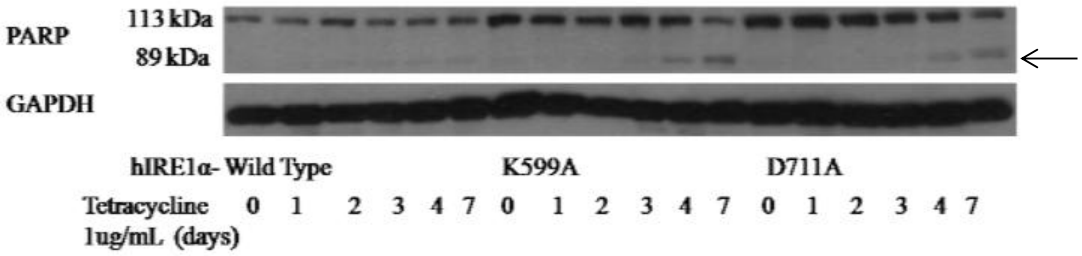

Figure A1.2: WB carried out by Louise Sutcliffe showing PARP-1 cleavage in WT-hIRE1α, K599A-hIRE1α, and D711A-hIRE1α MEFs after induction of hIRE1α expression using tetracycline (Sutcliffe, 2012). The arrow represents the cleaved fragment.

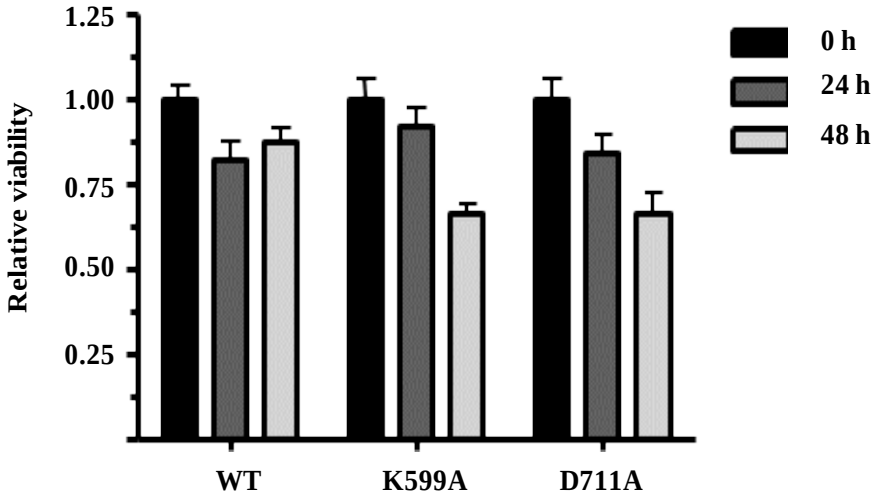

Figure A1.3: Results of an MTT assay carried out by Louise Sutcliffe, showing relative viabilities of WT-hIRE1α, K599A-hIRE1α, and D711A-hIRE1α MEFs after 0, 24, and 48 h of 100 ng/ml tunicamycin treatment (Sutcliffe, 2012).

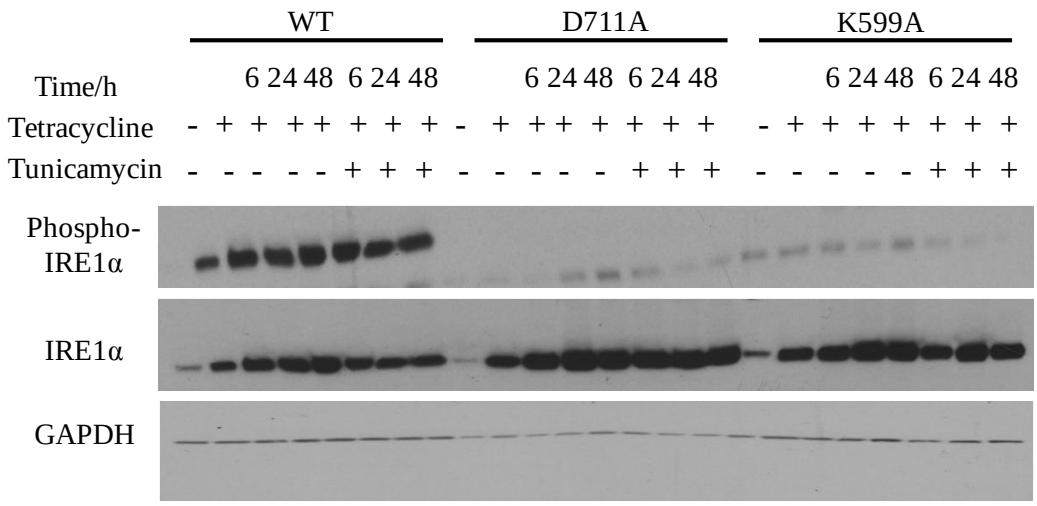

Figure A3.1: Western blot showing expression levels of IRE1α and its phospho-form from hIRE1α WT, D711A and K599A MEF lysates. – and + indicate absence or presence of the appropriate drug. Cells treated with tetracycline were harvested after 4 h, then after 6, 24 and 48 h of combined tetracycline and DMSO treatment. ER-stressed cells were harvested after 6, 24, and 48 h of combined tetracycline and tunicamycin treatment. GAPDH was used as the loading control.

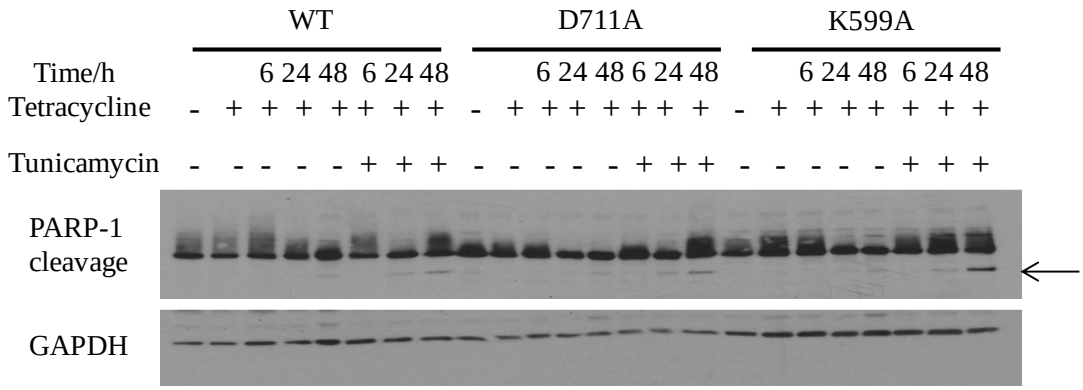

Figure A3.2: Western blot showing levels of PARP-1 cleavage from hIRE1α WT, D711A and K599A MEF lysates. The arrow indicates the cleaved fragment. – and + indicate absence or presence of the appropriate drug. Cells treated with tetracycline were harvested after 4 h, then after 6, 24 and 48 h of combined tetracycline and DMSO treatment. ER-stressed cells were harvested after 6, 24, and 48 h of combined tetracycline and tunicamycin treatment. GAPDH was used as the loading control.

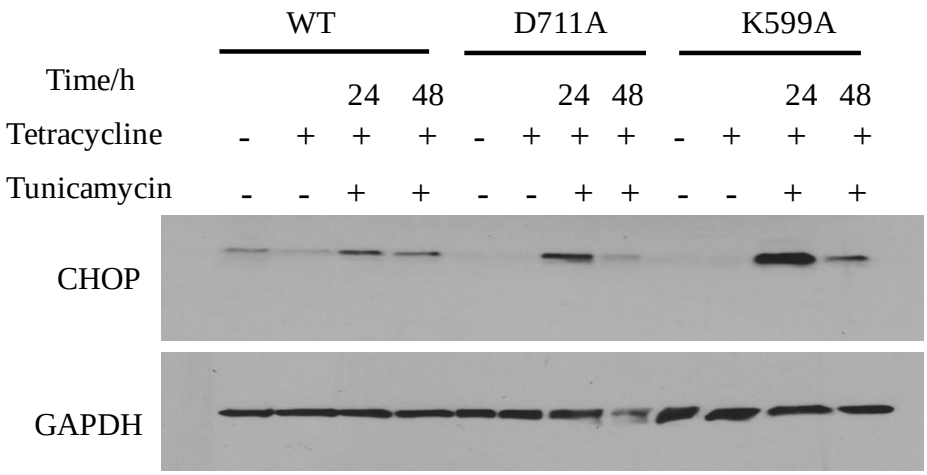

Figure A3.3: Western blot showing expression levels of CHOP from hIRE1α WT, D711A and K599A MEF lysates. – and + indicate absence or presence of the appropriate drug. The time/h indicates how long the cells have been treated with tunicamycin. Untreated cells were harvested at the end of the time course. Cells treated with tetracycline were harvested after 48 h of treatment. GAPDH was used as the loading control.

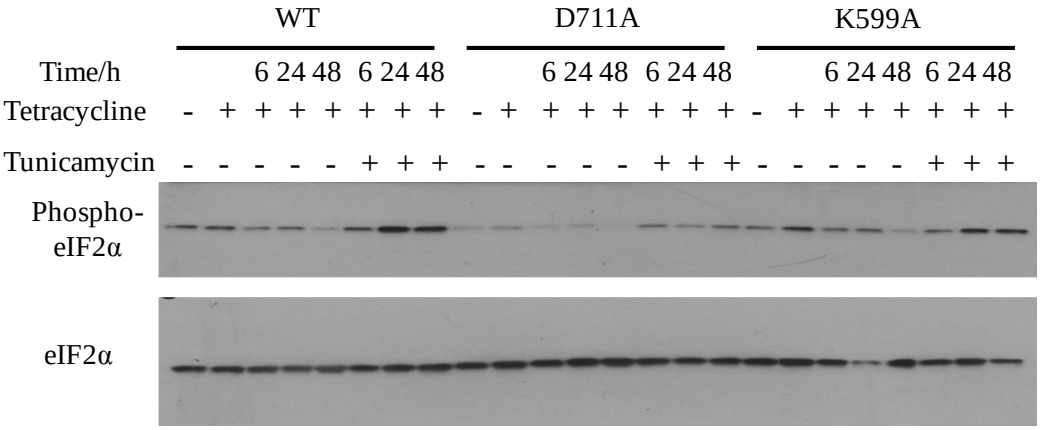

Figure A3.4: Western blot showing expression levels of total eIF2α and its phospho-form from hIRE1α WT, D711A and K599A MEF lysates. – and + indicate absence or presence of the appropriate drug. Cells treated with tetracycline were harvested after 4 h, then after 6, 24 and 48 h of combined tetracycline and DMSO treatment. ER-stressed cells were harvested after 6, 24, and 48 h of combined tetracycline and tunicamycin treatment.

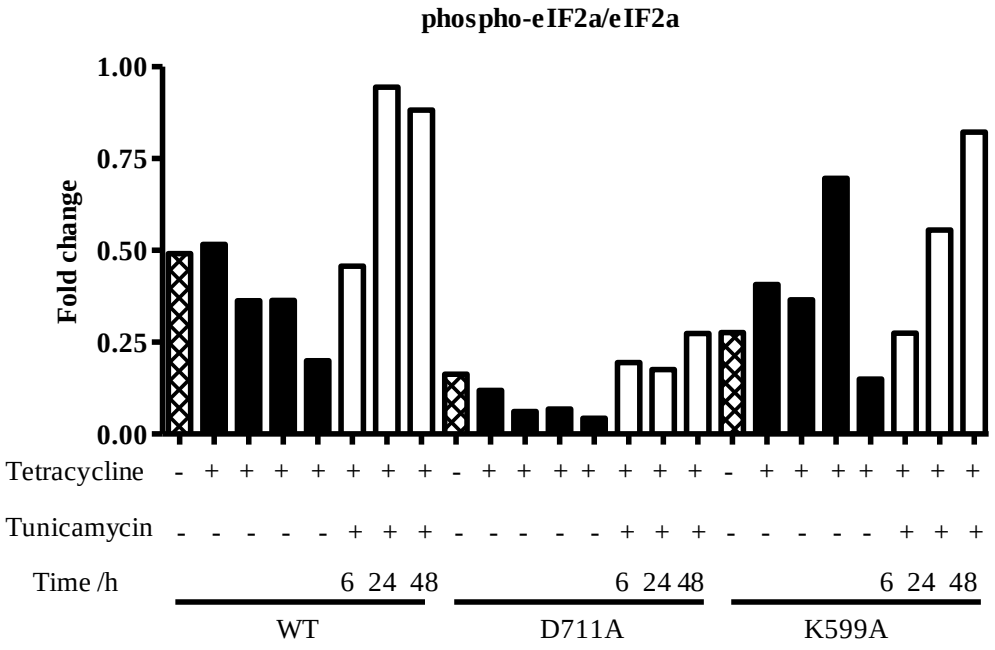

Figure A3.5: Graphical representation of the Western blot image in Figure A2.5. The bands were quantified using ImageJ and phospho-eIF2α/total eIF2α was calculated.

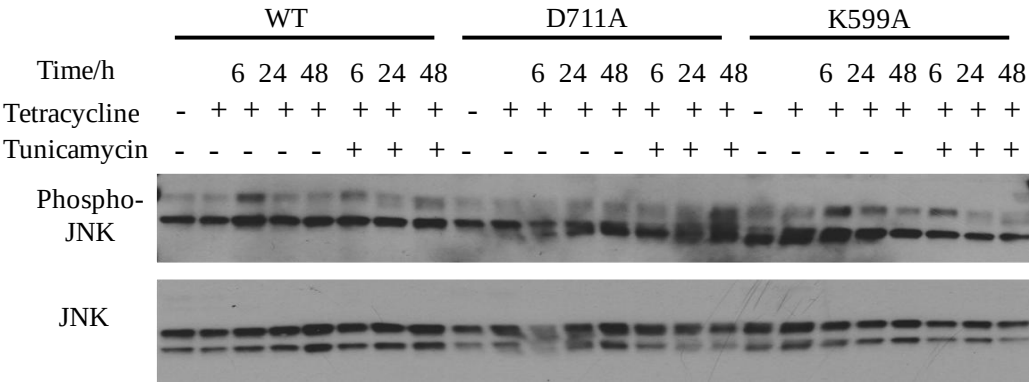

Figure A3.6: Western blot showing expression levels of total JNK and its phospho-form from WT, D711A and K599A lysates. – and + indicate absence or presence of the appropriate drug. Cells treated with tetracycline were harvested after 4 h, then after 6, 24 and 48 h of combined tetracycline and DMSO treatment. ER-stressed cells were harvested after 6, 24, and 48 h of combined tetracycline and tunicamycin treatment.

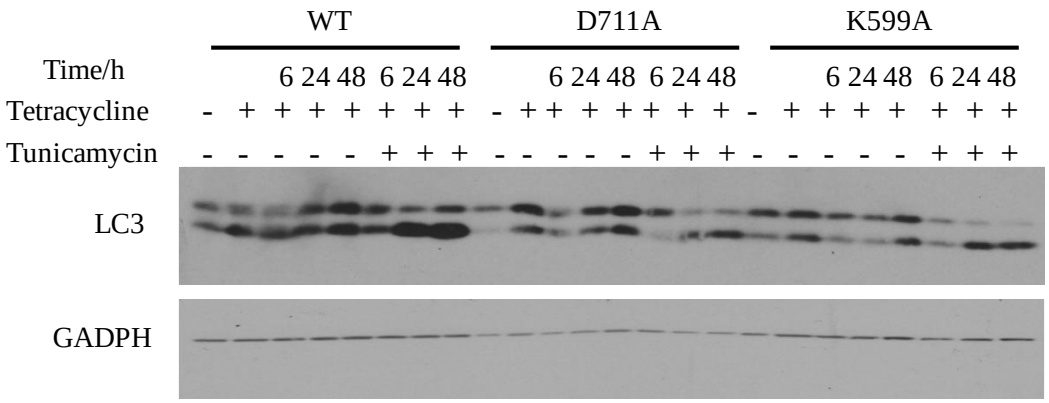

Figure A3.7: Western blot showing expression levels of LC3 from WT, D711A and K599A lysates. – and + indicate absence or presence of the appropriate drug. Cells treated with tetracycline were harvested after 4 h, then after 6, 24 and 48 h of combined tetracycline and DMSO treatment. ER-stressed cells were harvested after 6, 24, and 48 h of combined tetracycline and tunicamycin treatment. GAPDH was used as the loading control.

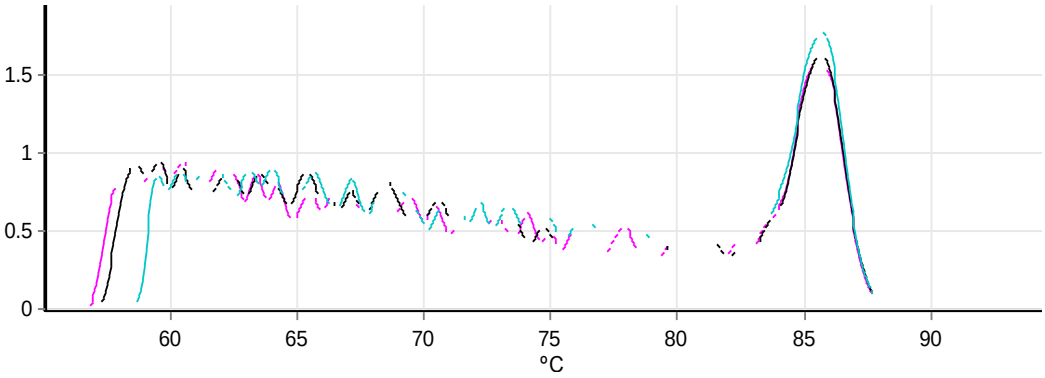

Figure A4.1: Melt curve for the* ACTB *gene in triplicate. The y-axis represents the change in fluorescence (F) over the change in temperature (T), and the x-axis shows the temperature in °C. The single peak represents the PCR product.

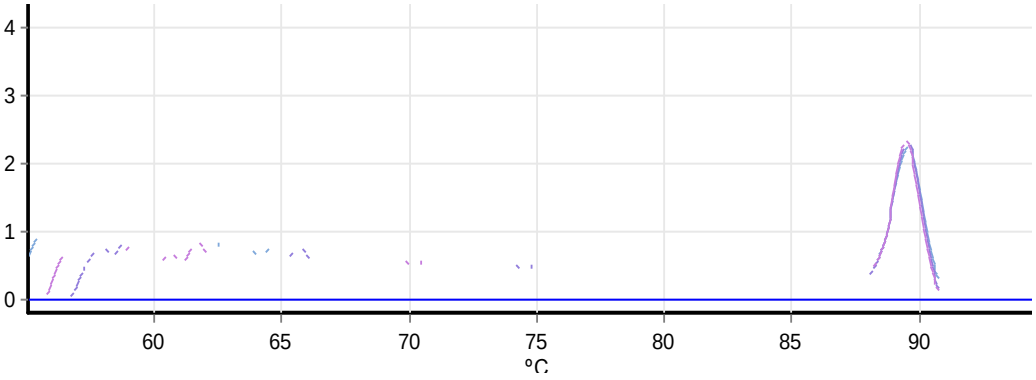

Figure A4.2: Melt curve for the* BIP *gene in triplicate. The y-axis represents the change in fluorescence (F) over the change in temperature (T), and the x-axis shows the temperature in °C. The single peak represents the PCR product.

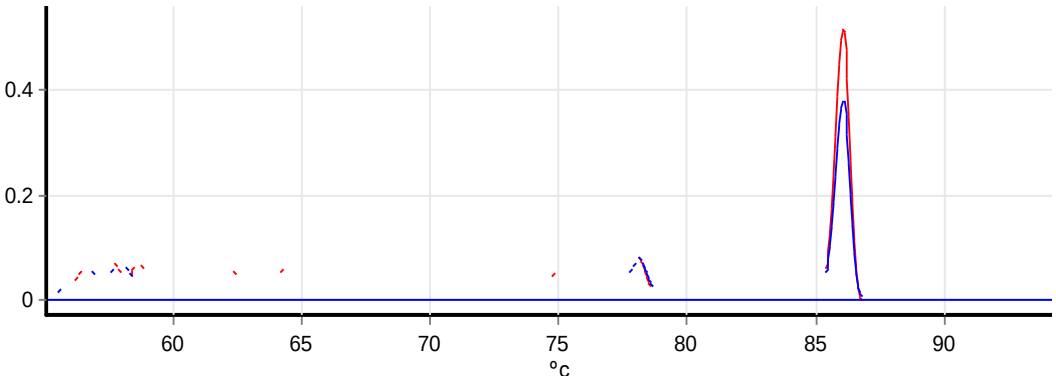

Figure A4.3: Melt curve for the* BLOS1 *gene in triplicate. The y-axis represents the change in fluorescence (F) over the change in temperature (T), and the x-axis shows the temperature in °C. The single peak represents the PCR product.

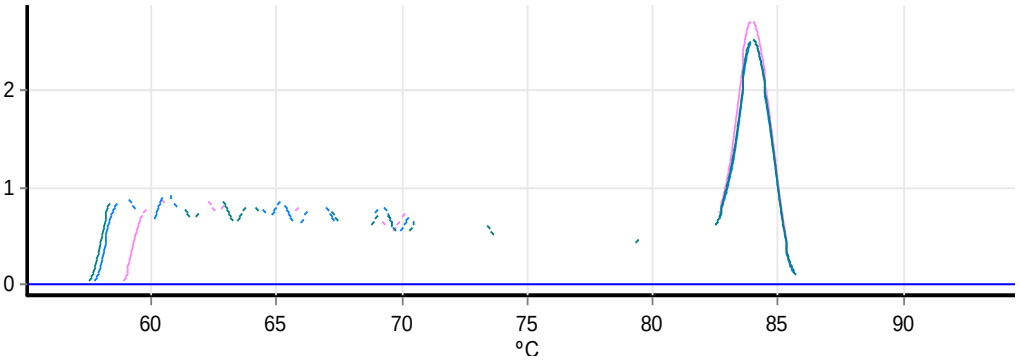

Figure A4.4: Melt curve for the* CHOP *gene in triplicate. The y-axis represents the change in fluorescence (F) over the change in temperature (T), and the x-axis shows the temperature in °C. The single peak represents the PCR product.

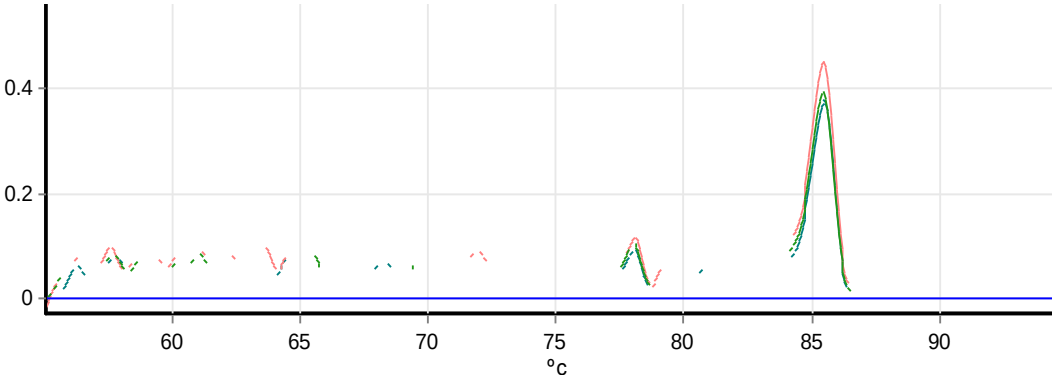

Figure A4.5: Melt curve for the* COL6 *gene in triplicate. The y-axis represents the change in fluorescence (F) over the change in temperature (T), and the x-axis shows the temperature in °C. The single peak represents the PCR product.

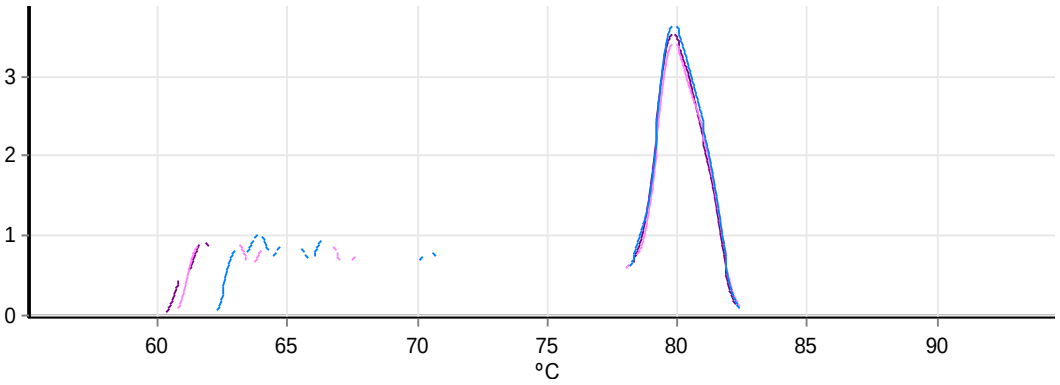

Figure A4.6: Melt curve for the* EDEM1 *gene in triplicate. The y-axis represents the change in fluorescence (F) over the change in temperature (T), and the x-axis shows the temperature in °C. The single peak represents the PCR product.

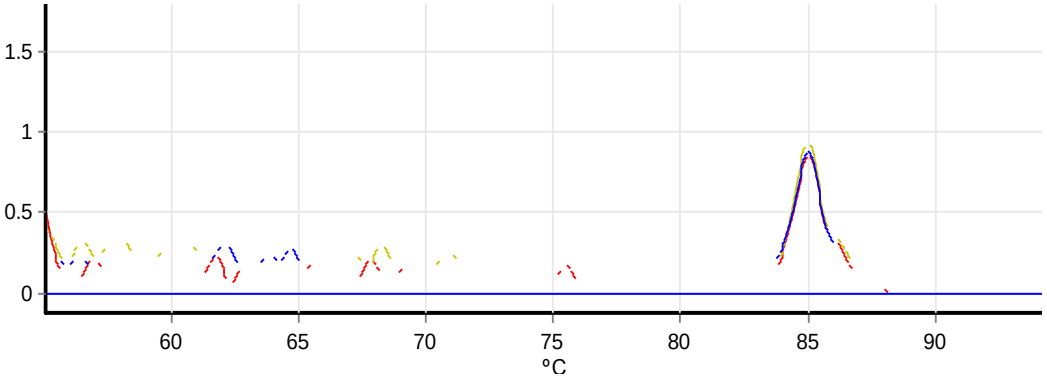

Figure A4.7: Melt curve for the* EPHRINB2 *gene in triplicate. The y-axis represents the change in fluorescence (F) over the change in temperature (T), and the x-axis shows the temperature in °C. The single peak represents the PCR product.

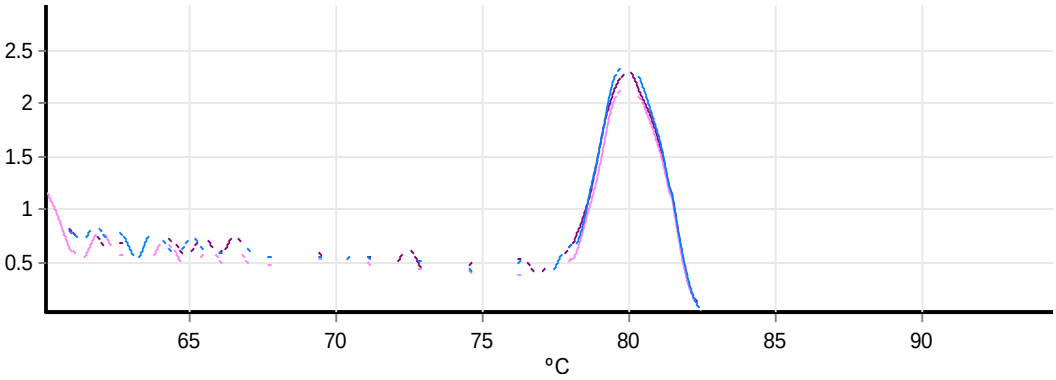

Figure A4.8: Melt curve for the* ERDJ4 *gene in triplicate. The y-axis represents the change in fluorescence (F) over the change in temperature (T), and the x-axis shows the temperature in °C. The single peak represents the PCR product.

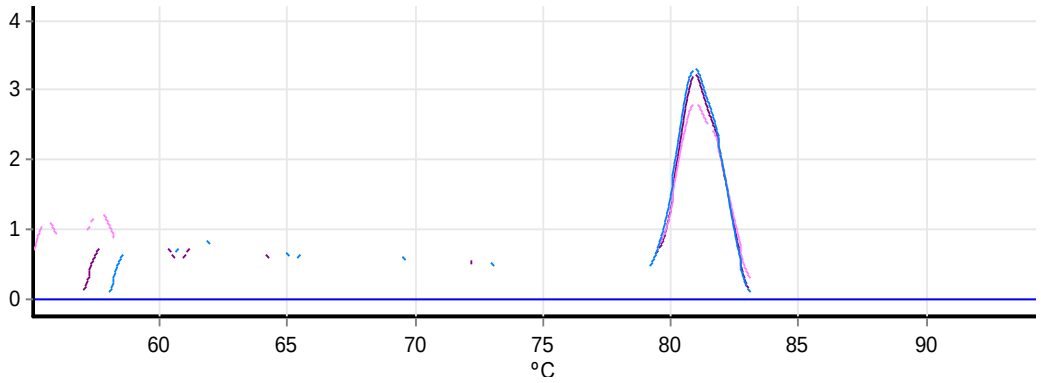

Figure A4.9: Melt curve for the* ERO1L-α *gene in triplicate. The y-axis represents the change in fluorescence (F) over the change in temperature (T), and the x-axis shows the temperature in °C. The single peak represents the PCR product.

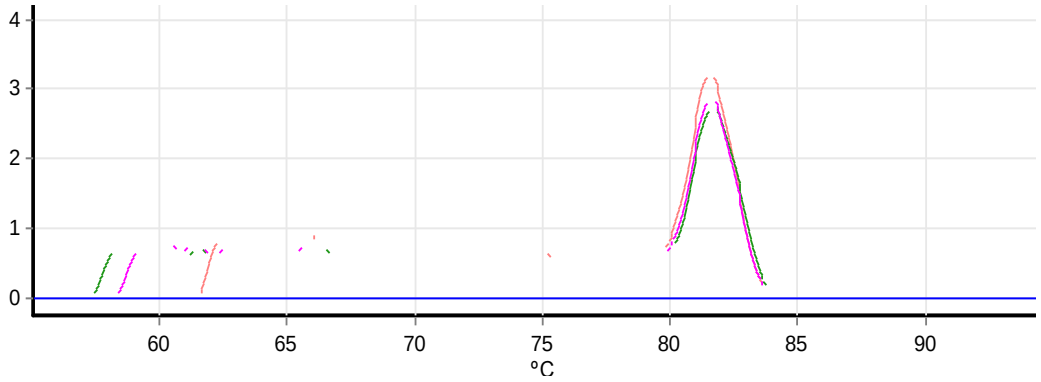

Figure A4.10: Melt curve for the* ERO1L-β *gene in triplicate. The y-axis represents the change in fluorescence (F) over the change in temperature (T), and the x-axis shows the temperature in °C. The single peak represents the PCR product.

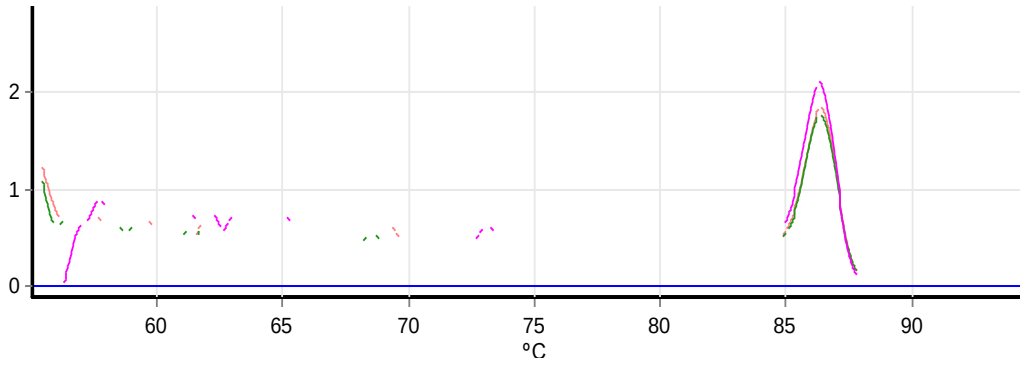

Figure A4.11: Melt curve for the* GADD34 *gene in triplicate. The y-axis represents the change in fluorescence (F) over the change in temperature (T), and the x-axis shows the temperature in °C. The single peak represents the PCR product.

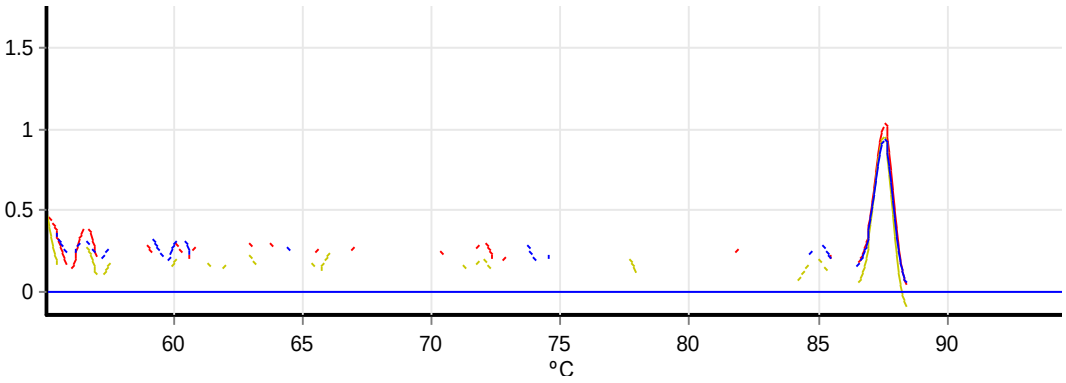

Figure A4.12: Melt curve for the* GALNT10 *gene in triplicate. The y-axis represents the change in fluorescence (F) over the change in temperature (T), and the x-axis shows the temperature in °C. The single peak represents the PCR product.

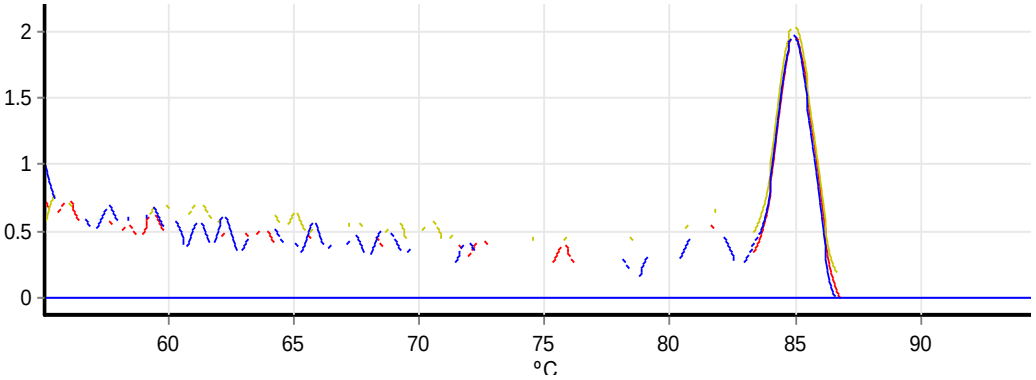

Figure A4.13: Melt curve for the* GRP94 *gene in triplicate. The y-axis represents the change in fluorescence (F) over the change in temperature (T), and the x-axis shows the temperature in °C. The single peak represents the PCR product.

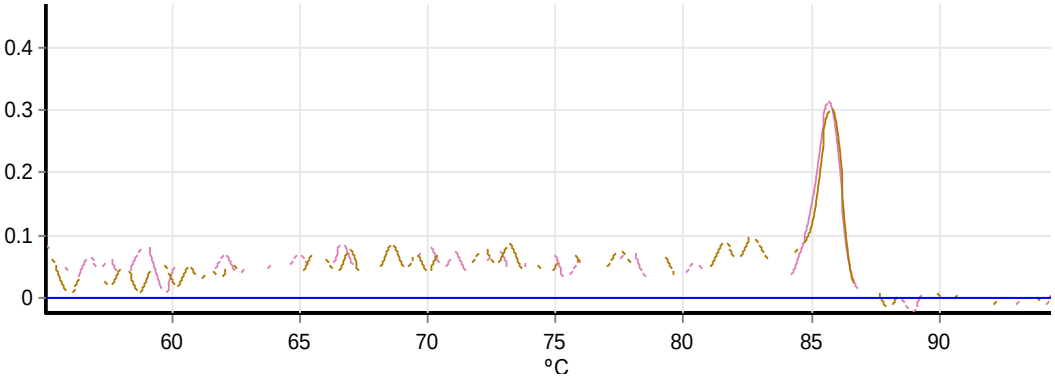

Figure A4.14: Melt curve for the* HEDJ *gene in triplicate. The y-axis represents the change in fluorescence (F) over the change in temperature (T), and the x-axis shows the temperature in °C. The single peak represents the PCR product.

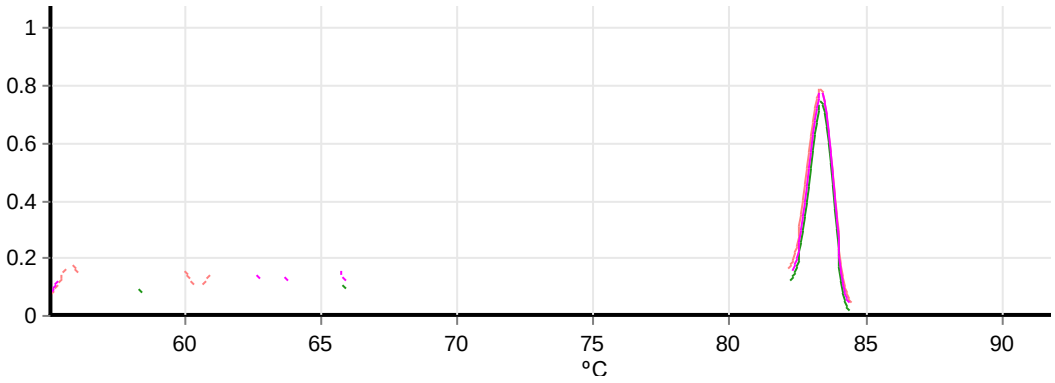

Figure A4.15: Melt curve for the* HERP *gene in triplicate. The y-axis represents the change in fluorescence (F) over the change in temperature (T), and the x-axis shows the temperature in °C. The single peak represents the PCR product.

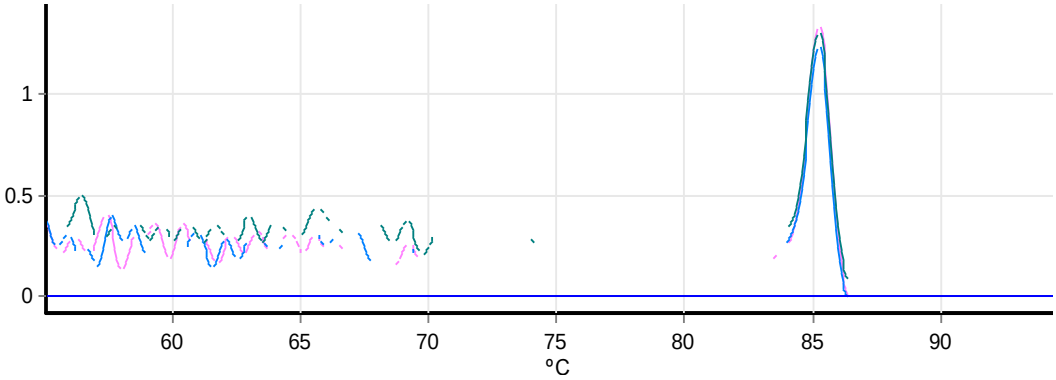

Figure A4.16: Melt curve for the* HGSNAT *gene in triplicate. The y-axis represents the change in fluorescence (F) over the change in temperature (T), and the x-axis shows the temperature in °C. The single peak represents the PCR product.

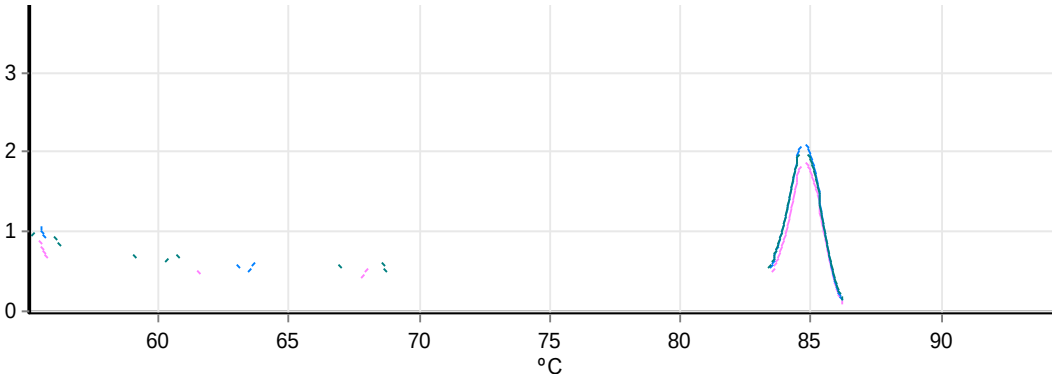

Figure A4.17: Melt curve for the* HRD1 *gene in triplicate. The y-axis represents the change in fluorescence (F) over the change in temperature (T), and the x-axis shows the temperature in °C. The single peak represents the PCR product.

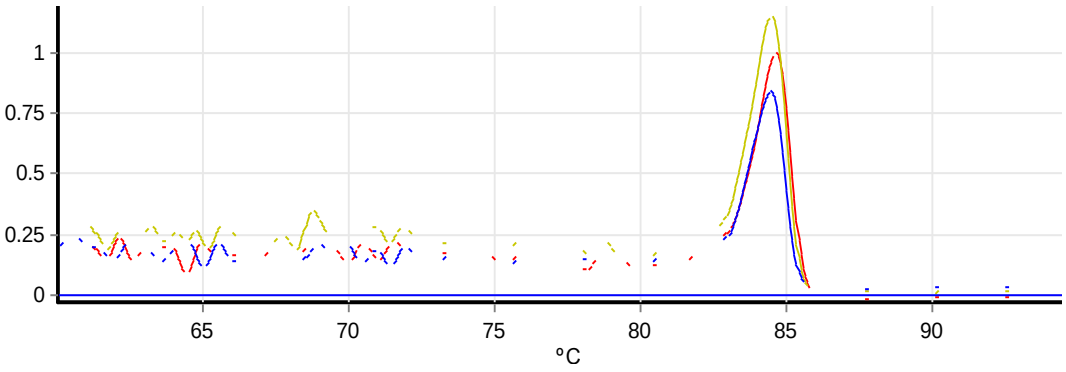

Figure A4.18: Melt curve for the* MAP7d1 *gene in triplicate. The y-axis represents the change in fluorescence (F) over the change in temperature (T), and the x-axis shows the temperature in °C. The single peak represents the PCR product.

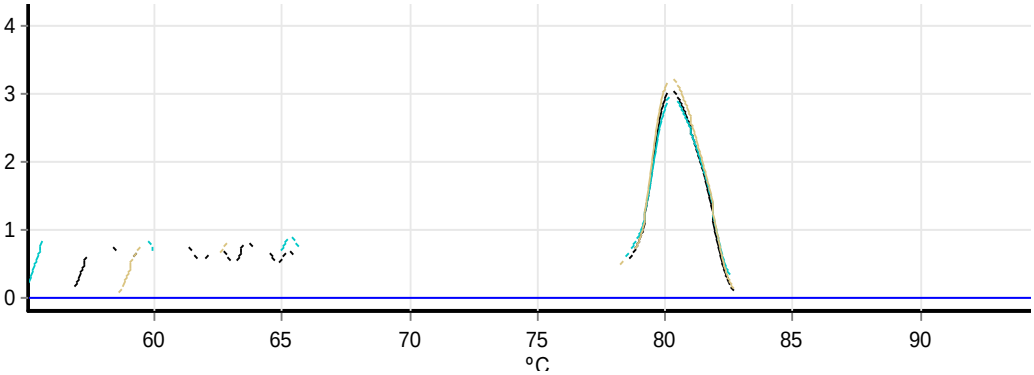

Figure A4.19: Melt curve for the* p58^{IPK} *gene in triplicate. The y-axis represents the change in fluorescence (F) over the change in temperature (T), and the x-axis shows the temperature in °C. The single peak represents the PCR product.

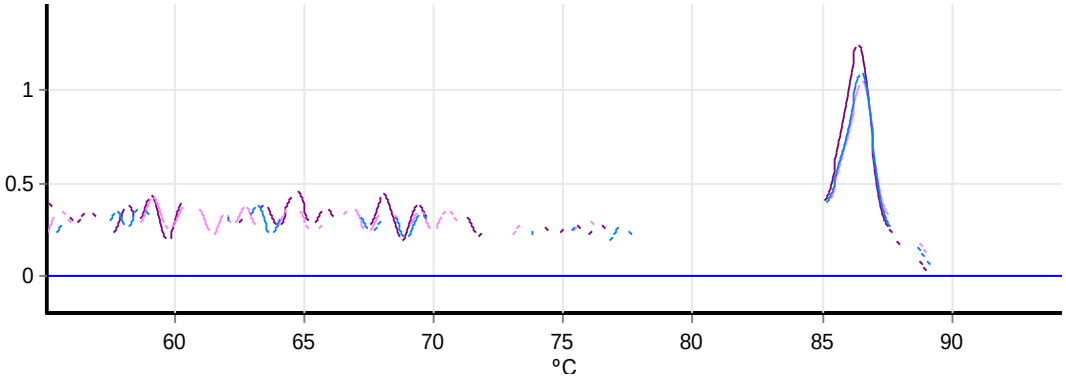

Figure A4.20: Melt curve for the* PDGFRB *gene in triplicate. The y-axis represents the change in fluorescence (F) over the change in temperature (T), and the x-axis shows the temperature in °C. The single peak represents the PCR product.

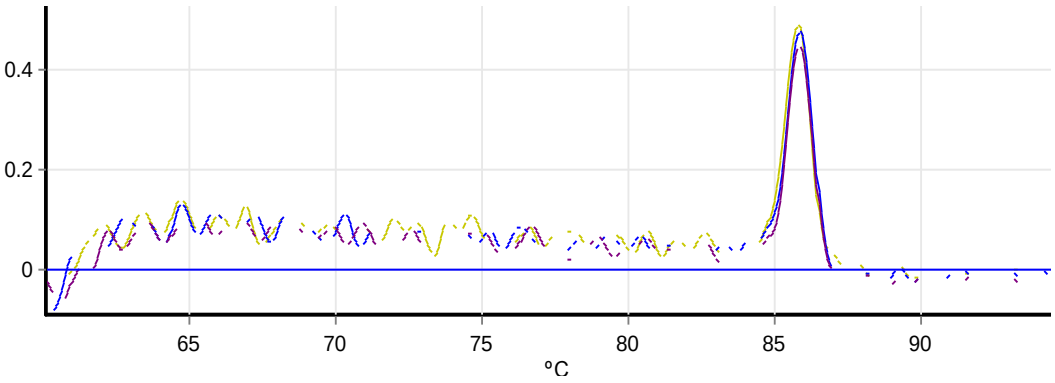

Figure A4.21: Melt curve for the* PMP22 *gene in triplicate. The y-axis represents the change in fluorescence (F) over the change in temperature (T), and the x-axis shows the temperature in °C. The single peak represents the PCR product.

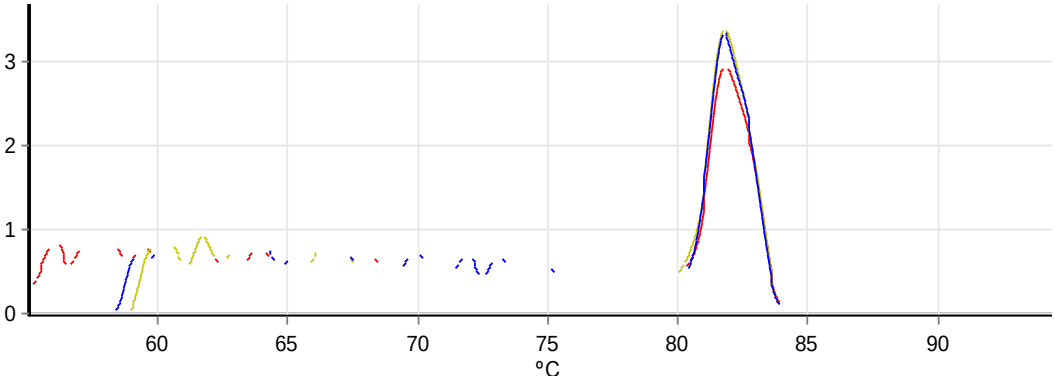

Figure A4.22: Melt curve for the* RAMP4 *gene in triplicate. The y-axis represents the change in fluorescence (F) over the change in temperature (T), and the x-axis shows the temperature in °C. The single peak represents the PCR product.

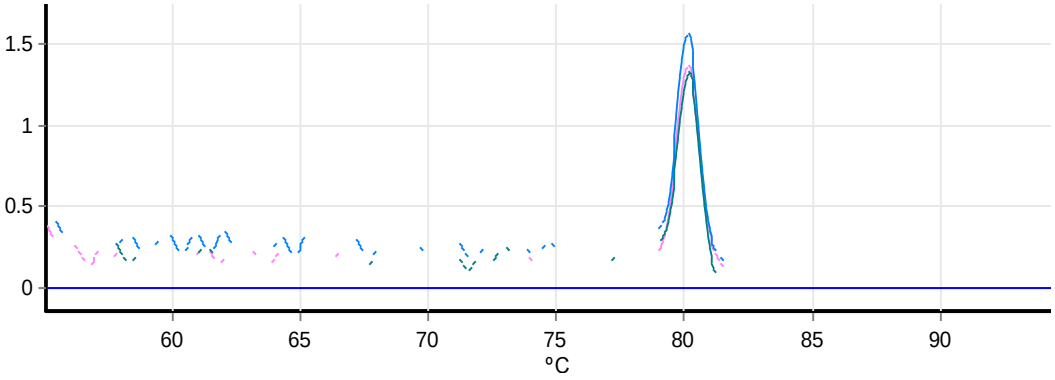

Figure A4.23: Melt curve for the* SRP20 *gene in triplicate. The y-axis represents the change in fluorescence (F) over the change in temperature (T), and the x-axis shows the temperature in °C. The single peak represents the PCR product.

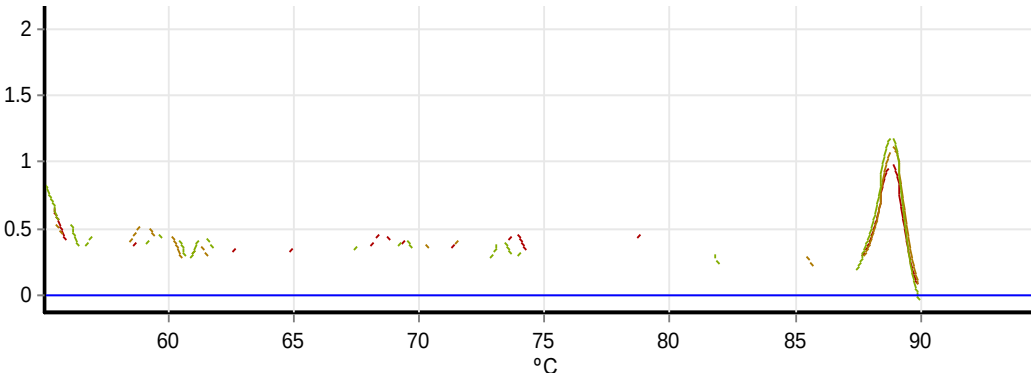

Figure A4.24: Melt curve for the* TRB3 *gene in triplicate. The y-axis represents the change in fluorescence (F) over the change in temperature (T), and the x-axis shows the temperature in °C. The single peak represents the PCR product.

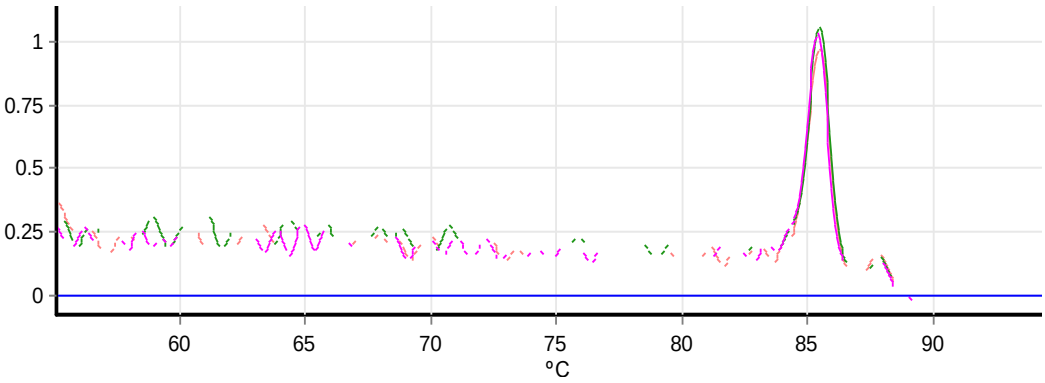

Figure A.4.25: Melt curve for the* TRIM16 *gene in triplicate. The y-axis represents the change in fluorescence (F) over the change in temperature (T), and the x-axis shows the temperature in °C. The single peak represents the PCR product.

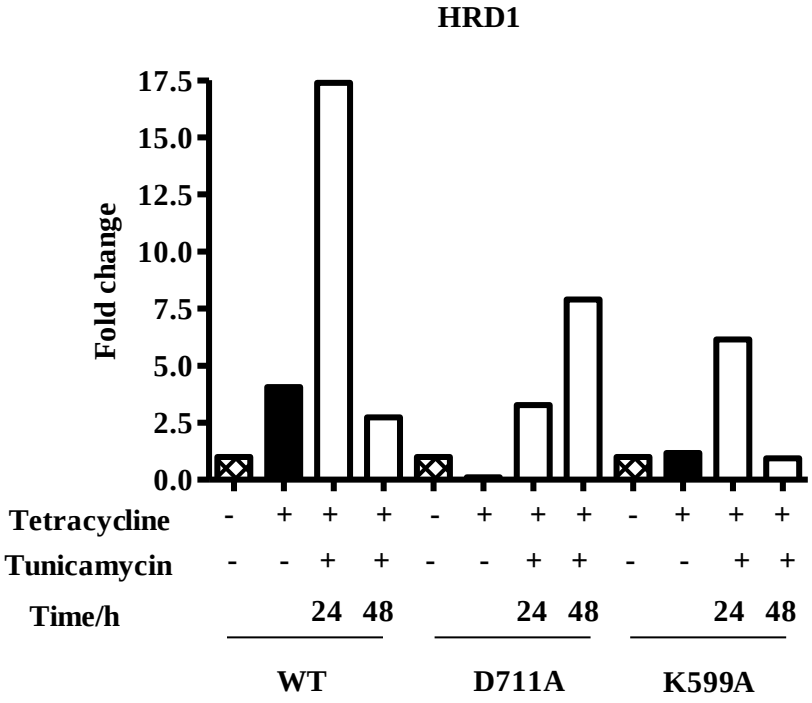

Figure A4.26: Qualitative repeat of the* HRD1 *expression profile determined by qPCR analysis using Rotor-Gene Q software. FAST 2xreal-time PCR MasterMix with SYBR Green was used. – and + indicate absence and presence of tetracycline and/or tunicamycin, respectively. Tetracycline-only treatment was for 48 h. The time is the number of hours that ER-stress was induced for. The average C_t value error was ± 0.48.

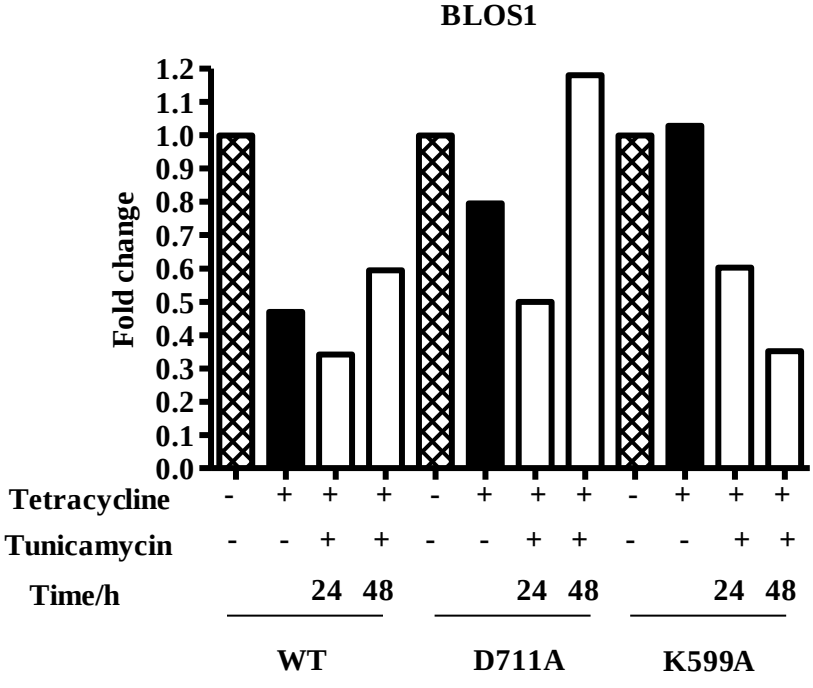

Figure A4.27:* BLOS1 *expression profile determined by qPCR analysis using Rotor-GeneQ software. 2xreal-time PCR MasterMix with SYBR Green was used. – and + indicate absence and presence of tetracycline and/or tunicamycin, respectively. Tetracycline-only treatment was for 48 h. The time is the number of hours that ER-stress was induced for. The average C_t value error was ± 0.13.

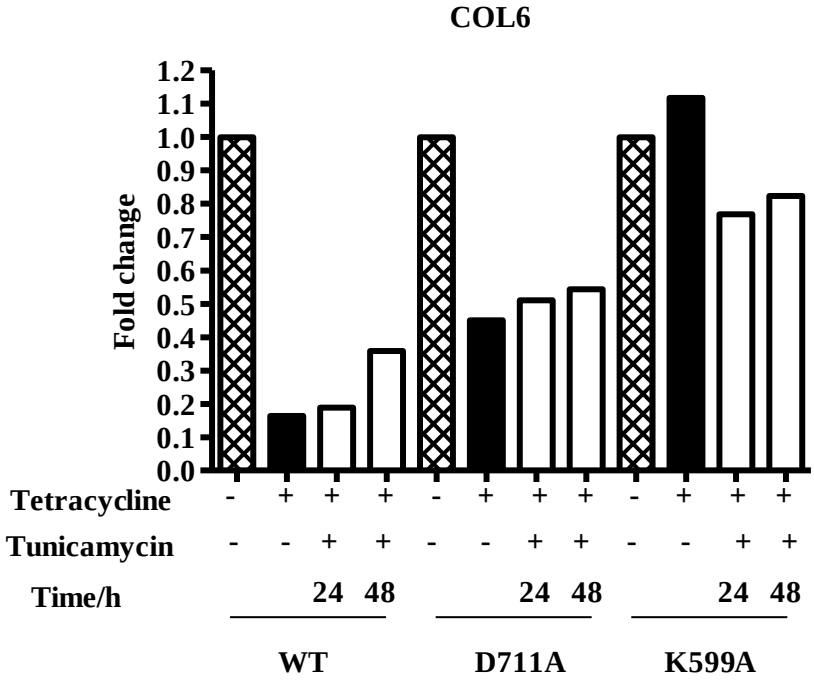

Figure A4.28: **COL6** ***expression profile determined by qPCR analysis using Rotor-Gene Q software. 2xreal-time PCR MasterMix with SYBR Green was used. – and + indicate absence and presence of tetracycline and/or tunicamycin, respectively. Tetracycline-only treatment was for 48 h. The time is the number of hours that ER-stress was induced for. The average*** C_t ***value error was ± 0.24.***

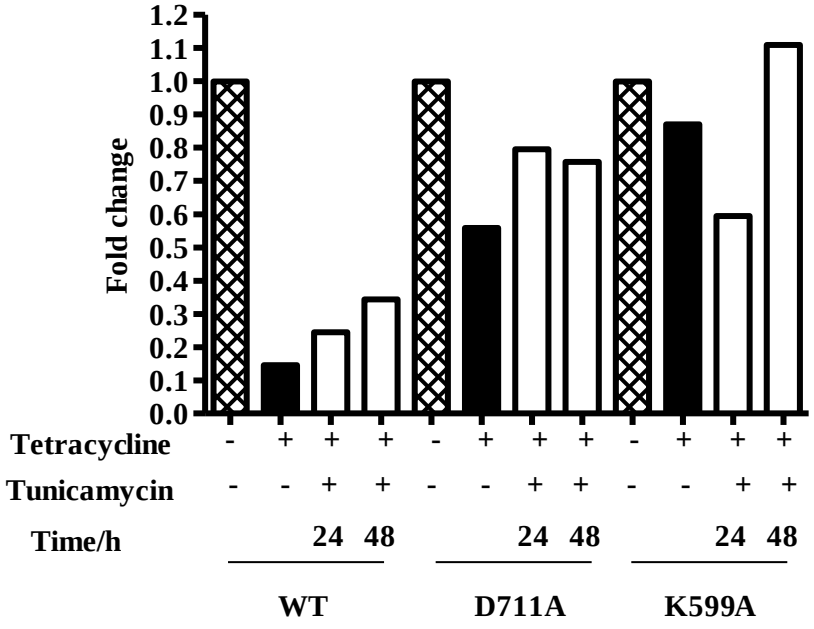

Figure A4.29: **EPHRINB2** ***expression profile determined by qPCR analysis using Rotor-Gene Q software. 2xreal-time PCR MasterMix with SYBR Green was used. – and + indicate absence and presence of tetracycline and/or tunicamycin, respectively. Tetracycline-only treatment was for 48 h. The time is the number of hours that ER-stress was induced for. The average*** C_t ***value error was ± 0.29.***

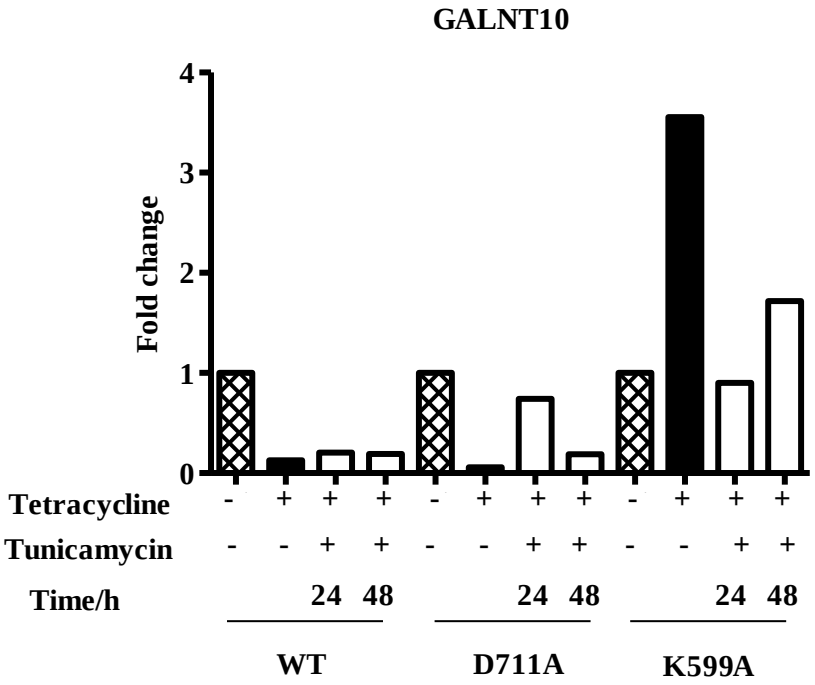

Figure A4.30: **GALNT10** *expression profile determined by qPCR analysis using Rotor-Gene Q software. 2xreal-time PCR MasterMix with SYBR Green was used. – and + indicate absence and presence of tetracycline and/or tunicamycin, respectively. Tetracycline-only treatment was for 48 h. The time is the number of hours that ER-stress was induced for. The average C_t value error was ± 0.24.*

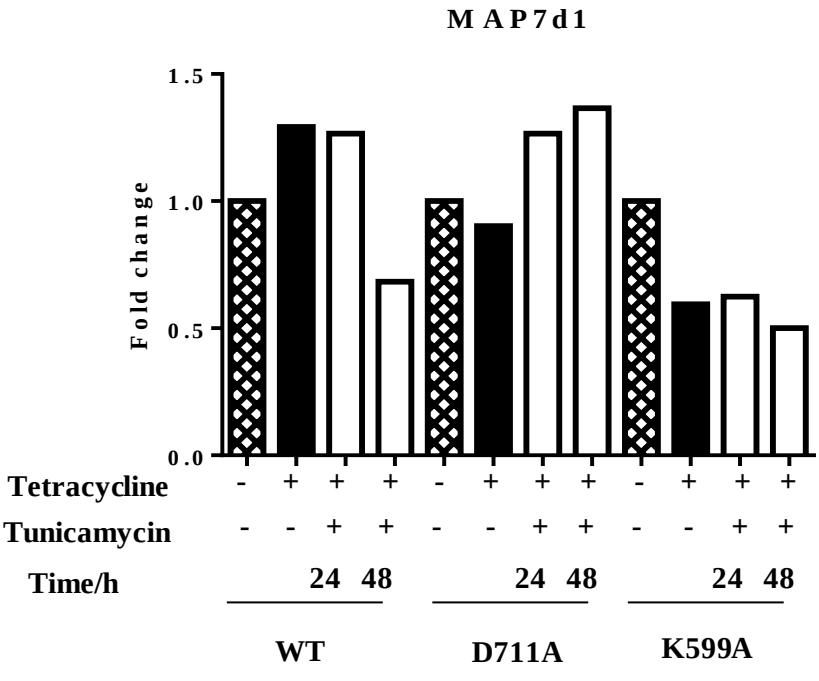

Figure A4.31: **MAP7d1** *expression profile determined by qPCR analysis using Rotor-Gene Q software. 2xreal-time PCR MasterMix with SYBR Green was used. – and + indicate absence and presence of tetracycline and/or tunicamycin, respectively. Tetracycline-only treatment was for 48 h. The time is the number of hours that ER-stress was induced for. The average C_t value error was ± 0.16.*

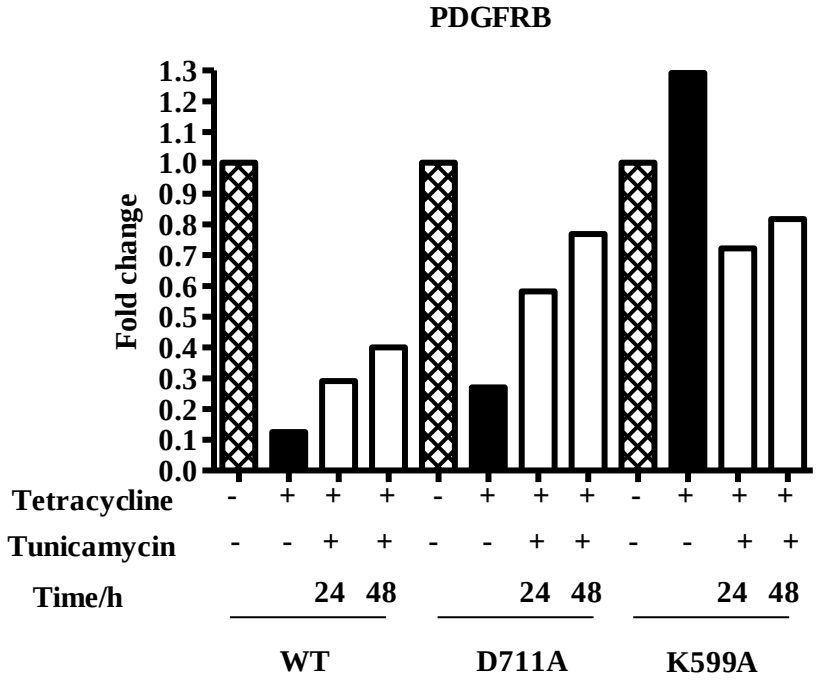

Figure A4.32: **PRDFRB** ***expression profile determined by qPCR analysis using Rotor-Gene Q software. 2xreal-time PCR MasterMix with SYBR Green was used. – and + indicate absence and presence of tetracycline and/or tunicamycin, respectively. Tetracycline-only treatment was for 48 h. The time is the number of hours that ER-stress was induced for. The average*** C_t ***value error was ± 0.27.***

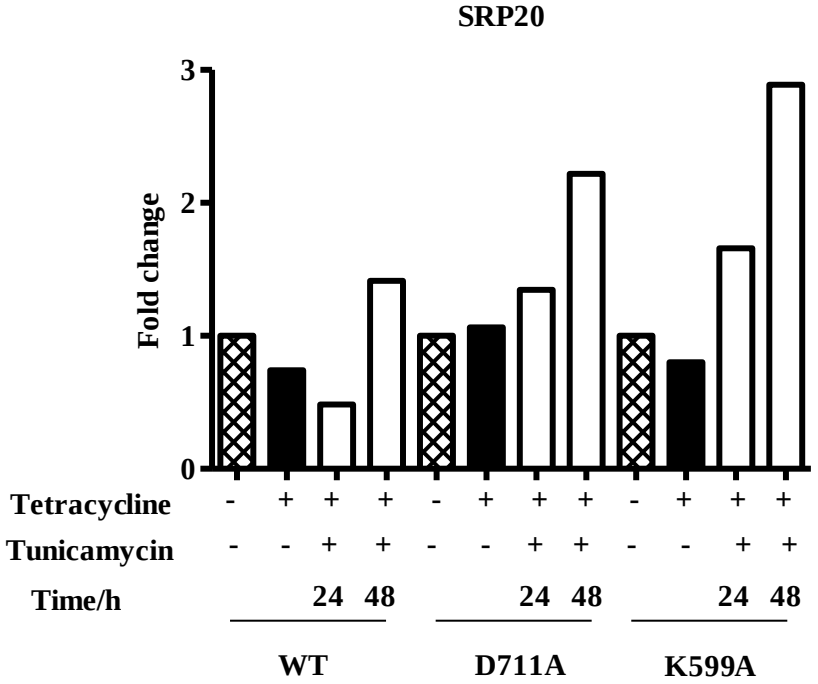

Figure A4.33: Qualitative repeat of the **SRP20** ***expression profile determined by qPCR analysis using Rotor-Gene Q software. FAST 2xreal-time PCR MasterMix with SYBR Green was used. – and + indicate absence and presence of tetracycline and/or tunicamycin, respectively. Tetracycline-only treatment was for 48 h. The time is the number of hours that ER-stress was induced for. The average*** C_t ***value error was ±0. 28.***

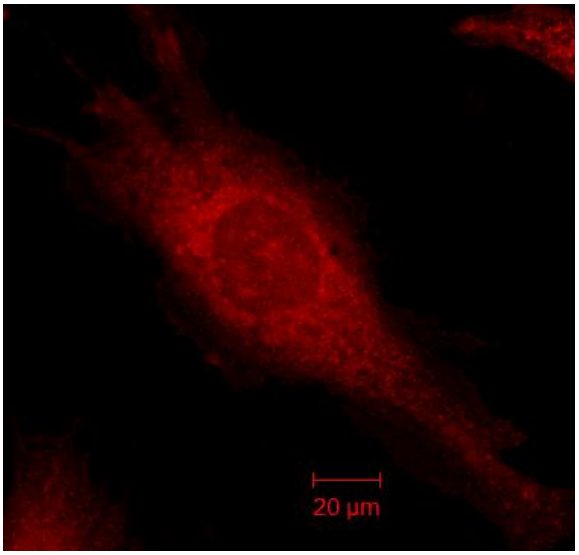

Figure A5.1: Untreated hIRE1α WT MEF cells incubated with ER-tracker dye. This image represents all untreated cell lines. The scale bar represents a distance of 20 µm.

References

- Adachi, Y., Yamamoto, K., Okada, T., Yoshida, H., Harada, A., and Mori, K. (2008) ATF6 Is a Transcription Factor Specializing in the Regulation of Quality Control Proteins in the Endoplasmic Reticulum. *Cell Structure and Function*. 33:75-89.
- Alberts, B., Johnson, A., Lewis, J., Riff, M., Roberts, K. and Walter, P. (2002) Molecular Biology of the Cell. In *Manipulating Proteins, DNA and RNA*, pp. 501-578. Garland Science, Abingdon.
- Ali, M.M.U., Bagaratuni, T., Davenport, E.L., Nowak, P.R., Silva-Santisteban, M.C., Hardcastle, A., McAndwers, C., Rowlands, M.G., Morgan, G.J., Aherne, W., Collins, I., Davies, F.E., and Pearl, L.H. (2011) Structure of the Ire1 autophosphrylation complex and implication for the unfolded protein response. *European Molecular Organisation Journal.* 30: 894-905.
- Amanso, A. M, Debbas, V, and Laurindo, F.R. (2011) Proteasome inhibition represses unfolded protein response and Nox4, sensitizing vascular cells to endoplasmic reticulum stress-induced death. *PLoS One.* 6: e14591.
- Aredia, F., Oriz, L.M.G., Giansanti, V., and Scovassi, A.I. (2012) Autophagy and Cancer. *Cells*. 1: 520-534.
- Back, S.H., Schröder, M., Lee, K., Zhang, K, and Kaufman, R.J. (2005) ER stress signalling by regulated splicing: IRE1/HAC1/XBP1. *Methods.* 35: 395-416.
- Badiola, N., Penas, C., Miñano-Molina, A., Barneda-Zahonero, B., Fadé, R., Sánchez-Opazo, G., Comella J. X., Sabriá, J., Zhu, C., Blomgran, K. and Rogríguez-Alvarez, J. (2011) Induction of ER stress in response to oxygen-glucose deprivation of cortical cultures involves the activation of the PERK and IRE-1 pathways and of caspase-12. *Cell Death and Disease.* 2: e149.
- Bassik, M.C., Scorrano, L., Oakes, S.A., Pozzan, T. and Korsemeyer, S.J. (2004) Phosphorylation of BCL-2 regulates ER Ca^{2+} homeostasis and apoptosis. *The European Molecular Organisation Journal.* 23: 1207-1216.
- Bernasconi, R., Galli, C., Kokame, K., and Molinari, M. (2013) Autoadaptive ER-Associated Degradation defines a Preemptive Unfolded Protein Response. *Molecular Cell.* 52: 1-11.
- Bertolotti, A., Zhang, Y., Hendershot, L.M., Harding, H.P., and Ron, D. (2000) Dynamic interaction of BiP and ER stress transducers in the unfolded-protein response. *Nature Cell Biology.* 2: 326-332.
- Birnboim, H.C., and Doly, J. (1979) A rapid alkaline extraction procedure for screening recombinant plasmid DNA. *Nucleic Acids Research.* 7: 1513-1523.
- Bommiasamy, H., Back, S.H., Fagone, P., Lee, K., Meshinchi, S., Vink, E., Sriburi, R., Matthew, F., Jackowski, Kaufman, R.J., and Brewer, J. (2009) ATF6α induces

XBP1-independant expansion of the endoplasmic reticulum. *Journal of Cell Science*. 122: 1626-1636.

- Brush, M., Welser, D.C. and Shenolikar, S. (2003) Growth Arrest and DNA Damage-Inducible Protein GADD34 Targets Protein Phosphatase 1α to the Endoplasmic Reticulum and Promotes Dephosphorylation of the α Subunit of Eukaryotic Translation Initiation Factor 2. *Molecular and Cellular Biology*. 23: 1292-1303.
- Chawla, A., Chakrabarti, S., Ghosh, G., and Niwa, M. (2011) Attenuation of yeast UPR is essential for survival and is mediated by *IRE1* kinase. *The Journal of Cell Biology*. 193: 41-50.
- Chiang, W.C., Messah, C., and Lin, J.H. (2011) IRE1 directs proteasomal and lysosomal degradation of misfolded rhodopsin. *Molecular Biology of the Cell.* 23:758-770.
- Cohen, M., Tzur, Y.B., Neufeld, E., Feinstein, N., Delannoy, M.R., Wilson, K.L., and Greunbaum, Y. (2002) Transmission electron microscope studies of the nuclear envelope in *Caenorhabditis elegans* embryos. *Journal of Structural Biology.* 140: 232-240.
- Cox, J.S., and Walter, P. (1996) A Novel Mechanism for Regulating Activity of a Transcription Factor That Controls the Unfolded Protein Response. *Cell*. 87: 391-404.
- Cox, J.S., Shamu, C., and Walter, P. (1993). Transcriptional Induction of Genes Encoding Endoplasmic Reticulum Resident Proteins Requires a Transmembrane Protein Kinase. *Cell*. 73: 1197-1206.
- Cross, B.C.S., Bond, P.J., Sadowski, P.G., Jha, B.K., Zak, J., Goodman, J.M., Silverman, R.H., Neubert, T.A., Baxendale, I.A., Ron, D., and Harding, H.P. (2012) The molecular basis for selective inhibition of unconventional mRNA splicing by an IRE1-binding small molecule. *Proceedings of the National Academy of Sciences.* E869-E878.
- Davis, J.M. (2002) Basic Cell Culture: A Practical Approach. Oxford University Press, Oxford.
- Dlugosz, P., Billen, L.P., Annis, M.G., Zhu, W., Zhang, Z., Lin, J., Leber, B., Andrews, D.W. (2006) Bcl-2 changes conformation to inhibit Bax oligomerisation. *The European Molecular Biology Organisation Journal.* 25: 2287-2296.
- Du, K., Herzig, S., Kulkarni, R.N, and Montminy, M. (2003) TRB3: A *tribbles* Homolog that Inhibits Akt/PKB Activation by Insulin in Liver. *Science.* 300: 1574-1577.

- Eskes, R., Desagher, S., Antonsson, B., and Martinou, J.C. (2000) Bid induced oligomerisation and insertion of Bax into the outer mitochondrial membrane. *Molecular Cell Biology.* 20: 929-935.
- Feldman, D.E., Chauhan, V., and Koong, A.C. (2005) The Unfolded Protein Response: A Novel Compenent of the Hypoxic Stress Response in Tumours. *Molecular Cancer Research.* 3: 596-605.
- Fomenko, D.E., and Galdyshev, V.N. (2003) Genomics Perspective on Disulphide Bond Formation. *Antioxidants & Redox Signalling.* 5: 397-402.
- Fujita, N., Itoh, T., Omori, H., Fukuda, M., Noda, T., and Yoshimori, T. (2008) The Atg16L Complex Specifies the Site of LC3 Lipidation for Membrane Biogenesis in Autophagy. *Molecular Biology of the Cell.* 19: 2092-2100.
- Gaddam, D., Stevens, N., and Hollien, J. (2012) Comparison of mRNA localisation and regulation during endoplasmic reticulum stress in *Drosophila* cells. *Molecular Biology of the Cell.* 24:14-20.
- Gao, B., Lee, S.M., Chen, A., Zhang, J., Zhang, D.D., Kannan, K., Ortmann, R.A., and Fang, D. (2008) Synoviolin promotes IRE1 ubiquitination and degradation in synovial fibroblasts from mice with collagen-induced arthritis. *European Molecular Biology Organisation*. 9: 480-485.
- Gardner, B.M., and Walter, P. (2011) Unfolded Proteins Are Ire1-Activating Ligands That Directly Induce the Unfolded Protein Response. *Science.* 333: 1891-1894.
- Giménez-Xavier, P., Francisco, R., Platini, F., Pérez, R., and Ambrosio, S. (2008) LC3-I conversion to LC3-II does not necessarily result in complete autophagy. *International Journal of Molecular Medicine.* 22: 781-785.
- Gobeil, S., Boucher, C.C., Nadeau, D., and Poirnier, G.G. (2001) Characterisation of the necrotic cleavage of poly(ADP-ribose) polymerase (PARP-1): implication of lysosomal proteases. *Cell Death & Differentiation.* 8: 588-594.
- Guo, F.J., Liu, Y., Zhou, J., Luo, S., Zhao, W., Li, X., and Liu, C. (2012) XBP1S protects cells from ER stress-induced apoptosis through Erk1/2 signalling pathways. *Histochemistry and Cell Biology*. 138: 447-460.
- Gupta, S., Deepti, A., Deegan, S., Lisbona, F., Hetz, C., and Samali, A. (2010) HSP72 Protects Cells from ER Stress-induced Apoptosis via Enhancement of IRE1α-XBP1 Signaling through a Physical Interaction. *PLoS Biology.* 8: e1000410.
- Han, D., Lerner, A.G., Vande walle, L., Upton, J., Xu, W., Hagen, A., Baces, B.J., Oakes, S.A., and Papa, F.R. (2009) IRE1α kinase Activation Modes Control Alternative Endoribonuclease Outputs to Determine Divergent Cell Fates. *Cell.* 138: 562-575.

- Han, D., Upton, J.P., Hagen, A., Callahan, J., Oakes, S.A., and Papa, F.R (2008) A kinase inhibitor activates the IRE1α RNase to confer cytoprotection against ER stress. *Biochemical and Biophysical Research Communications.* 365: 777-783.
- Harding, H.P., Novoa, I., Zhang, Y.H., Zeng, H.Q., Wek, R., Schapira, M., and Ron. D. (2000) Regulated translation initiation controls stress-induced gene expression in mammalian cells. *Molecular Cell*. 6: 1099-1108.
- Hershko, A., and Ciechanover, A. (1998) The Ubiquitin System. *Annual review of Biochemistry*. 67: 425-479.
- Hetz, C., Bernasconi, P., Fisher, J., Lee, A.H., Bassik, M.C., Antonsson, B., Brandt, G.S., Iwakoshi, N.N., Schinzel, A., Glimcher, L.H. and Korsemeyer, S.J. (2006) Proapoptotic BAX and BAK Modulate the Unfolded Protein Response by a Direct Interaction with Ire1α. *Science.* 312: 572-576.
- Hetz, C., Thielen, P., Matus, S., Nassif, M., Court, F., Kiffin, R., Martinez, Gabriela, Cuervo, A.M., Brown, R.H., and Glimcher, L.H. (2009) XBP-1 deficiency in the nervous system protects against amyotrophic lateral sclerosis by increasing autophagy. *Genes and Development*. 23: 2294-2306.
- Hodgson, D.R.W., and Schröder, M. (2011) Chemical approaches towards unravelling kinase-mediated signalling pathways. *Chemical Society Reviews.* 40: 1211-1223.
- Hollien, J., and Weissman, J.S. (2006) Decay of Endoplasmic Reticulum-localised mRNAs During the Unfolded Protein Response. *Science.* 313: 104-107.
- Hollien, J., Lin, J.H., Li, H., Stevens, N., Walter, P., and Weissman, J.S. (2009) Regulated Ire1-dependant decay of messenger RNAs in mammalian cells. *The Journal of Cell Biology*. 186: 323-361.
- Hussain, S.G. and Ramaiah, K.V.A. (2007) Endoplasmic Reticulum: Stress, signalling and apoptosis. *Current Science.* 93: 1684-1696.
- Inoue, H,. Nojima, H., and Okayama, H. (1990) High efficiency transformation of *Eschericia coli* with plasmids. *Gene*. 96: 23-28.
- Jin, Y., Zhuang, M., and Hendershot, L.M. (2009) ERdj3, a Luminal ER DnaJ Homologue, Binds Directly to Unfolded Proteins in the Mammalian ER: Identification of Critical Residues. *Biochemistry.* 48: 41-49.
- Karlin, A., and Bartels, E. (1966) Effects of blocking sulfhydryl groups and of reducing disulphide bonds on the acetylcholine-activated permeability system of the electroplax. *Biochimica et Biophysica Acta (BBA) - Biophysics including Photosynthesis.* 126: 525-535.

- Kato, H., Nakajima, S., Saito, Y., Takahashi, S., Katoh, R., and Kitamura, M. (2012) mTORC1 serves ER stress-triggered apoptosis via selective activation of the IRE1-JNK pathway. *Cell Death and Differentiation.* 19: 310-320.
- Kichipudi, S.V., Tellabati, M., Nelli, R.K., White, G.A., Perez, B.B., Sebastian, S., Slomka, M.J., Brookes, S.M., Brown, I.H., Dunham, S.P., and Chang, K.C. (2012) 18S *rRNA* is a reliable normalisation gene for real time PCR based on influenza virus infected cells. *Virology Journal*. 9: 230-237.
- Kim, I., Xu, W., and Reed, J.C. (2008) Cell death and endoplasmic reticulum stress: disease relevance and therapeutic opportunities. *Nature.* 7: 1013-1030.
- Kim, R., Emi, M., Tanabe, K., and Murakami, S. (2006) Role of the unfolded protein response in cell death. *Apoptosis.* 11: 5-13.
- Kimmig, P., Diaz, M., Zheng, J., Williams, C.C., Lang, A., Aragón, T., Li, H., and Walter, P. (2012) The unfolded protein response in fission yeast modulates stability of select mRNAs to maintain protein homeostasis. *eLife.* 1: e0048.
- Klopfenstein, D.R., Klumperman, J., Lustig, A., Kammerer, R.A., Oorschot, V., and Hauri, H.P. (2001) Subdomain-Specific Localization of Climp-63 (P63) in the Endoplasmic Reticulum Is Mediated by Its Luminal α-Helical Segment. *The Journal of Cell Biology.* 153: 1287-1300.
- Korennykh, A., and Walter, P. (2012) Structural Basis of the Unfolded Protein Response. *Annual Review of Cell and Developmental Biology.* 28: 251-277.
- Korennykh, A.V., Egea, P.F., Korostelev, A.A., Finer-Moore, J., Stroud, R.M., Zhang, C., Shokat, K.M., and Walter, P. (2011) Cofactor-mediated conformational control in the bifunctional kinase/RNase Ire1. *BMC Biology.* 9: 1-16.
- Korennykh, A.V., Egea, P.F., Korostelev, A.A., Finer-Moore, J., Zhang, C., Shokat, K.M., Stroud, R.M., and Walter, P. (2009) The unfolded protein response signals through high-order assembly of Ire1. *Nature.* 457: 687-693.
- Kozak, M. (2002) Pushing the limits of the scanning mechanism for initiation of translation. *Gene.* 299: 1-34.
- Krysko, D.V., Bergh, T.V., Herde, K.D., and Vandenabeele, P. (2008) Apoptosis and necrosis: Detection, discrimination and phagocytosis. *Methods.* 4: 205-221.
- Kundu, M., and Thompson, C.B. (2008) Autophagy: basic principles and relevance to disease. *Aunnual Review of Pathology.* 3:427-55.
- Lai, E., Teodoro, T., and Volchuk, A. (2006) Endoplasmic Reticulum Stress: Signalling the Unfolded Protein Response. *Physiology.* 22: 193-201.
- Lazebnik, Y.A., Kaufmann, S.H., Desnoyers, S., Poirier, G.G., and Earnshaw, W.C. (1994) Cleavage of poly(ADP-ribose) polymerase by a proteinase with properties like ICE. *Nature.* 371: 346-347.

- Lee, A.H., Chu, G.C., Iwakoshi, N.N., and Glimcher, L.H. (2005) XBP-1 is required for biogenesis of cellular secretory machinery of exocrine glands. *The European Molecular Organisation Journal.* 24: 4368-4380.
- Lee, A.H., Iwakoshi, N.N., and Glimcher, L.H. (2003) XBP-1 regulates a Subset of Endoplasmic Reticulum Chaperone Genes in the Unfolded Protein Response. *Molecular and Cellular Biology.* 23: 7448-7459.
- Lee, A.H., Iwakoshi, N.N., Anderson, K.C., and Glimcher, L.H. (2003) Proteasome inhibitors disrupt the unfolded protein response in myeloma cells. *Proceedings of the National Academy of Sciences of the United States of America.* 100: 9946-9951.
- Lee, H., Noh, J.Y. ,Oh, Y., Kim, Y, Chang, J.W., Chung, C.W., Lee, S.T., Kim, M., Ryu, H., and Jung, Y.K. (2012) IRE1 plays an essential role in ER stress-mediated aggregation of mutant huntintin via the inhibition of autophagy flux. *Human Molecular Genetics.* 21: 101-114.
- Lee, K.P.K., Dey, M., Neculai, D., Cao, C., Dever, T.E., Sicheri, F. (2008) Structure ofthe dual enzyme Ire1 reveals the basis for catalysis and regulation in non-conventional RNA splicing. *Cell*. 132: 89-100.
- Lei, K. and Davis, R. (2003) JNK phosphorylation of Bim-related members of the Bcl2 family induces Bax-dependent apoptosis. *Proceedings of the National Academy of Sciences.* 100: 2432-2437.
- Lerner, A.G., Upton, J.P., Praveen, P.V.K., Ghosh, R., Nakagawa, Y., Igbaria, A., Shen, S., Ngugen, V., Nackes, B.J., Heiman, M., Heintz, N., Greengard, P., Hui, S., Tang, Q., Trusina, A., Oakes, S.A., and Papa, F.R. (2012) IRE1α Induces Thioredoxin-Interacting Protein to Activate the NLRP3 Inflammasome and Promote Programmed Cell Death under Irremediable ER Stress. *Cell Metabolism.* 16: 250-264.
- Li, H., Korennykh, A.V., Behrman, S.L., and Walter,P. (2010) Mammalian endoplasmic reticulum stress sensor IRE1 signals by dymanic clustering. *Proceedings of the National Academy of Sciences.* 107: 16113-16118.
- Lin, J.H., Li, H., Yasumura, D., Cohen, H.R., Zhang, C., Panning, B., Shokat, K.M., LaVail M.M. and Walter, P. (2007) IRE1 Signalling Affects Cell Fate During the Unfolded Protein Response. *Science.* 318: 944-949.
- Lin, J.H., Li, H., Zhang, Y., Ron, D., and Walter, P. (2009) Divergent Effects of PERK and IRE1 Signaling on Cell Viability. *PLoS.* 4(1): e4170.
- Livak, K., and Schmittgen, T.D. (2001) Analysis of Relative Gene Expression Data Using Real-Time Quantitative PCR and the $2^{-\Delta\Delta C}{}_t$ Method. *Methods.* 25: 402-408.
- Lui, J., and Lin, A. (2005) Role of JNK activation in apoptosis: A double-edged sword. *Cell Research.* 15: 36-42.

- Luo, D., He, Y., Zhang, H., Yu, L., Chen, H., Xu, Z., Tang, S., Urano, F., and Min, W. (2008) AIP1 is Critical in Trnasducing IRE1-mediated Endoplasmic Reticulum Stress Response. *Journal of Biological Chemistry.* 283: 11905-11912.
- Lykidis, A., and Jackowski, S. (2001). Regulation of mammalian cell membrane biosynthesis. *Progress in nucleic acid research and moluecular biology.* 65: 361-393.
- Lytton, J., Westlin, M., and Hanley, M.R. (1991) Thapsigargin inhibits the sarcoplasmic or endoplasmic Ca-ATPase family of calcium pumps. *The Journal of Biological Chemistry.* 266: 17067-17071.
- Ma, J., Brewer, J.W., Dielh, A. and Hendershot, L.M. (2002) Two Distinct Stress Pathways Converge Upon the CHOP Promoter During the Mammalian Unfolded Protein Response. *Journal of Molecular Biology.* 318: 1351-1365.
- Ma, Y., and Hendershot, L.M. (2004) Herp Is Dually Regualted by Both the Endoplasmic Reticulum Stress-specific Branch of the Unfolded Protein Response and a Branch That Is Shared with Other Cellular Reponses. *The Journal of Biological Chemistry.* 279: 13792-13799.
- Ma, Y., and Hendershot, L.M. (2004) Herp Is Dually Regulated by Both the Endoplasmic Reticulum Stress-specific Branch of the Unfolded Protein Response and a Branch That Is Shared with Other Cellular Stress Pathways. *The Journal of Biological Chemistry.* 279: 13792-13799.
- Marciniak, S.J., Yun, C.Y., Oyadomari, S., Novoa, I., Zhang, Y., Jungreis, R., Nagata, K., Harding, H.P., and Ron, D. (2004) CHOP induces death by promoting protein synthesis and oxidation in the stressed endoplasmic reticulum. *Genes and Development.* 18: 3066-3077.
- Mikhailov, V., Mikhailova, M., Pulkrabek, D.J., Dong, Z., Venkatachalam, M.A., Saikumar, P. (2001) Bcl-2 Prevents Bax Oligomerisation in the Outer Mitochondrial Membrane. *The Journal of Biological Chemistry.* 276: 18361-18374.
- Mizushima, N., Kuma, A., Kobayashi, Y., Yamamoto, A., Matsubae, M., Takao, T., Natsume, T., Ohsumi, Y., and Yoshimori, T. (2003) Mouse Apg16L, a novel WD-repeat protein, targets to the autophagic isolation membrane with he Apg12-Apg5 conjugate. *The Journal of Cell Science.* 116: 1679-1688.
- Mizushima, N., Yamamoto, A., Hatano, M., Kobayashi, Y., Kabeya, Y., Suzuki, K., Tokuhisa, T., Ohsumi, Y., and Yoshimori, T. (2001) Dissection of Autophagosome Formation Using Apg5-Deficient Mouse Embryonic Stem Cells. *The Journal of Cell Biology.* 152: 657-668.
- Mori, K., Ma, W., Gething, M.J., and Sambrook, J. (1993) A transmembrane protein with a cdc2+/CDC28-related kinase activity is required for signaling from the ER to the nucleus. *Cell.* 74:743-756.

- Mori, K., Ogawa, N., Kawahara, T., Yanagi, H., and Yura, T. (2000) mRNA splicing-mediated C-terminal replacement of transcription factor Hac1p is required for efficient activation of the unfolded protein response. *Proceedings of the National Academy of Sciences of the United States of America.* 97: 4660-4665.
- Morishima, N., Nakanishi, K., Takenouchi, H., Shibata, T. and Yasuhiko, Y. (2004) An Endoplasmic Reticulum Stress-specific Caspase Cascade in Apoptosis Cytochrome c-independent activation of caspase-9 by caspase-12. *The Journal of Biological Chemistry.* 277: 34287-34294.
- Morris, J.A., Dorner, A.J., Edwards, C.A., Hendershot, L.M., and Kaufman, R.J. (1997) Immunoglobulin Binding Protein (BiP) Function Is Required to Protect Cells from Endopalsmic Reticulum Stress but Is Not Required for the Secretion of Selective Proteins. *The Journal of Biological Chemistry.* 272: 4237-4334.
- Nataksukasa, K, and Brodsky, J.L. (2009) The Recognition and Retrotranslocation of Misfolded Proteins from the Endoplasmic Reticulum. *Traffic.*9: 861-870.
- Neutzner, A., Neutzner, M., Benischke, A.S., Ryu, S.W., Frank, S., Youle, R.J., and Karbowski, M. (2011) A systematic search for endoplasmic reticulum (ER) membrane-associated RING finger proteins identifies Nixin/ZNRF4 as a regulator of calnexin stability and ER homeostasis. *The Journal of Biological Chemistry.* 286: 8633-8643.
- Nutt, L.K., Chandra, J., Pataer, A., Fang, B., Roth, J.A., Swisher, S.G., O'Neil, R.G. and McConkey, D.J. (2002) Bax-mediated Ca^{2+} Mobilisation Promotes Cytochrome c Release during Apoptosis. *The Journal of Biological Chemistry.* 277: 20301-20308.
- Ogata, M., Hino, S., Saito, A., Morikawa, K., Kondo, S., Kanemoto, S., Murakami, T., Taniguchi, M., Tanii, I., Yoshinaga, K., Shiosaka, S., Hammarback, J.A., Urano, F., and Imaizumi, K. (2006) Autophagy Is Activated for Cell Survival after Endoplasmic Reticulum Stress. *Molecular and Cell Biology.* 26: 9220-9231.
- Ohoka, N., Yoshii, S., Hattori, T., Onozaki, K. and Hayashi, H. (2005) *TRB3,* a novel ER stress-inducible gene, is induced via the ATF4-CHOP pathway and is involved in cell death. *The European Molecular Biology Organisation Journal.* 24: 1243-1255.
- Okada, T., Yoshida, H., Akazawa, R., Negishi, M. and Mori, K. (2002) Distinct roles of activating transcription factor 6 (ATF6) and double-stranded RNA-activated protein kinase-like endoplasmic reticulum kinase (PERK) in transcription during the mammalian unfolded protein response. *Biochemical Journal.* 366: 585-594.
- Okada, T., Yoshida, H., Akazawa, R., Negishi, M., and Mori, K. (2000) ATF6 activated by proteolysis binds in the presence of NF-Y (CBF) directly to the cis-

acting element responsible for the mammalian unfolded protein response. *Molecular and Cellular Biology.* 1: 585-594.

- Oliver, F.J., de la Rubia, G., Rolli, V., Ruiz-Ruiz, M.C., de Murcia, G., and Ménissier-de Murcia, J. (1998) Importance of poly(ADP-ribose) polymerase and its cleavage in apoptosis. Lesson from an uncleavable mutant. *The Journal of Biological Chemistry.* 273: 33533-33539.
- Oyadomari, S., and Mori, M. (2004) Role of CHOP/GADD153 in endoplasmic reticulum stress. *Cell Death and Differentiation.* 11: 381-389.
- Oyadomari, S., Yun, C., Fisher, E.A., Kreglinger, N., Kreibich, G., Oyadomari, M., Harding, H.P., Goodman, A.G., Harant, H., Garrison, J.L., Taunton, J., Kayze, M.G., and Ron, D. (2006) Cotranslational degradation Protects the Stressed Endoplasmic Reticulum from Protein Overload. *Cell*. 126: 727-739.
- Padmakumar, V.C., Libotte, T., Lu, W., Zaim, H., Abraham, S., Noegel, A.A., Gotzmann, J., Foisner, R., and Karakesisoglou, I. (2005) The inner nuclear membrane protein Sun1 mediates the anchorage of Nesprin-2 to the nuclear envelope. *Journal of Cell Science.* 118: 3419-3430.
- Papa, F.R., Zhang, C., Shokat, K., and Walter, P. (2003) Bypassing a kinase activity with an ATP-competitive drug. *Science.* 203: 1533-1537.
- Paton, A.W., Beddoe, T., Thorpe, C.M., Whisstock, J.C., Wilce, M.C., Rossjohn, J., Talbot, U.M., and Paton, J.C. (2006) AB_5 subtilase cytotoxin inactivates the endoplasmic reticulum chaperone BiP. *Nature.* 443: 548-552.
- Pattingre, S., Tessa, A., Qu, X., Garuti, R., Liang, X.H., Mizushima, N., Packer, M., Schneider, M.D., and Levine, B. (2005) Bcl-2 antiapoptotic proteins inhibit Beclin-1 dependent autophagy. *Cell*. 122: 927-936.
- Putcha, G.V., Le, S., Frank, S., Besirli, C.G., Clark, K., Chu, B., Axil, S., Youle, R.J., LaMarche, A., Maroney, A. and Johnson, Jr. E.M. (2003) JNK-Mediated BIM Phosphorylation Potentiates BAX-Dependent Apoptosis. *Neuron.* 38: 899-914.
- Reed, R., Holmes, D., Weyers, J., and Jones, A. (2013) Practical Skills in Biomolecular Sciences. In *Molecular genetics II – PCR and related applications*, pp. 467-473. Pearson Education Limited, Essex.
- Reich, E., Franklin, R.M., Shatkin, A.J., and Tatum, E.L. (1961) Effect of actinomycin D on cellular nucleic acid synthesis and virus production. *Science.* 134: 556-557.
- Reimold, A.M., Etkin, A., Clauss, I., Perkins, A., Friend, D.S., Zhang, J., Horton, H.F., Scott, A., Orkin, S.H., Byrne, M.C., Grusby, M.J., and Glimcher, L.H. An essential role in liver development for transcription factor XBP-1. *Genes and Development.* 14: 152-157.

- Reynold, E.S. (1963) The use of lead citrate at high pH as an electron-opaque stain in electron microscopy. *The Journal of Cell Biology.* 17: 208-212.
- Ron, D. and Walter, P. (2007) Signal integration in the endoplasmic reticulum unfolded protein response. *Nature.* 8: 519-529.
- Rubio, C., Pincus, D., Korennykh, A., Schuck, S., El-Samad, H., and Walter, P. (2011) Homeostatic adaptation to endoplasmic reticulum stress depends on Ire1 kinase activity. *The Journal of Cell Biology.* 193: 171-184.
- Sado, M., Yamasaki, Y., Iwanaga, T, Onaka, Y., Ibuki, T, Nishihara, S., Mizuguchi, H., Momota, H., Kishibuchi, R., Hashimoto, T., Wada, D., Kitagawa, H. and Watanabe, T.K. (2008) Protective effect against Parkinson's disease-related insults though the activation of XBP-1. *Brain Research.* 1257: 16-24.
- Salazar, M., Carracedo, A., Salanueva, I.J., Hernández-Tiedra, S., Lorente, M., Egia, A., Vázquez, P., Blázquez, C., Torres, S., García, S., Nowak, J., Fimia, G.M., Piacentini, M., Cecconi, F., Pandolfi, P.P., González-Feria, L., Iovanna, J.L., Guzmán, M., Boya, P., and Velasco, G. (2009) Cannabinoid action induces autophagy-mediated cell death through stimulation of ER-stress in human glioma cells. *The Journal of Clinical Investigation.* 119: 1359-1372.
- Scheuner, D., and Kaufman, R.J. (2008) The Unfolded Protein Response: A Pathway That Links Insulin Demand with β-cell Failure and Diabetes. *Endocrine Reviews.* 29: 317-333.
- Scheuner, D., Song, B., McEwen, E., Liu, C., Laybutt, R., Gillespie, P., Saunders, T., Bonner-Wier, S., and Kaufman, R.J. (2001) Translational Control Is Required for the Unfolded Protein Response and In Vivo Glucose Homeostasis. *Molecular Cell.* 7: 1165-1176.
- Schröder, M., Kaufman, R.J. (2005) The Mammalian Unfolded Protein Response. *Annual review of Biochemistry.* 74: 739-789.
- Schuck, S., Prinz, W.A., Thorn, K.S., Voss, C., and Walter, P. (2009) Membrane expansion alleviated endoplasmic reticulum stress independently of the unfolded protein response. *The Journal of Cell Biology.* 187: 525-536.
- Shamu, C.E., and Walter, P. (1996). Oligomerisation and phosphorylation of the Ire1p kinase during intracellular signalling from the endoplasmic reticulum to the nucleus. *EMBO.* 15: 3028-3039.
- Shang, Y.Y., Zhong, M., Zhang, L.P., Guo, Z.X., Wang, Z.H., Zhang, Y., Deng, J.T. and Zhang, W. (2010) Tribble 3, a novel oxidized low-density lipoprotein-inducible gene, is induced via the activating transcription factor 4-C/EBP homologous protein pathway. *Clinical and Experimental Pharmacology and Physiology.* 37: 51-55.

- Shibata, Y., Shemesh, T., Prinz, W.A., Palazzo, A.F., Kozlov, M.M., and Rapport, T.A. (2010) Mechanisms determining the morphology of the peripheral ER. *Cell*. 143: 774-788.
- Shoulders, M.D., Ryno, L.M., Genereux, J.C., Moresco, J.J., Tu, P.G., Wu, C., Yates III, J.R., Su, A.I., Kelly, J.W., and Weissman, L. (2013) Stress-Independent Activation of XBP1s and/or ATF6 Reveals Three Functionally Diverse ER Proteostasis Environments. *Cell*. 3: 1279-1292.
- Sitia, R. and Braakman, I. (2003) Quality control in the endoplasmic reticulum protein factory. *Nature*. 426: 891–894.
- Sriburi, R., Bommiasamy, H., Buldak, G.L., Robbins, G.R., Frank, M., Jackowski, S., and Brewer, J.S. (2007) Coordinate Regulation of Phospholipid Biosynthesis and Secretory Pathway Gene Expression in XBP-1(S)-induced Endoplasmic Reticulum Biogenesis. *Journal of Biological Chemistry.* 282: 7024-7034.
- Sriburi, R., Jackowski, S., Mori, K., and Brewer, J. (2004) XBP1: a link between the unfolded protein response, lipid biosynthesis, and biogenesis of the endoplasmic reticulum. *The Journal of Cell Biology.* 167: 35-41.
- Sutcliffe, L.K. (2012) *Chemical genetic dissection of efferent IRE1α signalling.* Ph.D. Thesis. Durham University: UK.
- Tabas, I., and Ron, D. (2011) Integrating the mechanisms of apoptosis induced by endoplasmic reticulum stress. *Nature Cell Biology.* 13: 184-190.
- Takatsuki, A., Kohno, K., and Tamura, G. (1975) Inhibition of biosynthesis of polyisoprenol sugar in chick embryo microsomes by tunicamycin. *Agricultural and Biological Chemistry*. 39: 2089–2091.
- Tan, Y., Dourdin, N., Wu, C., De Verya, T., Elce, J.S., and Greer, P.A. (2006) Ubiquitous Calpains Promote Caspase-12 and JNK Activation during Endoplasmic Reticulum Stress-induced Apoptosis. *Journal of Biological Chemistry.* 281: 16016-16024.
- Tirasophon, W., Lee, K., Callaghan, B., Welihinda, A., and Kaufman, R.J. (2000) The endoribonuclease activity of mammalian IRE1 autoregulated its mRNA and it required for the unfolded protein response. *Genes and Development.* 14: 2725-2736.
- Tirasophon, W., Welihinda, A.A., and Kaufman, R.J. (1998) A stress response pathway from the endoplasmic reticulum to the nucleus requires a novel bifunctional protein kinase/endoribonuclease (Ire1p) in mammalian cells. *Genes and Development.* 12: 1812-1824.
- Todd-Corlett, A., Jones, E., Seghers, C., and Gething, M.J. (2007) Lobe IB of the ATPase Domain of Kar2p/BiP Interacts with Ire1p to Negatively Regulate the

Unfolded Protein Response in *Saccharomyces cerevisiae. The Journal of Molecular Biology*. 367: 770-787.

- Tooze, S.A., and Yoshimori, T. (2010) The origin of the autophagosomal membrane. *Nature Cell Biology*. 12: 831-835.
- Travers, K.J., Patil, C.K., Wodicka, L., Lockhart, D.J., Weissmann, J.S., and Walter, P. (2000) Functional and Genomic Analyses reveal an Essential Coordination between the Unfolded Protein Response and ER-Associated Degradation. *Cell*. 101: 249-258.
- Upton, J.P., Wang, L., Han, D., Wang, E.S., Huskey, N.E., Lim, L., Truitt, M., McManus, M.T., Ruggero, D., Goga, A., Papa, F.R., and Oakes, S.A. (2012) IRE1α Cleaves Select microRNAs During ER Stress to Derepress Translation of Proapoptotic Caspase-2. *Science*. 338: 818-822.
- Urano, F., Wang, X., Bertolotti, A., Zhang, Y., Chung, P., Harding, H.P. and Ron, D. (2000) Coupling of Stress in the ER to Activation of JNK Protein Kinases by Transmembrane Protein Kinase IRE1. *Science*. 287: 646-666.
- Vandermoere, F., Yazidi-Belkoura, I.E., Slomiamy, C., Demont, Y., Bidaux, G., Adriaenssens, E., Lemoine, J., and Hondermarck, H. (2006) The Valsolin-containing Protein (VCP) Is a Target of Akt Signaling Required for Cell Survival. *The Journal of Biological Chemistry*. 281: 14360-14313.
- Vattem, K.M., and Wek, R.C. (2004). Reinitiation involving upstream ORFs regulates *ATF4* mRNA translation in mammalian cells. *Proceedings of the National Academy of Sciences.* 101: 11269-11274.
- Wang, X., Olberding, K.E., White, C., Li, C. (2011) Bcl-2 proteins regulate ER membrane permeability to luminal proteins during ER stress-induced apoptosis. *Cell Death and Differentiation.* 18: 38-47.
- Wang, X.Z., and Ron, D. (1996) Stress-induced phosphorylation and activation of the transcription factor CHOP (Gadd153) by p38 MAK kinase. *Science*. 272: 1347-1349.
- Warburg, O., and Christian, W. (1942) Isolation and crystallisation of enolase. *Biochemische Zeitschrift.* 310: 384-421.
- Wei, M.C., Lindsten, T., Mootha, V.K., Weiler, S., Gross, A., Ashiya, M., Thompson, C.B., and Korsemeyer, S.J. (2000) tBID, a membrane-targeted death ligand, oligomerises BAK to release cytochrome c. *Genes and Development.* 14: 2060-2071.
- Wei, M.C., Zong, W.X., Cheng, E.H.Y., Lidsten, T., Panoutsakopoulou, V., Ross, A.J., Roth, K.A., MacGregor, G.R., Thompson, C.B. and Korsemeyer, S.J. (2001) Proapoptotic BAX and BAK: A Requisite Gateway to Mitochondrial Dysfunction and Death. *Science.* 292: 727-730.

- Wei, Y., Pattingre, S., Sinha, S., Bassik, M., and Levine, B. (2008) JNK1-Mediated Phosphorylation of Bcl-2 Regulates Starvation-Induced Autophagy. *Molecular Cell.* 30: 678-688.
- Williams, J.A., Hou, Y., Ni, H.M., and Ding, W.X. (2013) Role of intracellular calcium in proteasome inhibitor-induced endoplasmic reticulum stress, autophagy, and cell death. *Pharmaceutical Research.* 30: 2279-2289.
- Wócjik, C., Rowicka, M., Kudlicki, A., Nowis, D., McConnell, E., Kujawa, M., and DeMartino, G.N. (2006) Valsolin-containing Protein (p97) Is a Regulator of Endoplasmic Reticulum Stress and of the degradation of N-End Rule and Ubiquitin-Fusion degradation Pathway Substrates in Mammalian Cells. *Molecular Biology of the Cell*. 17: 4604-4618.
- Wojciechowicz K, Gledhill K, Ambler CA, Manning CB, Jahoda CAB (2013) Development of the Mouse Dermal Adipose Layer Occurs Independently of Subcutaneous Adipose Tissue and Is Marked by Restricted Early Expression of FABP4. PLoS ONE 8: e59811.
- Wójcik, C., Rowicka, M., Kudlicki, A., Nowis, D., McConnell, E., Kujawa, M., and DeMartino, N. (2006) Valsolin-containing Protein (p97) Is a Regulator of Endoplasmic Reticulum Stress and of the Degradation of N-End Rule and Ubiquitin-Fusion Degradation Pathway Substrates in Mammalian Cells. *The American Society for Cell Biology.* 17: 4806-4618.
- Xie, Z., Nair, U., and Klionsky, D.J. (2008) Atg8 Controls Phagophore Expansion during Autophagosome formation. *Molecular Biology of the Cell.* 19: 3290-3298.
- Xu, P., Raden, D., Doyle III, F.J., and Robinson, A.S. (2005) Analysis of unfolded protein response during single-chain antibody expression in *Saccharomyces cerevisiae* reveals different roles for BiP and PDI in folding. *Metabolic Engineering.* 7: 269-279.
- Yamamoto, K., Ichijo, H., and Korsemeyer, S.J. (1999) BCL-2 Is Phosphorylated and Inactivated by an ASK1/Jun N-Terminal Protein Kinase Pathway Normally Activated at G_2/M. *Molecular and Cellular Biology.* 19: 8469-8478.
- Yamamoto, K., Sato, T., Matsui, T., Sato, M., Okada, T., Yoshida, H., Harada, A., and Mori, K. (2007) Transcriptional Induction of Mammalian ER Quality Control Proteins Is Mediated by Single or Combined Action of ATF6α and XBP1. *Developmental Cell.* 13: 365-376.
- Yoneda, T, Imaizumi, K., Oono, K., Yui, D., Gomi, F., Katayama, T. and Tohyama, M. (2001) Activation of Caspase-12, an Endoplamic Reticulum (ER) Resident Caspase, thought Tumor Necrosis Factor Receptor-associated Factor 2-dependent Mechanism in Response to the ER Stress. *The Journal of Biological Chemistry.* 276: 13935-13940.

- Yoshida, H., Matsui, T., Hosokawa, N., Kaufman, R.J., Nagata, K., and Mori, K. (2003) A Time-Dependent Phase Shift in the Mammalian Unfolded Protein Response. *Developmental Cell.* 4: 265-271.
- Yoshida, H., Matsui, T., Yamamoto, A., Okada, T., and Mori, K. (2001) XBP1 mRNA Is Induced by ATF6 and Spliced by IRE1 in Response to ER Stress to Produce a Highly Active Transcription Factor. *Cell*. 107: 881-891.
- Yu, C., Minemoto, Y., Zhang, J., Liu, J., Tang, F., Bui, T.N., Xiang, J. and Lin, A. (2004) JNK Suppresses Apoptosis via Phosphorylation of the Proapoptotic Bcl-2 Family Protein BAD. *Molecular Cell.* 13: 329-340.
- Zhang, B., Shozu, M., Okada, M., Ishikawa, H., Kasai, T., Murakami, K., Nomura, K., Harada, N., and Inoue, M. (2010) Insulin-Like Growth Factor I Enhances the Expression of Aromatose P450 by Inhibiting Autophagy. *Endocrinology.* 151: 4949-4958.
- Zinszner, H, Kuroda, M., Wang, X.Z., Batchvarova, N., Lightfoot, R.T., Remotti, H., Stevens, J.L., and Ron, D. (1998) CHOP is implicated in programmed cell death in response to impaired function of the endoplasmic reticulum. *Genes and Development.* 12: 982-995.
- Zong, W.X., Li, C., Hatzivassiliou, G., Lindsten, T., Yu, Q.C., Yuan, J. and Thompson, C.B. (2003) Bax and Bak can localise to the endoplasmic reticulum to initiate apoptosis. *The Journal of Cell Biology*. 162: 59-69.